

AWARD NUMBER: W81XWH-11-2-0021

TITLE: "Threshold-Switchable Particles (TSPs) To Control Internal Hemorrhage."

PRINCIPAL INVESTIGATOR: James H. Morrissey, Ph.D.

CONTRACTING ORGANIZATION: University of Illinois, Urbana, IL 61801-3620

REPORT DATE: December 2015

TYPE OF REPORT: Annual

PREPARED FOR: U.S. Army Medical Research and Materiel Command
Fort Detrick, Maryland 21702-5012

DISTRIBUTION STATEMENT: Approved for Public Release;
Distribution Unlimited

The views, opinions and/or findings contained in this report are those of the author(s) and should not be construed as an official Department of the Army position, policy or decision unless so designated by other documentation.

REPORT DOCUMENTATION PAGE				Form Approved OMB No. 0704-0188	
Public reporting burden for this collection of information is estimated to average 1 hour per response, including the time for reviewing instructions, searching existing data sources, gathering and maintaining the data needed, and completing and reviewing this collection of information. Send comments regarding this burden estimate or any other aspect of this collection of information, including suggestions for reducing this burden to Department of Defense, Washington Headquarters Services, Directorate for Information Operations and Reports (0704-0188), 1215 Jefferson Davis Highway, Suite 1204, Arlington, VA 22202-4302. Respondents should be aware that notwithstanding any other provision of law, no person shall be subject to any penalty for failing to comply with a collection of information if it does not display a currently valid OMB control number. PLEASE DO NOT RETURN YOUR FORM TO THE ABOVE ADDRESS.					
1. REPORT DATE December 2015		2. REPORT TYPE Annual		3. DATES COVERED 23 NOV 2014 - 22 Nov 2015	
4. TITLE AND SUBTITLE "Threshold-Switchable Particles (TSPs) To Control Internal Hemorrhage."				5a. CONTRACT NUMBER W81XWH-11-2-0021	
				5b. GRANT NUMBER	
				5c. PROGRAM ELEMENT NUMBER	
6. AUTHOR(S) James H. Morrissey, Rustem Ismagilov, Ying Liu, Galen Stucky, and Christian Kastrup E-Mail: jhmorris@illinois.edu				5d. PROJECT NUMBER	
				5e. TASK NUMBER	
				5f. WORK UNIT NUMBER	
7. PERFORMING ORGANIZATION NAME(S) AND ADDRESS(ES) UNIVERSITY OF ILLINOIS GRANTS AND CONTRACTS OFFICE 506 S WRIGHT ST, 364 HENRY ADMIN BLDG URBANA IL 61801-3620				8. PERFORMING ORGANIZATION REPORT NUMBER	
9. SPONSORING / MONITORING AGENCY NAME(S) AND ADDRESS(ES) U.S. Army Medical Research and Materiel Command Fort Detrick, Maryland 21702-5012				10. SPONSOR/MONITOR'S ACRONYM(S)	
				11. SPONSOR/MONITOR'S REPORT NUMBER(S)	
12. DISTRIBUTION / AVAILABILITY STATEMENT Approved for Public Release; Distribution Unlimited					
13. SUPPLEMENTARY NOTES					
14. ABSTRACT The final goal of this project is to develop smart particles to stop internal hemorrhage at local sites. Four collaborating laboratories are working together under this contract to define threshold levels of activators of blood clotting such that the candidate clotting activators will circulate in the blood at a concentration below the threshold necessary to trigger clotting, but accumulation of the activators at sites of internal injury/bleeding will cause the local concentration of clotting activators to exceed the clotting threshold and restore hemostasis. During the past year we have applied our improved methods for covalently attaching inorganic polyphosphate (a potent initiator and accelerator of blood clotting) to nanoscale solid supports including silica- and gold-based nanoparticles that have been fabricated using a variety of derivatization and passivation methods. We have conducted extensive testing of candidate procoagulant nanoparticles to quantify their ability to trigger and/or accelerate blood clotting and have made significant progress toward the goal of adjustable procoagulant activities of the particles to render them sub- or supra-threshold with regard to initiation of the clotting cascade.					
15. SUBJECT TERMS Internal hemorrhage; Bleeding; Blood clotting; Nanoparticles; Trauma					
16. SECURITY CLASSIFICATION OF:			17. LIMITATION OF ABSTRACT	18. NUMBER OF PAGES	19a. NAME OF RESPONSIBLE PERSON
a. REPORT	b. ABSTRACT	c. THIS PAGE			USAMRMC
Unclassified	Unclassified	Unclassified	Unclassified	59	19b. TELEPHONE NUMBER (include area code)

Table of Contents

	<u>Page</u>
Introduction.....	1
Keywords.....	1
Overall Project Summary	2
Key Research Accomplishments.....	23
Conclusion.....	24
Publications, Abstracts and Presentations.....	25
Inventions, Patents and Licenses.....	25
Reportable Outcomes.....	26
Other Achievements.....	26
References.....	26
Appendices	27

DECEMBER 2015 ANNUAL REPORT FOR WQ81XWH-11-2-0021:

"Threshold-Switchable Particles (TSP) to Control Internal Hemorrhage"

1. INTRODUCTION

The final goal of our research is to develop smart particles to stop internal hemorrhage at local sites. Our research comprises five collaborating laboratories working to develop new types of pro-hemostatic nanoparticles and to define threshold levels of these particles such that the candidate nanoparticles will circulate in the blood at a concentration below the threshold necessary to trigger clotting. On the other hand, when the particles accumulate at sites of internal injury/bleeding, their local concentration should exceed the clotting threshold and restore hemostasis. Our continuing approaches include the development and application of chemistries for attaching inorganic polyphosphate (polyP; a potent trigger and accelerator of blood clotting) to nanoscale solid supports, development of candidate nanoparticles with varying abilities to trigger and/or accelerate blood clotting, and defining the threshold levels under which these particles will or will not trigger blood clotting.

2. KEYWORDS

- Internal hemorrhage
- Bleeding
- Blood clotting
- Nanoparticles
- Trauma

3. OVERALL PROJECT SUMMARY

Comments on Administrative and Logistical Matters

Overview of subcontracts — Five laboratories participate in this project, headed by Drs. James Morrissey (University of Illinois at Urbana-Champaign), Ying Liu (University of Illinois at Chicago), Rustem Ismagilov (Caltech), Galen Stucky (University of California at Santa Barbara), and Christian Kastrup (University of British Columbia in Vancouver, BC, Canada).

No-cost extension — Relocating the Ismagilov lab to Caltech delayed progress on certain subtasks, and granting our request for a new subaward to Dr. Kastrup resulted in further unavoidable delays in this project. We therefore requested and received an additional, one-year, no-cost extension, resulting in a new expiration date of 22 June 2016.

Human Anatomical Substances use approval (Milestone #2) — Some of the studies to be conducted in Dr. Ismagilov's lab were designed to employ blood samples from human volunteer blood donors. Dr. Ismagilov obtained IRB approval from Caltech for these studies (RI-334, approved on December 5, 2011) and Dr. Ismagilov was notified on March 20, 2012 that the protocol was approved by the Office of Research Protections. During 2014, the Ismagilov concluded these studies with samples from human volunteers, and on 28 October 2014 submitted a request to close the protocol to the US Army Medical Research and Materiel Command (USAMRMC), Office of Research Protections (ORP), Human Research Protection Office (HRPO). The final report and supporting documents were reviewed by HRPO and found to be acceptable. The protocol was therefore closed in October 2014 and no additional studies with human subjects will be undertaken for the remainder of this project.

Approval for animal studies (Task #5) — We are now in a position to test candidate TSPs in a mouse tail bleeding model. We have received local IACUC approval for these studies at the University of Illinois at Urbana-Champaign, and are now proceeding to obtain approval from the USAMRMC Animal Care Use and Review Office (ACURO) for these studies. No animal studies will be undertaken under this award until full approval is obtained.

Scientific Progress

BACKGROUND

Inorganic polyphosphates (polyP) are linear polymers of phosphate monomers. Ubiquitous across a diverse range of organisms, its physiological function in humans and other complex eukaryotes has only recently been investigated in detail [1]. PolyP is secreted from activated blood platelets and research from the Morrissey lab and others has shown that polyP acts at various stages of the coagulation cascade, depending on its polymer length [2]. Long-chain polyP (>300 phosphates long) is a potent activator for the contact pathway of blood clotting, while shorter polyP polymers of 60-100 phosphate units (the size secreted by platelets) accelerate the activation of coagulation factor V and slow fibrin clot lysis [2, 3]. With its role now clearly established as a critical hemostatic agent within the body, polyP could potentially serve as a useful and safe procoagulant compound to address multiple bleeding disorders including internal hemorrhage.

When intravenously administered, nanoparticle therapies have been devised to target activated platelets with some success, but the goal of functionally delivering a procoagulant therapy to treat internal hemorrhage in practice has yet to be fully realized [4]. We are developing novel approaches for the targeted delivery of nanoparticles functionalized with controlled amounts of polyP. These tunable particles will then be able to selectively target sites of injury in response to appropriate stimuli such as a drop in temperature without the induction of clotting anywhere else in the body, a property that aqueous polyP unfortunately does not possess. Therefore, the overall goal of this study is to understand the process of particle-induced blood clotting, eventually leading to optimally engineered particles for treating internal bleeding.

Task 1 — Conduct spatially-defined numerical simulations to identify threshold conditions. The simulations will utilize Comsol Multiphysics modeling software to screen concentrations of activators and particles, reaction rates, temporal dynamics, shear and external fields.

Progress and completion of Milestone 1 by the Ismagilov lab and Kastrup lab was summarized in the December 2014 annual report. A manuscript describing this work has been submitted for publication to *Thrombosis and Haemostasis*, entitled “Localization of short-chain polyphosphate enhances its ability to clot flowing blood plasma,” by Ju Hun Yeon, Nima Mazinani, Travis S. Schlappi, Karen Y. T. Chan, James R. Baylis, Stephanie A. Smith, Alexander J. Donovan, Damien Kudela, Galen D. Stucky, Ying Liu, James H. Morrissey, Rustem F. Ismagilov, and Christian J. Kastrup.

Task 2 — Conduct in vitro experiments to test recommended threshold conditions with human plasma and whole blood.

Progress and completion of Milestone 2 by the Ismagilov lab and Kastrup lab was summarized in the December 2014 annual report. A manuscript describing this work has been submitted for publication to *Thrombosis and Haemostasis*, entitled “Localization of short-chain polyphosphate enhances its ability to clot flowing blood plasma,” by Ju Hun Yeon, Nima Mazinani, Travis S. Schlappi, Karen Y. T. Chan, James R. Baylis, Stephanie A. Smith, Alexander J. Donovan, Damien Kudela, Galen D. Stucky, Ying Liu, James H. Morrissey, Rustem F. Ismagilov, and Christian J. Kastrup.

Task 3 — Design and test particles that will function as candidate TSPs.

Our collaborative efforts made additional progress in generating and in vitro testing of candidate TSPs, spearheaded by the production in the Liu lab of “artificial dense granules” and gold nanoparticles; and by the production in the Stucky lab of porous silicon-based nanoparticles. In addition, materials were tested in vitro in the originating labs and also in the Kastrup and Morrissey labs.

The Liu group focused on creating candidate TSPs exploiting a facile, biomimetic synthetic program, which entailed the nanoprecipitation of platelet-sized polyP in aqueous calcium and subsequent encapsulation of the bare particles in sterically stabilized liposomes. The resulting nanostructures closely resemble the secreted procoagulant phosphate bodies of human platelets (platelet dense granules). The artificial dense granules (ADGs) have been systematically characterized by dynamic light scattering (DLS) and high-resolution electron microscopy (HREM). Immediately after encapsulation, the ADG particle size is approximately 180 nm, with narrow polydispersity index (PDI) (**Figure 1A**). ADG stability in suspension has been demonstrated in previous reports. After 5 hr, the intensity-weighted ADG particle population consists of a major peak close to 180 nm and a minor peak (<10%) centered near two microns (**Figure 1B**). The ADGs were gently vortexed for 30 s prior to the 5 hr light scattering measurement. This suggests that very little irreversible aggregation has occurred and that the ADGs are very stable in aqueous suspension on a timescale of hours.

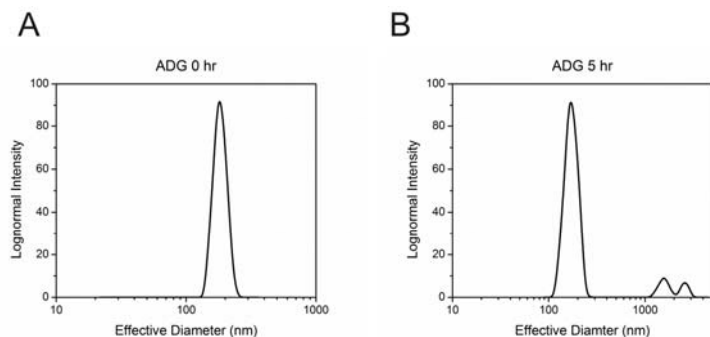


Figure 1. Intensity-weighted, lognormal particle size distribution by dynamic light scattering of ADGs prepared for HREM. A: ADG particle size distribution immediately after encapsulation. ADGs are monodisperse and approximately 180 nm in diameter. B: ADG particle size at 5 hr after 30 s of gentle vortexing. The ADG intensity-weighted particle size distribution has a major peak at 180 nm and a minor peak above 1 micron. Very little irreversible aggregation has occurred.

ADG structure, morphology, and elemental composition were then investigated by HREM and electron energy loss spectroscopy (EELS). Bare polyP NPs and ADGs were prepared on graphene monolayer sandwiches following C. Wang et al. *Adv. Mater.*, **2014**, 26: 3410–3414 for imaging on a scanning transmission electron microscope (STEM). **Figure 2** shows ADGs in dry cells that manifest a core-shell architecture consisting of an electron dense core ~150 nm with a shell thickness of ~25 nm. Total particle size ~190 nm, closely corroborating light scattering data. Most likely, the core consists of the polyP NP, which is encapsulated in the PEGylated phospholipid vesicle, resulting in less electron density in the corona. In contrast, **Figure 3** demonstrates that the bare polyP NPs are uniformly electron dense in dark-field imaging. Bare NPs are generally 150-200 nm, equivalent to DLS data in solution; however, there are some larger particles >200 nm (**Figure 3C**), most likely the result of sample preparation. During the drying process, the calcium concentration significantly increases. As the nanoprecipitation of PolyP in aqueous salt solutions is thermodynamic driven by the metal ion concentration, increased divalent metal ion concentration will result in larger NPs.

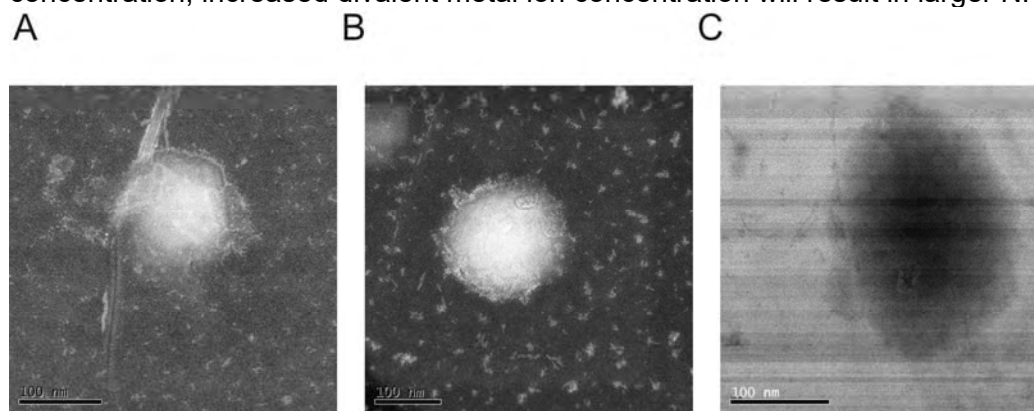


Figure 2. Core-shell architecture of ADGs. A: Dark-field image of a 160-nm diameter ADG with 24-nm shell thickness. B: Another ADG with similar core-shell architecture. Particle size is approximately 190 nm. C: Bright-field image of an ADG.

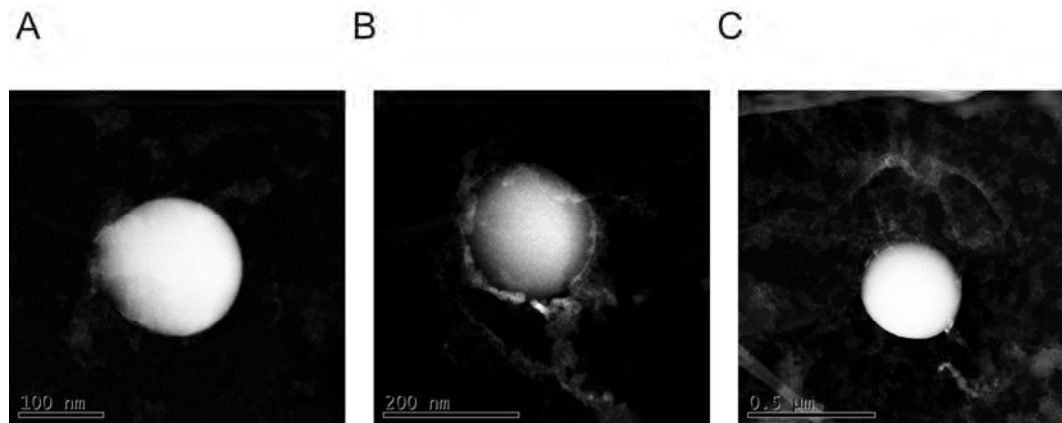


Figure 3. STEM images of bare polyP NPs highlighting its homogeneous electron density. A: 166-nm polyP NP. B: Bare particle ~184 nm. C: A larger, 401-nm bare polyP NP.

Electron energy loss spectroscopy (EELS) is a common technique used to determine the elemental constituents of nanostructured materials in concert with electron-dispersive X-Ray spectroscopy (EDS). The Liu group reported previously that bare polyP NPs contain the elements P, Ca, and O, with the P:Ca stoichiometry being 2.01 by EDS (Donovan et al. *Biomacromolecules* **2014**, 15(11): 3976-3984.). EELS exploits the inelastic scattering of the electron beam characteristic of certain elements to construct a two-dimensional elemental map of the sample in question. EELS allowed the Liu group to conclude that the core-shell architecture observed in **Figure 2** was most

likely a consequence of encapsulation of polyP NPs in the sterically stabilized liposomes. **Figure 4B** shows the location of oxygen, calcium, and phosphorous in an ADG, and the locations where the elements are co-localized. The core consists of P, Ca, and O while the corona contains more P and O. Additional analysis indicates that the shell contains small amounts of carbon (possibly from the phospholipid acyl tails) after subtraction of the graphene background (data not shown).

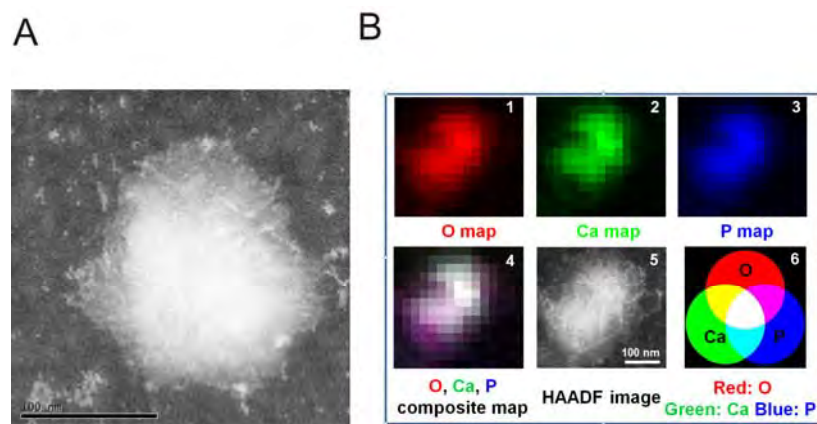


Figure 4. Core-shell structure, morphology, and 2-D elemental mapping of Artificial Dense Granules. A: STEM microscopy of ADG highlighting its core-shell structure. The ADG is 163 nm across. The shell is approximately 20 nm. B: Electron energy loss spectroscopy (EELS) of an ADG

revealing the colocalization of P, O, and Ca in the dense core and only P and O in the corona. Additional analysis confirms the presence of C in the shell after subtraction from the graphene background. This suggests that the PEGylated vesicle has encapsulated a polyP NP, corroborating light scattering data.

Both the bare polyP NP and ADG specimens contained several irregular 10-20 nm-scale features besides the ~200 nm particles. The high resolution afforded by sample preparation in the graphene monolayer sandwich and the intrinsic abilities of STEM allowed for careful examination of these smaller nanostructures at atomic resolution (**Figure 5**). **Figure 5A** shows that the background is composed of rectangular nanocrystals approximately 5 nm wide and 20 nm long. The ordered array of individual atoms is clearly resolved in **Figure 5B**. Each bright white spot in the high-resolution dark-field image is a single atom. The image in **Figure 5A** was filtered to obtain information on the object's crystal symmetry (**Figure 5C**). After subtraction of the graphene background, the nanocrystals clearly possess hexagonal symmetry. Fast-Fourier transform (FFT) analysis will allow the Liu group to compare the structure's symmetry group to other specimens in the crystal databank. Most likely, the nanostructures are crystalline calcium phosphate salts. Apatites ($\text{Ca}_{10}(\text{PO}_4)_6(\text{OH}, \text{Cl}, \text{F})_2$), common structural biomaterials, including hydroxyapatite, the key constituent of tooth dentin and a bone mineral, have hexagonal pyramidal symmetry. It is most plausible that these nanocrystals, which were not detected in solution-phase by DLS, formed after sample preparation. Upon drying, the calcium concentration may have increased sufficiently to promote polyP polymer hydrolysis, even at mildly acidic conditions. In addition, the polyP preparation is relatively heterodisperse, with some chains as short as 25-mer. These short polyP oligomers may co-crystallize with calcium upon drying.

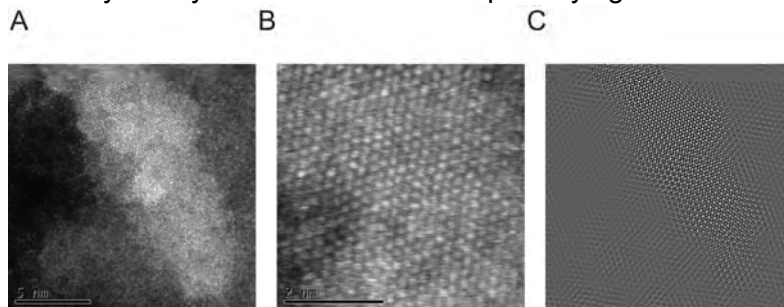


Figure 5. Atomic resolution imaging of the background. A: Rectangular nanocrystal with dimensions 5 nm X 20 nm. The grid contains several nanometer-scale features in addition to the polyP NPs. High-resolution imaging of one particular area shows unequivocally that they are crystalline. B: Atomic resolution of nanocrystal in A revealing the ordered arrangement of individual atoms.

The dark-field image reveals the location of single atoms, as distinguished by the intense white areas of high electron density. C: Hexagonal crystal symmetry after image processing. The nanocrystals have hexagonal crystal

symmetry ubiquitous among calcium phosphate salts, including apatites, an important structural biomaterial.

The Liu group has identified a class of secreted phospholipase enzymes (sPLA₂) released from human platelets during activation, which will allow for the targeting and margination of the ADG candidate TSPs at sites of internal incompressible hemorrhage. sPLA₂ is secreted from the α granules of human platelets upon activation by thrombin or other inflammatory markers. The interfacially-active enzyme catalyzes the hydrolysis of the acyl tail from phospholipids, yielding lysophospholipids and arachidonic acid. Concentrations of sPLA₂ are substantially elevated in inflammatory diseases and can locally reach ~1-10 $\mu\text{g/ml}$ near sites of trauma. Control experiments were performed with bare polyP NPs and 10 $\mu\text{g/ml}$ sPLA₂ from bee venom (bvsPLA₂) to identify any possible interactions between the polymer and protein. Platelet-sized polyP was nanoprecipitated in 5 mM CaCl₂, pH 5.4 and the stability in suspension was monitored by DLS for 30 min before addition of the enzyme. Before introduction of the enzyme, the particle aggregation behavior manifests typical power-law growth kinetics, with an initial diameter ~175 nm, slowly increasing to slightly above 200 nm. 10 minutes after addition of sPLA₂, however, the scattering count rate had dropped significantly (below 200 kcps, data not shown), and the effective diameter was well above 3000 nm. The Liu Group suspects that polyP complexes in some fashion with sPLA₂, possibly forming an electrostatic interaction between the multiple positively charged lysines in bvsPLA₂'s anticoagulant site (responsible for binding to the prothrombinase complex) and the negatively charged monophosphate residues of polyP. New evidence recently presented by Ursula Jakob and colleagues at the University of Michigan (cf. M.J. Gray et al. *Molecular Cell*. **2014**, 53: 689-699) argues that polyP is an ancient and general protein chaperone, capable of binding to a multitude of proteins with diverse tertiary structures, protecting the cell from oxidative stress and other environmental insults. Indeed, work from the Liu and Morrissey groups have determined by DLS and surface plasmon resonance (SPR) that polyP is capable of binding to a myriad of serum and coagulation proteins. Therefore, it seems plausible polyP may be binding to sPLA₂.

The Liu group has demonstrated in previous reports that ADGs are able to activate the Factor XII (FXII) zymogen in an *in vitro* assay after solubilization of the liposomal envelope with the non-ionic detergent Tween 20 following the protocol outlined in Engel et al. *J. Thromb. Haemost.* **2014**, 12:1-10. Progress has been made this past year on characterizing the functional stability of ADGs after freeze drying. ADGs were synthesized as described previously and then 100X, 300X, and 500X (w:w) trehalose was added as an excipient before freeze drying. The ability of the freeze-dried ADGs after resuspension to activate FXII was then interrogated to determine if the ADGs had retained their procoagulant ability. **Figure 6A** shows the activation kinetics of freshly nanoprecipitated polyP measured against freeze-dried ADGs using various amount of trehalose. The bare polyP NPs manifest the highest intrinsic FXII activity followed by the freeze-dried ADGs treated with detergent. The freeze-dried ADGs not treated with Tween 20 show little activity. The activation of FXII correlates with the amount of trehalose excipient added. High weight fractions of sugar excipients are needed to guarantee stability after freeze-drying and prevent aggregation after resuspension. It may be possible that the trehalose is interfering with mass transport due to changes in solution viscosity and diffusivity of FXIIa, thereby slowing FXII activation kinetics. **Figure 6B** shows a control experiment with freshly precipitated bare polyP NPs with and without trehalose (equivalent to ADG with 100X trehalose in **Figure 6A**) and Tween 20. It is clearly evident that the bare particles with trehalose and Tween 20 possess less FXII activity. Indeed, it is comparable to the curve in **Figure 6A** representing ADG with 100X trehalose + Tween 20. Work is ongoing to optimize the freeze-drying process so that ADGs retain close to maximal procoagulant effect for several months.

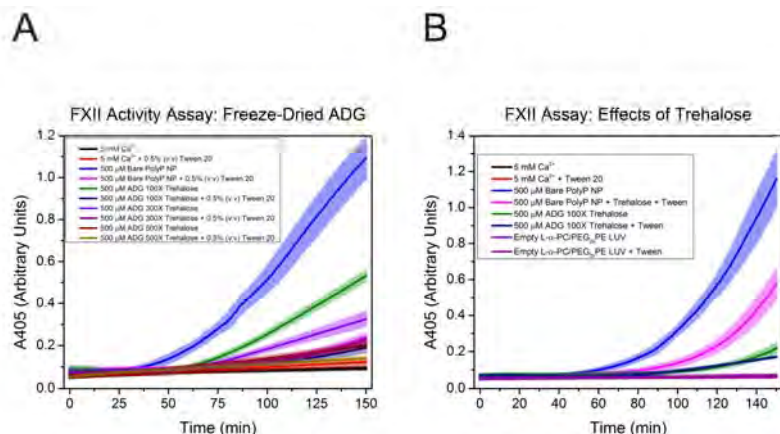
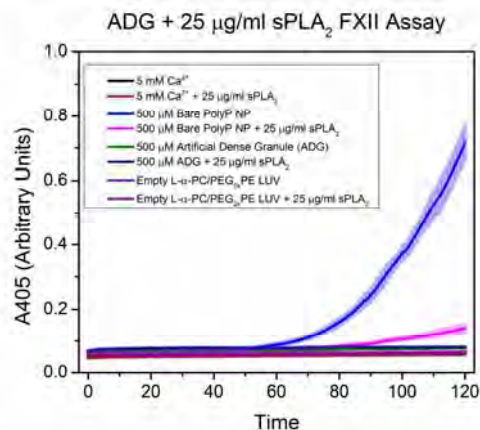


Figure 6. *In vitro* contact activity assays of lyophilized ADGs contrasted against freshly precipitated polyP NPs. A: FXII autoactivity of freeze-dried ADGs using trehalose as excipient. ADGs were freeze-dried with 100X, 300X, and 500X trehalose by weight phosphate. 500 μM bare PolyP NPs are able to activate FXII most rapidly. Freeze-dried ADGs with detergent possess attenuated FXII activity compared to the fresh bare particles, while freeze-dried ADGs without detergent are comparable to control, with only minimal activity. **B: Effects of trehalose on the activation of FXII.** Bare particles with trehalose and Tween 20 at the same monophosphate concentration manifest slower activation kinetics.

In addition to using detergent to expose the polyP cargo, the Liu group is currently devising strategies to use phospholipases to degrade the phospholipid envelope. Given that bvsPLA₂ possibly interacts with polyP as shown above with DLS, the Liu group suspected that this polymer-protein complexation may adversely affect polyP's ability to activate the contact pathway of coagulation. The autoactivation of FXII by ADGs treated with and without 25 $\mu\text{g}/\text{ml}$ bvsPLA₂ for 15 min is shown in **Figure 7**. Bare particles were also incubated with bvsPLA₂ to ascertain any functional consequences of polyP-bvsPLA₂ on contact activity. Bare PolyP without bvsPLA₂ manifests the highest rate of activation. Both ADGs treated with and without enzyme possess minimal FXII activity. Interestingly, bare particles incubated with enzyme show drastically reduced FXII activity. This is likely a result of polyP-bvsPLA₂ interaction. Favorable electrostatic interactions between the positively charged lysine residues on bvsPLA₂ may shield the negatively charged monophosphate residues from the FXII zymogen, abrogating its role as a negatively charged contact surface required for initiation of the contact pathway of blood clotting.

Figure 7. *In vitro* FXII activity assay with 25 $\mu\text{g}/\text{ml}$ bvsPLA₂. The ability of polyP to activate the FXII zymogen is severely abrogated in the presence of enzyme.



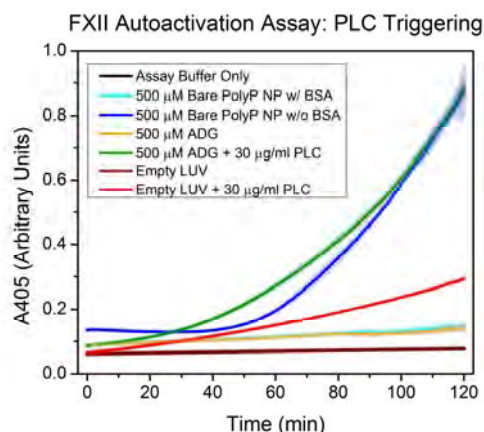


Figure 8. *In vitro* FXII activity assay with 30 $\mu\text{g/ml}$ PLC from *C. perfringens*. ADGs triggered with PLC autoactivate FXII zymogen in the same manner as bare polyP NPs, whereas ADG without trigger are functionally inert.

The Liu group continues to pursue phospholipase-dependent triggering strategies, focusing on a related isoform called phospholipase C (PLC), which is intimately involved in the platelet degranulation process, the exocytosis of dense and α granules into circulation. While human isoforms exclusively hydrolyze phosphoinositides, certain PLC bacterial toxins, often referred to as lecithinases, manifest robust enzymatic activity for phosphatidylcholines and phosphatidylethanolamines, potentially suitable for hydrolyzing the ADG phospholipid envelope. The ability of PLC to function as a trigger for ADGs to initiate the autoactivation of FXII zymogen was assessed again following protocol detailed in Engel et al. *J. Thromb. Haemost.* **2014**, 12:1-10. 500 μM ADGs were pre-incubated with 30 $\mu\text{g/ml}$ PLC from *C. perfringens* for 20 min at 37°C before addition of zymogen and chromogenic substrate. ADG + 30 $\mu\text{g/ml}$ PLC is able to initiate FXII autoactivation at approximately the same rate as 500 μM bare polyP NPs (**Figure 8**) Empty LUVs + 30 $\mu\text{g/ml}$ PLC demonstrate a modest rise in turbidity; however, it is significantly less than ADG + 30 $\mu\text{g/ml}$ PLC and 500 μM bare polyP NPs. Moreover, the increase in absorbance could be attributed to other underlying processes mechanistically unrelated to autoactivation of FXII such as vesicle fusion. PLC concentration dependence on FXII autoactivation was observed (data not shown for 10 and 60 $\mu\text{g/ml}$), with optimal activity achieved at 30 $\mu\text{g/ml}$ PLC.

Investigation of the procoagulant and potentially prohemostatic function of ADGs in biological fluids such as human pooled normal plasma has recently been a primary objective of the Liu group in order to transform it from a proof-of-concept into a viable drug delivery system (DDS). Biological media present certain challenges and add much complexity into the creation a prohemostatic DDS, and, inevitably, certain modifications must be carried out in the design of the delivery vector. The ADG phospholipid envelope was modified with 30 mol% cholesterol to a final composition of 5 mol% DPPE-PEG₂₀₀₀, 65 mol% L- α -PC, and 30 mol% cholesterol. The change was implemented to increase membrane rigidity, and prevent transport of polyP and/or ions across the bilayer. The ability of modified ADGs (30 mol% cholesterol) to initiate the contact pathway of blood coagulation was assayed by 96-well turbidity microplate assay at room temperature. Modified ADGs were pre-incubated with 30 $\mu\text{g/ml}$ PLC for 20 min before addition to recalcified plasma. Emphasis must be placed that the citrated plasma was recalcified first, and then the sample was immediately added, contrary to conventional protocol. Nonetheless, the time to clot is a time scale of several minutes instead of seconds, so it was deemed experimentally justifiable. Modified ADGs triggered with 30 $\mu\text{g/ml}$ PLC manifest fibrin formation in approximately 10 minutes compared to a time of approximately 30 min for control with no activator present (**Figure 9**). ADG without enzyme begins to coagulate at statistically the same time as granular polyP NPs, which suggests that further modifications in the envelope must be considered.

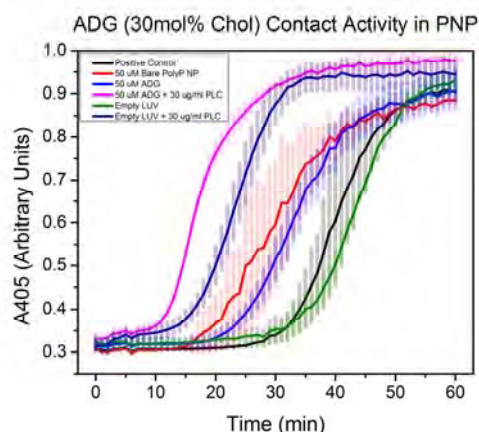


Figure 9. Contact activity assay of modified ADGs with PLC in PNP. Modified ADGs with 30 $\mu\text{g}/\text{ml}$ PLC are robust contact pathway activators compared to control with no activator present. However, modified ADGs without trigger still initiate the contact pathway in a manner equivalent to precipitated polyP NPs.

Stucky group studies on silicon-based nanoparticles: In developing candidate nanometer- and micron-scale particles to serve as suitable support for TSPs and to further our study of silicon based inorganic materials, the Stucky lab looked at porous silicon nanoparticles and microparticles as a potential TSP candidate and carrier for polyphosphate. Porous silicon is of interest for study as a TSP because of the tunable particle size, pore size, and pore volume; the options for a number of surface and pore modification techniques to control the amount, identify, and therapeutic agent release rate; the biodegradability of the porous silicon; and the optical properties that allow for *in vivo* monitoring.¹⁻⁵ In addition, the porosity of the silicon allows for more surface area as a carrier for functionalized polyphosphate. Another option is to load and encapsulate a secondary therapeutic agent in the pores of the silicon particle structure for slow, low dose, and longer term drug release, while functionalizing the surface of the silicon particle with polyphosphate for more rapid blood clotting activity. For instance, a scenario where the silicon particle surface functionalized with polyphosphate accelerates blood clotting, while a secondary drug is released over time to minimize inflammation or infection resulting from the injury.

The porous silicon work was conducted with the assistance of Professor Michael Sailor at University of California San Diego. Porous silicon nanoparticles were prepared using electrochemistry techniques that utilized a silicon wafer as the anode and working electrode, and a platinum wire as the cathode and counter electrode, in the presence of a hydrofluoric acid and ethanol electrolyte solution (**Figure 10**). Particle size, pore size, and pore volume are tunable from nanometer to micron size by controlling the current density applied during the electrochemical synthesis process, the type and concentration of dopant and the crystalline orientation of the silicon wafer, and the electrolyte solution concentration.¹

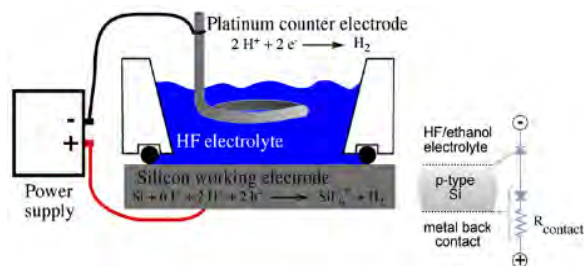


Figure 10. Schematic of the etch cell system used to prepare porous silicon particles. The electrochemical half-reactions and the equivalent circuit for etching of a p-type silicon wafer are shown.¹

To prepare luminescent porous silicon nanoparticles (LPSiNP) (**Figure 11**), porous p-type silicon is first etched into the single-crystal silicon wafer substrate depicted in **Figure 9**. The entire porous nanostructure is removed from the silicon substrate by application of a current pulse and then fractured into multi-sized particles by overnight ultrasonication in an aqueous solution. The particles are then filtered through a filtration membrane to obtain porous p-type silicon nanoparticles of a particular size range. To activate their luminescence, the porous silicon nanoparticles are incubated in an aqueous solution.²

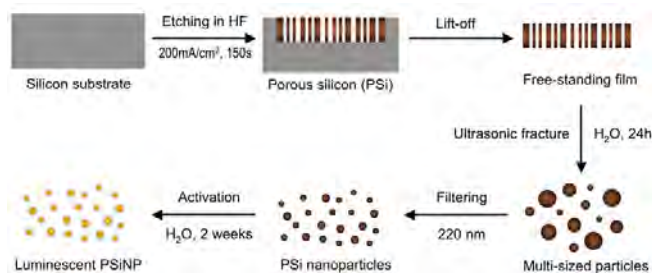


Figure 11. Schematic of the synthesis of luminescent porous silicon nanoparticles (LPSiNP).²

To further improve on the size control of the electrochemically etched porous p-type silicon nanoparticles, two different current pulses can be applied that results in a lower current primary layer and a higher current perforated layer (**Figure 12**).⁶ The illustration below depicts the ultrasonic fracture process used to prepare porous p-type silicon nanoparticles from porous silicon film and the result of introducing perforations into the silicon film. The introduction of a secondary perforated layer provides an additional fracture plane to allow for better size control upon ultrasonic fracturing.

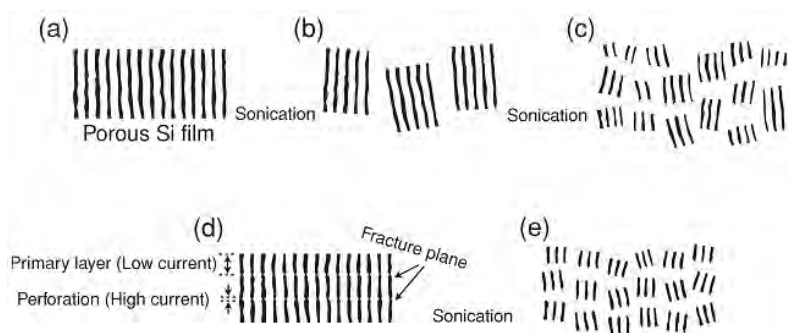


Figure 12. Illustration of the ultrasonic fracture process with etched (a) primary layer only and (d) primary and perforated layers. (a) Porous silicon film with pores that run primarily perpendicular to the wafer surface. (b) Fragments from ultrasonic fracturing along pore walls. (c) Additional ultrasonic fracturing further fragments particles into smaller, irregularly sized, and polydispersed particles. (d) Introduction of perforated layers as fracture planes for improved size selectivity. (e) Result is smaller, regularly sized, and uniform porous silicon particles.⁶

Using the above described etching procedure and perforation technique, we electrochemically synthesized (**Figure 13**) and characterized porous p-type silicon nanoparticles for consideration as a suitable TSP. Characterization data for porous silicon nanoparticles serve as a baseline for comparison in subsequent functionalization efforts. Post-etching, all work with porous silicon nanoparticles was conducted in ethanol to minimize oxidative effect

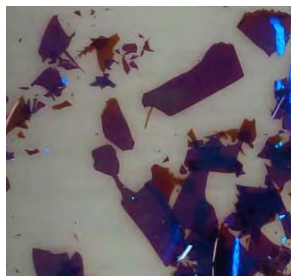


Figure 13. Etched porous silicon layer fragments in ethanol pre-ultrasonic fracturing.

Below are scanning electron microscopy (SEM) and transmission electron microscopy (TEM) images of porous silicon after ultrasonic fracturing (**Figure 14**), and three iterations of ethanol washes followed by centrifugation at 21,128 x g for 15 minutes (**Figure 15**). Post ultrasonic fracturing resulted in nanometer to micron size particles. Further washing and processing resulted in porous p-type silicon nanoparticles with diameters of approximately 125 nm and pore size as measured from SEM to be approximately 30 nm. SEM images showed post-wash porous silicon nanoparticles to be of uniform size. The particles under SEM appear agglomerated due to the effect of drying, but the particles show similar packed and individual morphologies. However, TEM images show particles of varying sizes. TEM allows for better imaging of particles in different orientation.

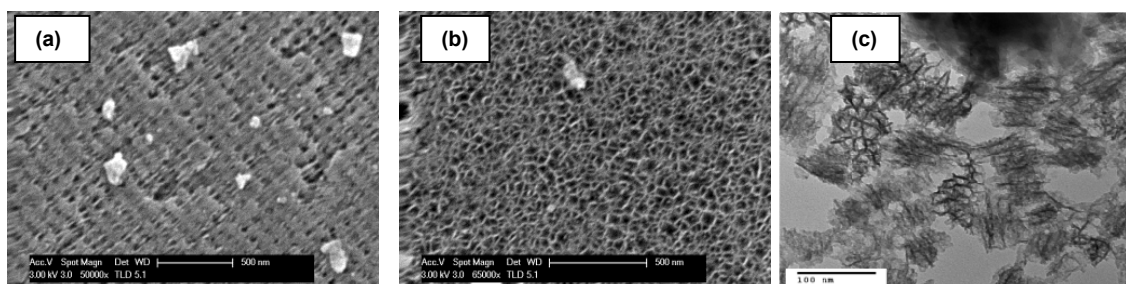


Figure 14. (a, b) SEM images of porous silicon post ultrasonic fracturing (a) along pore wall and (b) top down. (c) TEM image of porous silicon post ultrasonic fracturing.

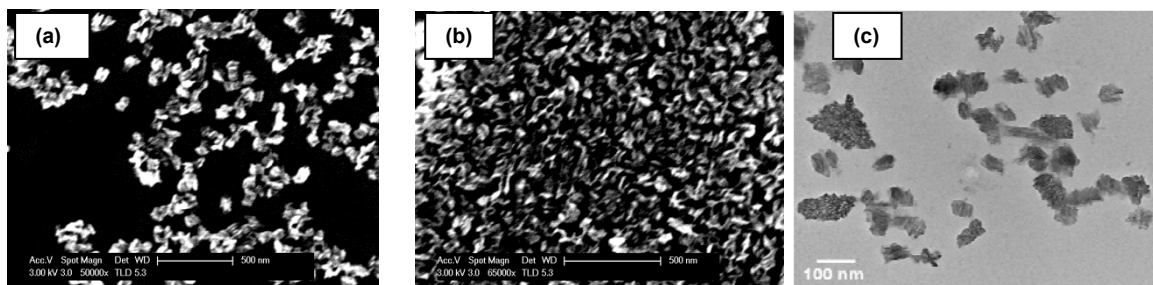


Figure 15. (a, b) SEM of porous silicon post ultrasonic fracturing and washing. Nanoparticles appear agglomerated due to drying effect. (c) TEM image of porous silicon post ultrasonic fracturing and washing.

Dynamic light scattering (DLS) post ultrasonic fracturing, and washing and centrifugation, indicated porous p-type silicon nanoparticles to be 151.8 ± 9.508 nm with a reasonable polydispersity index (PDI) of 0.183, which confirmed the size and uniformity results obtained by SEM. Electrophoretic light scattering (ELS) indicated that the zeta potential was -27.2 ± 3.90 mV. The magnitude of the zeta potential was indicative of the particles' colloidal stability, while the strongly negative zeta potential suggested that the silicon nanoparticle surface was oxidized to silicon dioxide, which was expected due to the transition from predominantly brown colored porous silicon to a lighter brown to white oxidized porous silicon over time.

Supernatants after ethanol washes and centrifugation retain smaller porous silicon nanoparticles. This can serve as a means for further size selection other filtration, which may capture larger particles

and make them unsalvageable for subsequent use. Whereas with centrifugation, larger particles that precipitate out can be collected, redispersed, and undergo further ultrasonic fracturing to give smaller particles that are more uniform and monodisperse. DLS of porous silicon collected from the supernatant with further washing resulted in nanoparticles of 78.74 ± 1.370 nm with a Pdl of 0.071. ELS measurement gave a zeta potential of -8.52 ± 0.777 mV. The lower magnitude zeta potential indicated a less stable colloidal system. However, based on the Pdl, the nanoparticles remain monodisperse. The less negative zeta potential may be due to a higher proportion of porous silicon in the sample that has not yet been oxidized to silicon dioxide.

Raman spectroscopy confirmed the presence of silicon in the sample of porous silicon with a strong signal at 500 cm^{-1} (**Figure 16**). Depending on orientation of the sampling location, the Raman shift may vary, but the signal remains predominantly between 500 cm^{-1} and 517 cm^{-1} , and occasionally below 500 cm^{-1} . The signal at 300 cm^{-1} is due to the acoustic phonon with a second order signal at 600 cm^{-1} .⁷

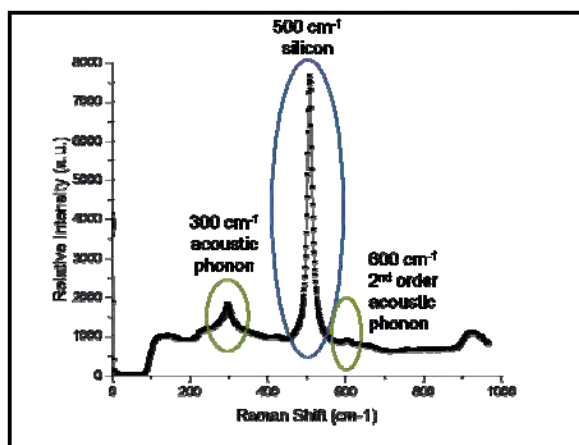


Figure 16. Raman spectroscopy spectrum shows clear evidence of silicon in the porous silicon sample at 500 cm^{-1} with an acoustic phonon at 300 cm^{-1} and a second order signal at 600 cm^{-1} .

Fourier transform infrared spectroscopy (FTIR) spectrum for porous silicon is provided below (**Figure 17**). The advantage of FTIR over Raman spectroscopy is that there are more infrared active modes, which provide more detailed information about the sample. The broad absorption band centered at 1075 cm^{-1} is due to the Si-O-Si stretch. The rocking or bending vibration of O in the Si-O-Si is located at 487 cm^{-1} . Double peaks at 625 cm^{-1} and 650 cm^{-1} are from SiH₂ and SiH wagging modes, respectively. The signal at 912 cm^{-1} is from the SiH₂ scissoring mode with the signal at 975 cm^{-1} from the SiF₃ stretching mode. The double peaks at 2087 cm^{-1} and 2100 cm^{-1} are from stretching vibration modes of SH and SH₂, respectively. The broad band at approximately 3400 cm^{-1} is due to the O-H stretch from water vapor absorption.⁷

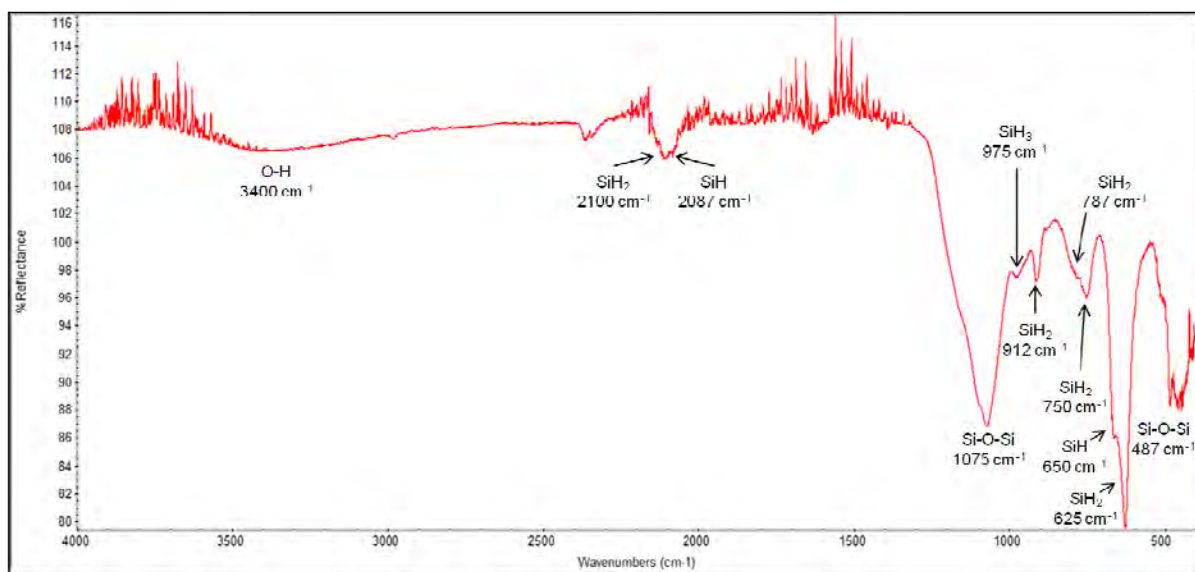


Figure 17. FTIR spectrum of porous silicon with peak assignments.

In summary for this portion of the report, the Stucky lab successfully prepared porous p-type silicon nanoparticles via an electrochemical process. Characterization results provided above confirmed our findings. The study into porous p-type silicon nanoparticles advances our pursuit in designing and testing particles that may function as a candidate nanometer scale particle suitable for supporting TSPs that do not trigger clotting when finely dispersed in plasma/blood.

Using the aforementioned electrochemically synthesized porous silicon nanoparticles, the Stucky lab proceeded to covalently attach molecules that can trigger or enhance blood clotting. This was accomplished by functionalizing the surface of the nanoparticles with (3-aminopropyl)-triethoxysilane (APTES), (3-aminopropyl)trimethoxysilane (APTMS), and (3-aminopropyl)dimethylethoxysilane (APDES) in order to obtain primary amine end groups. The primary amine end groups served as covalent binding sites for subsequent functionalization of polyphosphate onto the porous silicon nanoparticles.

Using porous silicon nanoparticles that were determined by DLS and ELS to be 78.74 ± 1.370 nm with a Pdl of 0.071 and a zeta potential of -8.52 ± 0.777 mV, the porous silicon nanoparticles were incubated overnight at room temperature with stirring in a ratio of 200 mole silicon to 1 mole APTES, APTMS, or APDES. The purpose of these experiments was to compare the binding efficiencies of APTES, APTMS, and APDES. This information allowed us to determine the best amine reagent for our work. The mole ratio of silicon to amine reagent was based on literature, which provided that a 200:1 silica:silane weight ratio was the ideal condition to prevent aggregation.⁸ In this situation, we substituted silicon for silica.

DLS and ELS characterization were conducted in ethanol for porous silicon-APTES, -APTMS, and -APDES functionalized nanoparticles post-ethanol wash and collection by centrifugation, which was repeated three times. The porous silicon-APTES nanoparticle sample was determined to be 80.36 ± 2.722 nm in size with a Pdl of 0.257, and a zeta potential measurement of 42.0 ± 1.68 mV. The size of the APTES functionalized porous silicon nanoparticle was slightly larger with a higher standard deviation and Pdl than the bare porous silicon. The zeta potential magnitude showed stability with a positive value typical of amines.

The size of porous silicon-APTMS was determined to be 67.66 ± 5.129 nm with a Pdl of 0.127, and a zeta potential measurement of 40.2 ± 0.937 mV. The size of APTMS functionalized porous silicon was smaller than the bare porous silicon, but with a higher standard deviation and a larger Pdl. This trend needs to be further investigated. The zeta potential magnitude showed stability with the positive value typical of amines. However, the zeta potential magnitude for APTMS functionalized porous silicon was lower than that of APTES functionalized porous silicon nanoparticles.

The size of porous silicon-APDES was determined to be 58.56 ± 3.052 nm with a Pdl of 0.146, and a zeta potential measurement of 29.4 ± 0.918 mV. The size of APDES functionalized porous silicon was smaller than the bare porous silicon, but with a higher standard deviation and a larger Pdl. This trend needs to be further investigated. The zeta potential magnitude showed stability with the positive value typical of amines. However, the zeta potential magnitude for APDES functionalized porous silicon was lower than that of APTES and APTMS functionalized porous silicon nanoparticles.

SEM (**Figure 18**) and energy-dispersive x-ray spectroscopy (EDS) characterization were conducted to determine changes, if any, in porous silicon nanoparticle morphology and chemical composition post covalent modification with APTES, APTMS, and APDES. SEM images of the particles show irregular particle size and morphology. The agglomeration of the particles may be an artifact of drying the sample. Overall, particle morphology did not appear to be affected by the functionalization effort. EDS showed no indication of nitrogen present. However, the concentration of APTES, APTMS, and APDES used was well below the 1% detection limit, so the result was expected.

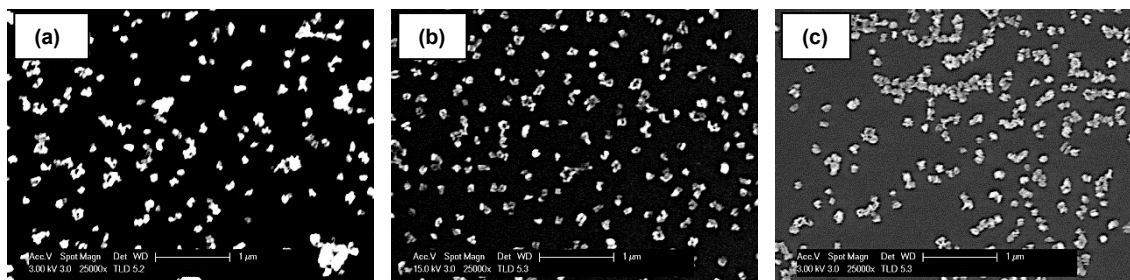


Figure 18. SEM images of porous silicon nanoparticles functionalized with (a) APTES, (b) APTMS, and (c) APDES.

Using the amine functionalized samples described above, polyphosphate 70mer provided by the Morrissey lab, was covalently attached via the zero length 1-ethyl-3-(3-dimethylaminopropyl)carbodiimide (EDAC) cross-linker.⁹ Use of a primary amine and EDAC to covalently attach the polyphosphate allowed us improved control of the amount and mechanism by which the polyphosphate attached to the porous silicon nanoparticles. This control allowed for qualitative and quantitative characterization techniques and calculations based on mole ratios that serve as feedback for formulation refinement to correlate composition with TSP effectiveness *in vitro*.

The amount of sample collected allowed only enough dried sample material for characterization by DLS, SEM (**Figure 19**), EDS (**Figure 20**) and x-ray photoelectron spectroscopy (XPS) (**Figure 21**). In preparing the samples for characterization, the samples appeared hygroscopic, which is atypical of silicon and polyphosphate, but is characteristic of lithium chloride. A 2 M lithium chloride solution was used in the washing process to remove unbound polyphosphate. In an attempt to retain a sufficient amount of sample for characterization, two additional water washes to remove the lithium chloride was not conducted. It was evident from EDS and XPS results that significant amounts of lithium chloride remained in the sample. The concentration of lithium chloride in the wash solution exceeded the amount of porous silicon nanoparticles and polyphosphate 70mer in the sample. Reagent amounts need to be scaled up and washing procedure needs to include final water washes. Concentration of lithium chloride used in the wash may also need to be decreased.

Although DLS experiments were conducted, the data quality was poor with particles in the micron size regime and a Pdl of greater than 0.500. SEM visually confirmed the DLS result. SEM images showed unexpected sample morphology post APTES, APTMS, or APDES treatment and polyphosphate 70mer functionalization followed by two washes with a 2 M lithium chloride solution. Image resolution was lost at higher magnification, thereby limiting us to micron scale micrographs.

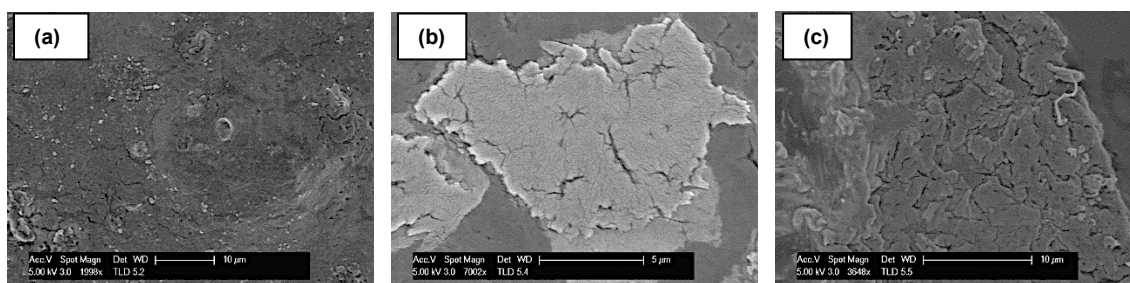


Figure 19. SEM images of porous silicon nanoparticles functionalized with (a) APTES, (b) APTMS, and (c) APDES (10 μm scale bar) and polyphosphate 70mer showed unusual sample morphology.

EDS spectra (**Figure 20**) showed the presence of phosphorus and not nitrogen post amine and polyphosphate 70mer functionalization of the porous silicon nanoparticles. In theory, given the mole ratios used and the average number of phosphorus repeating units in polyphosphate 70mer, the ratio of silicon to nitrogen to polyphosphate should be 200 silicon:1 nitrogen:70 phosphorus. This may be why silicon and phosphorus were detected by EDS, but not nitrogen. In all the EDS results, the presence of Cl was significant as illustrated by the counts for the element extending well beyond the spectra scale. By weight percent, of the elements of interest, the APTES functionalized sample showed 37.33% Si, 33.37% O, 26.30% C, and 3.00% P, while the APTMS sample showed 19.59% Si, 14.05% O, 65.25% C, and 1.11% P; and the APDES sample showed 17.74% Si, 17.43% O, 64.06% C, and 0.77% P. The EDS data reflected sampling locations that provided the highest weight percent of phosphorus collected during the data collection session. There were sampling locations that provided less or no phosphorus detection. Most likely, the silicon and phosphorus signals were due solely to the samples, while the oxygen signal may be due to silicon that oxidized to silicon dioxide, phosphate, the sample surface, and the environment; and the carbon signal may be due to covalently bound APTES, APTMS, or APDES, and the adhesive used to mount the sample.

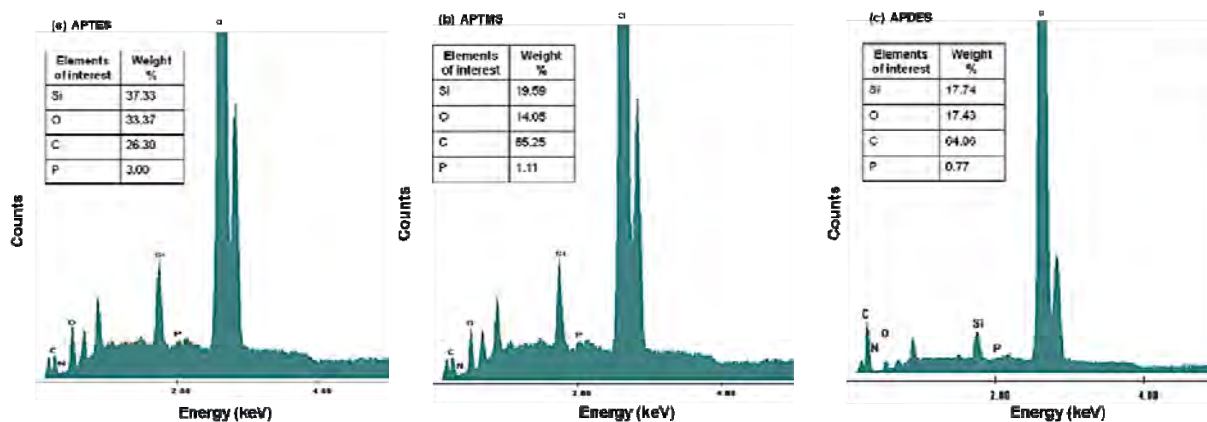


Figure 20. EDS spectra of porous silicon nanoparticles functionalized with (a) APTES, (b) APTMS, and (c) APDES and polyphosphate 70mer consistently showed the presence of phosphorus.

XPS spectra (**Figure 21**) showed the presence O 1s at 532 eV, N 1s at 399 eV, C 1s at 284 eV, Cl 2s at 270 eV, and Cl 2p at 200 eV to varying degrees in all three porous silicon nanoparticle functionalized APTES, APTMS, or APDES with polyphosphate 70mer samples. The APDES sample showed the strongest nitrogen signal. However, only the APTMS sample showed the presence of Si 2s at 149 eV and Si 2p at 99 eV. XPS demonstrated greater sensitivity for detection of nitrogen than EDS post amine and polyphosphate 70mer functionalization even though there should be more

phosphorus than amine based on the theoretical elemental ratio of 200 silicon:1 nitrogen:70 phosphorus. In addition, XPS showed a more pronounced carbon signal, which is attributed to the adhesive that kept the sample in place and the functionalized amine, than EDS. EDS on the other hand, showed a stronger chlorine signal from the lithium chloride introduced in the wash process than XPS. Differences in detection limitation and methodology may explain the differences in XPS and EDS results.

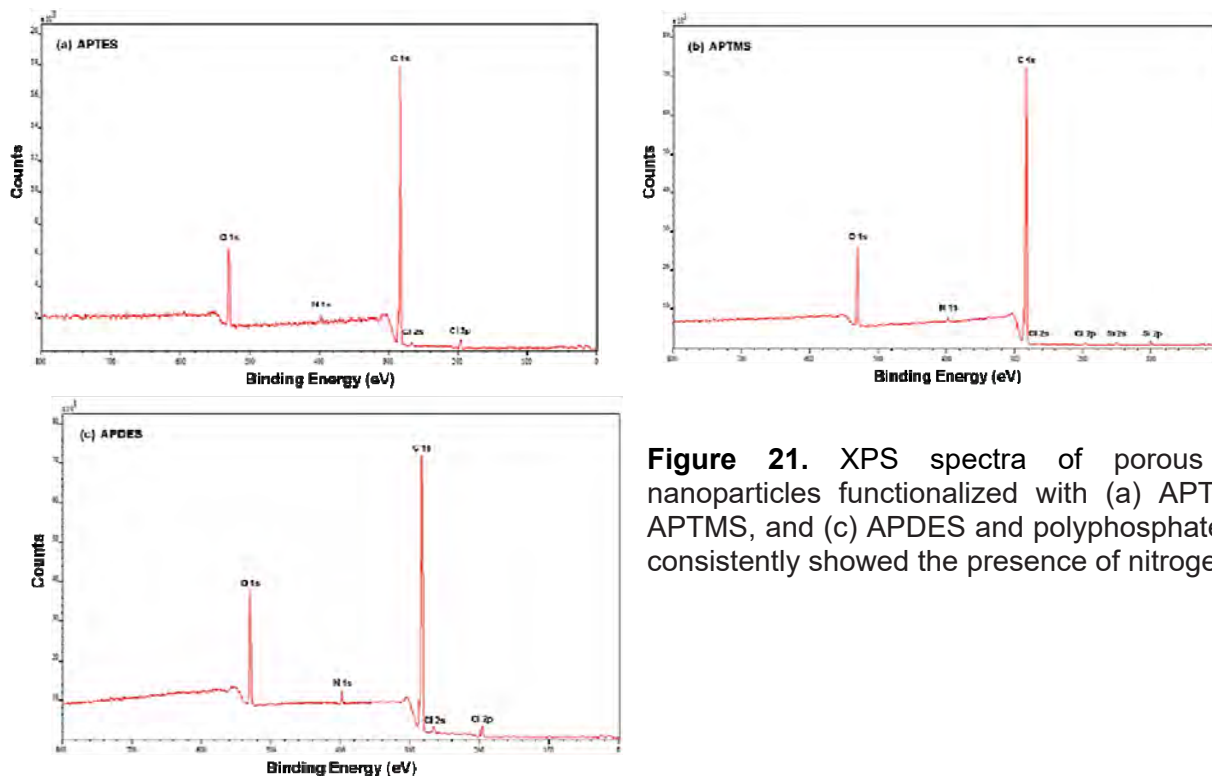


Figure 21. XPS spectra of porous silicon nanoparticles functionalized with (a) APTES, (b) APTMS, and (c) APDES and polyphosphate 70mer consistently showed the presence of nitrogen.

In summary for this portion of the report, the Stucky lab successfully covalently attached molecules, such as APTES, APTMS, and APDES, that allowed for subsequent binding of molecules that enhance blood clotting, such as polyphosphate, to a solid support. In this case, the solid support consisted of porous silicon nanoparticles. Although progress was made into understanding the porous silicon nanoparticle system with regards to the chemistry pertinent to developing a suitable TSP, additional characterization and chemical process refinement are still required.

The Stucky lab efforts to incorporate a clotting triggering/enhancing agent, such as polyphosphate, onto porous silicon nanoparticles looked at encapsulation and surface modification approaches. Encapsulation of polyphosphate required the pores to be large enough for the polyphosphate to enter or the polyphosphate to be small enough to enter the pores. A linear polyphosphate 70mer was calculated to be 24 nm based on bond length. To improve the chances of encapsulation, the Morrissey lab provided us with platelet size polyphosphate that went through a rigorous sizing technique that they developed. To encapsulate and surface modify the porous silicon, 0.33 mg/mL platelet size polyphosphate in water was added to porous silicon nanoparticles and allowed to react overnight at room temperature with gentle agitation.

DLS and ELS measurements of the components of the platelet sized polyphosphate functionalized porous silicon nanoparticles were taken at each step for systematic comparison purposes. Pre-modification with platelet size polyphosphate, the porous silicon nanoparticles were determined to be 142.4 ± 9.144 nm with a Pdl of 0.238, and a zeta potential of -30.2 ± 0.458 mV. The focus of this experiment was on modification of the porous silicon nanoparticles with polyphosphate,

so the size of the nanoparticles was not a concern. The zeta potential was comparable to that of what we saw with silica.

The platelet size polyphosphate was determined to be 112.8 ± 31.57 nm with a Pdl of 0.537, and a zeta potential of -28.1 ± 4.82 mV. As indicated by the Pdl, there was significant size variation with the polyphosphate. The zeta potential was also saw significant fluctuation. In addition, the polyphosphate seemed to be of a lower magnitude than what it should be given that once functionalized onto the porous silicon nanoparticle, the zeta potential had a more negative value. These anomalies may be due to the low concentration (0.33 mg/mL) of the platelet size polyphosphate used in the measurements.

The encapsulated and surface functionalized porous silicon with platelet size polyphosphate was determined by DLS and ELS post wash to be 163.3 ± 2.515 nm with a Pdl of 0.211, and a zeta potential of -45.5 ± 0.954 mV. The size of the final modified porous silicon-polyphosphate nanoparticle system seemed reasonable. The magnitude of the negative zeta potential also seemed aligned with previous studies on silica functionalized polyphosphate. As a system, the porous silicon-polyphosphate nanoparticle showed less polydispersity and a higher zeta potential magnitude, which indicated that the system was more uniform and stable than its components.

SEM and EDS (Figure 22) characterization of platelet size polyphosphate encapsulated and surface modified porous silicon nanoparticle was conducted to compare with the DLS findings. The particle size and morphology remain varied. Depending on the orientation of the particles, pores can be seen from a top down perspective and in parallel to the pore direction. In the pre-wash sample, EDS confirmed the presence of silicon at 73.18% weight, oxygen at 21.62% weight, phosphorus at 5.38% weight, and sodium at 1.62% weight. Sodium is probably due to the preparation process of the polyphosphate. In the post-wash sample, EDS only showed the presence of silicon and oxygen, which indicated the phosphorus signal in the pre-wash sample was due to unbound polyphosphate, or that the bound phosphorus signal was too low for detection.

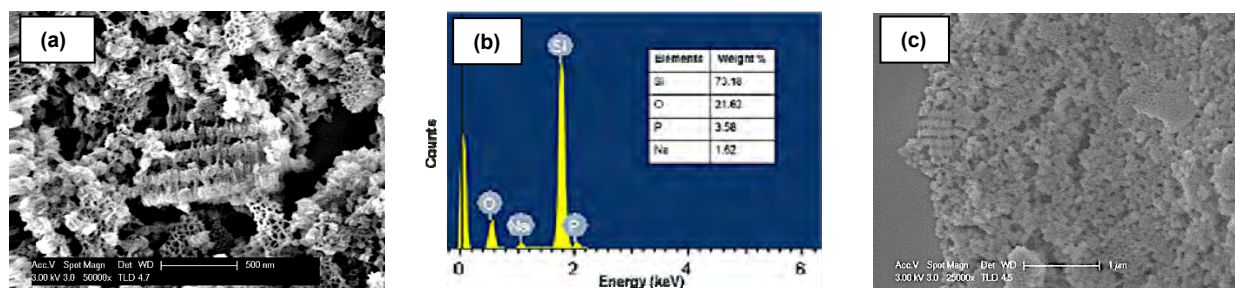


Figure 22. (a) Pre-wash SEM image, (b) pre-wash EDS spectrum, (c) post-wash SEM image of platelet size polyphosphate encapsulated and surface functionalized porous silicon nanoparticle.

The aforementioned characterization techniques do not differentiate between encapsulated polyphosphate and surface modified polyphosphate. Polyphosphate attachment to the porous silicon nanoparticle in this approach was taken as a whole to establish maximum binding capacity. Additional characterization via malachite green and inductively coupled plasma is needed to quantitatively determine the moles of bound polyphosphate via phosphate or phosphorus.

One method to ensure polyphosphate encapsulation was to allow polyphosphate to react with the porous silicon nanoparticles followed by the addition of a divalent cationic solution, such as calcium chloride at acidic pH, to cap the pores. The introduction of the 4 M calcium chloride under moderate agitation at room temperature allowed a network of calcium and silicon to form, thereby forming a cap to contain the polyphosphate. The particles were then washed and characterized. SEM image no longer showed the usual porous silicon morphology and EDS confirmed the presence of Ca and Cl and no Si (Figure 23). The calcium chloride coated the porous silicon nanoparticles. In repeating this experiment, a lower concentration of calcium chloride and additional washing may mitigate the issue.

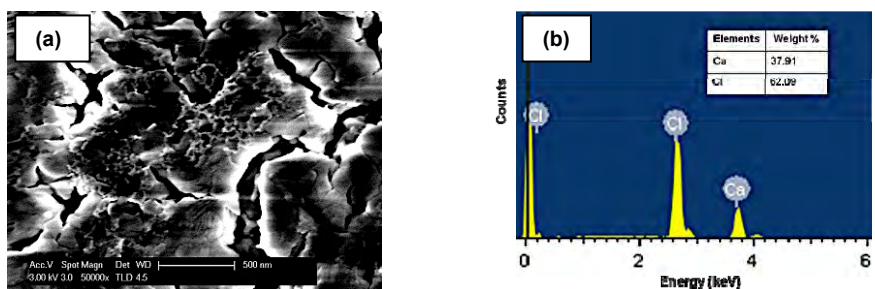


Figure 23. (a) SEM (500 nm scale bar) and (b) EDS characterization of encapsulated platelet size polyphosphate in porous silicon nanoparticle capped with calcium chloride.

Another approach was to focus the study on the use of polyphosphate in the surface modification of the porous silicon nanoparticles by using polyphosphate 200-1300mer. The size of the polyphosphate 200mer should have prevented its entrance into the pores, thereby ensuring any activity with the porous silicon nanoparticle was on the surface. For this experiment, 6.0 mM polyphosphate 200-1300mer in water was added to porous silicon nanoparticles and allowed to react at room temperature under gentle agitation overnight. The porous silicon nanoparticles used were determined by DLS and ELS to be 78.74 ± 1.370 nm with a Pdl of 0.071 and a zeta potential of -8.52 ± 0.777 mV.

DLS and ELS measurements post wash and collection by centrifugation showed that the porous silicon-polyphosphate 200-1300mer system was 72.00 ± 3.864 nm with a Pdl of 0.084 and a zeta potential of -29.8 ± 0.1531 mV. The polyphosphate 200-1300mer functionalized porous silicon nanoparticles were smaller than the bare porous silicon nanoparticles, which was unexpected and may be due to a variation in the refractive index that was not taken into account with the functionalized polyphosphate-porous silicon nanoparticle system. The refractive index used for all porous silicon nanoparticle based samples was porous silicon. Another factor may be that the porous silicon nanoparticles are not uniform, which may affect the scattered light needed for DLS measurements. The change in magnitude of the zeta potential is consistent with previous results.

SEM and EDS (**Figure 24**) characterization of polyphosphate 200-1300mer functionalized porous silicon nanoparticles appear similar to images of unfunctionalized porous silicon nanoparticles. The polyphosphate 200-1300mer did not alter the morphology of the porous silicon nanoparticles based on SEM. EDS spectrum showed only the presence of silicon, which indicated the lack of polyphosphate 200-1300mer presence, or the presence was too low for detection. The latter hypothesis of a presence too low for ELS detection was supported by the zeta potential data.

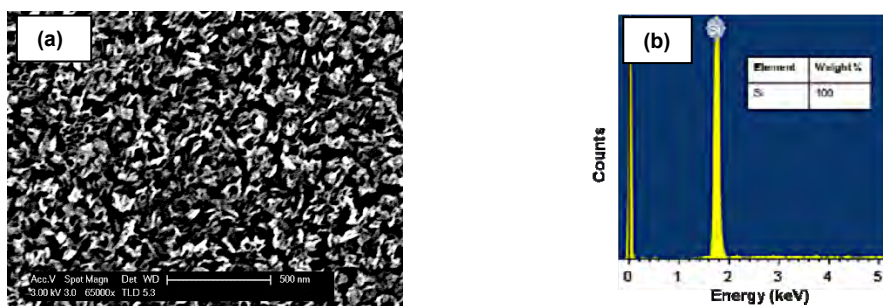


Figure 24. (a) SEM image and (b) EDS spectrum of post-wash polyphosphate 200-1300mer functionalized porous silicon nanoparticles.

In summary for this portion of the report, the Stucky lab attempted and obtained inclusive characterization results on the attachment of molecules that enhance blood clotting, such as polyphosphate, to a solid support consisting of porous silicon nanoparticles via physisorption. Additional chemical process refinement and characterization efforts are required to determine the best

approach to attaching polyphosphate to porous silicon nanoparticles as part of the effort in developing a suitable TSP candidate.

Using a thromboelastograph (TEG), the Stucky lab compared the procoagulant activity of porous silicon nanoparticles to previously characterized and published results by the group and collaborators on silica nanoparticles and silica nanoparticles functionalized with polyphosphate 70mer as a function of concentration (**Figure 25**).¹⁰ Initial studies indicated that porous silicon nanoparticles performed better to slightly better than silica nanoparticles in reducing clot time. However, porous silicon nanoparticles took longer to clot than silica nanoparticles functionalized with polyphosphate 70mer. Procoagulant studies were conducted under the same conditions, which consisted of the use of pooled normal plasma at 37°C with the nanoparticles dispersed in phospholipid.

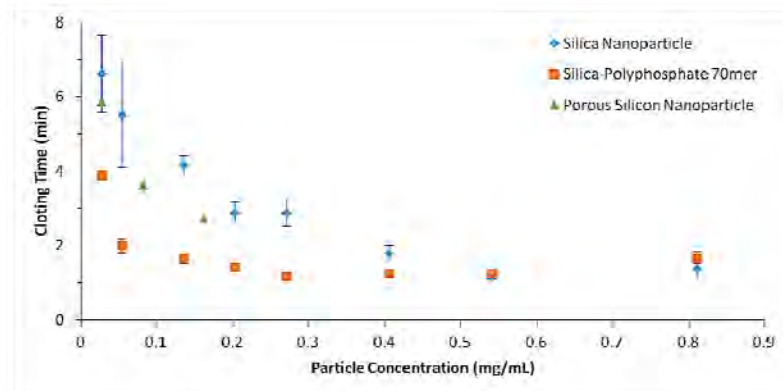


Figure 25. TEG data comparing clotting time as a function of concentration for porous silicon nanoparticles compared to silica nanoparticles and silica nanoparticles functionalized with polyphosphate 70mer. Porous silicon nanoparticles clotted faster than silica nanoparticles, but not as fast as silica nanoparticles functionalized with polyphosphate 70mer.

Also during Q1 2015, the Stucky lab conducted assays to compare the effectiveness of the polyphosphate (polyp)-silica nanoparticle (SNP) (polyp-SNP) as a therapeutic to that of FVIIa. Recombinant factor VIIa (rFVIIa, Novoseven) is currently used by the military as an intravenous hemostat. rFVIIa promotes hemostasis through its activation of the extrinsic coagulation pathway. However, the excessive cost and safety questions in using these biological agents are major concerns that often limit their use until late stage blood loss in trauma patients.¹¹ Despite anecdotal successes, multiple studies showed that the use of rFVIIa does not significantly improve outcomes in bleeding patients and may result in thrombotic complications.¹²⁻¹⁵ As a result, rFVIIa has fallen out of favor in the trauma community in favor of other agents including prothrombin complex concentrates and antifibrinolytics. However, these treatments still retain drawbacks. For our studies, a supratherapeutic dose (270 ug/ml) of FVIIa was chosen as the current therapeutic baseline (**Figures 26-28**).

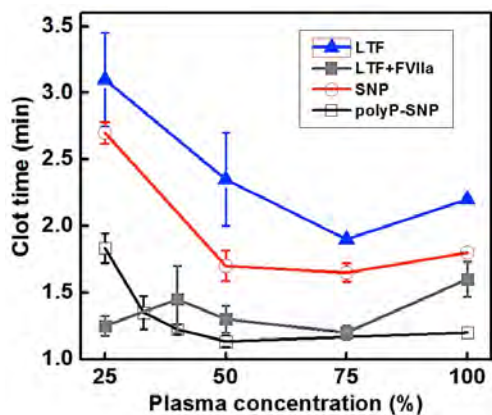


Figure 26. PolyP-SNP outperformed supratherapeutic levels of FVIIa except at 25 % (75 % saline).

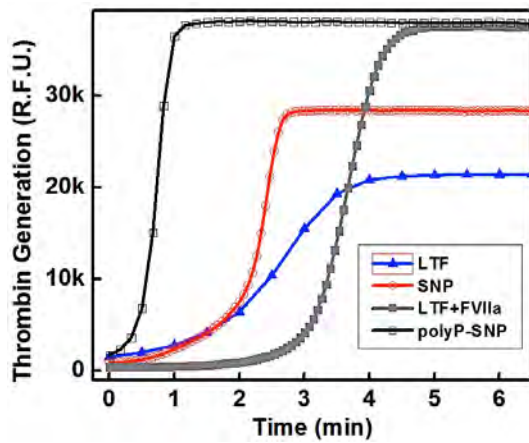


Figure 27. At 50 % hemodilution, polyP-SNP generates thrombin much faster when compared to FVIIa, bare SNPs and lipidated tissue factor (LTF).

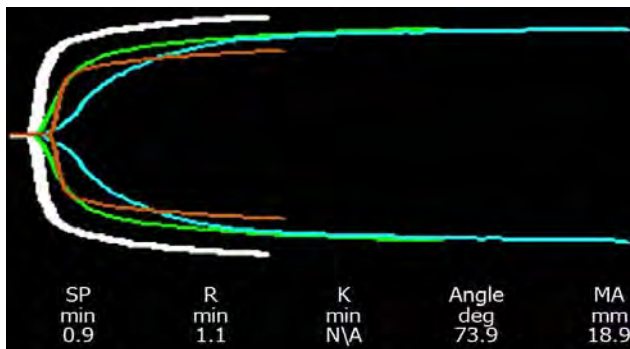


Figure 28. TEG curves comparing polyP-SNP (white), FVIIa (green), bare SNP (brown), and LTF (teal) at 50 % plasma.

Using TEG, we were able to compare FVIIa and polyP-SNP at both hemodilute and hypothermic conditions. For all data points except 25 % plasma, polyP-SNP outperformed the protein FVIIa. Thrombin generation assays also confirmed that polyP-SNP produces thrombin faster than FVIIa even under suboptimal conditions. In addition to clot time, polyP-SNP also produced the optimal or similar rate of clot formation (α) and overall clot size (MA) when compared with FVIIa, bare SNP, and LTF as measured by TEG. Given polyP-SNP's long-term stability and clotting accelerant nature, the *in vitro* data suggests that polyP-SNP may be a superior pre-hospital intravenous treatment than protein-based therapeutics such as FVIIa (**Figures 29-31**).

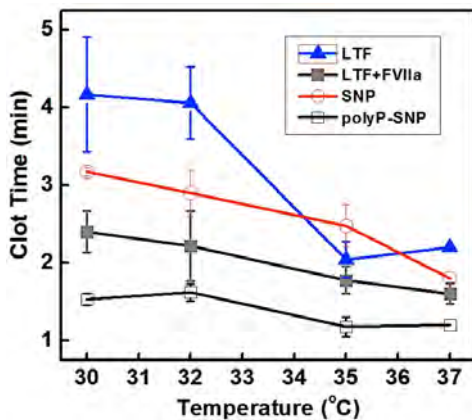


Figure 29. PolyP-SNP outperformed supratherapeutic levels of FVIIa at all normal and hypothermic temperatures.

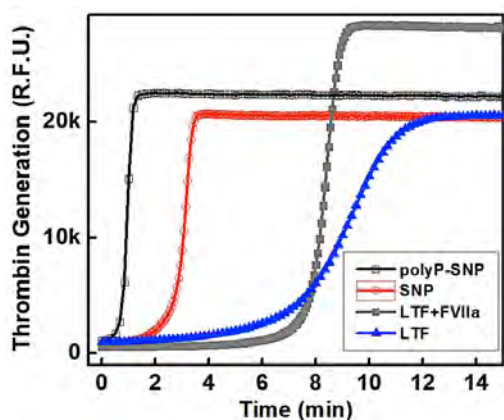


Figure 30. At 32°C, polyP-SNP generates thrombin quicker than FVIIa, bare SNP, or LTF.

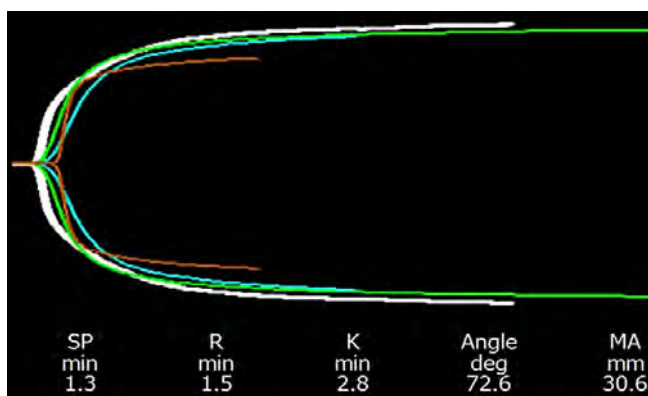


Figure 31. TEG curves comparing polyP-SNP (white), FVIIa (green), bare SNP (brown), and LTF (teal) at 32°C.

In summary for this portion of the report, the Stucky lab conducted initial quantification of the procoagulant activity of porous silicon nanoparticles. The initial results are promising and indicate that porous silicon nanoparticles may be suitable as a solid support for our TSP. Further procoagulant studies are needed for polyphosphate functionalized porous silicon nanoparticles. In addition, we looked at polyP-SNP's clotting ability under hypothermic and hemodilute conditions. In comparison with supratherapeutic levels of the currently in use intravenous hemostat FVIIa, polyP-SNP accelerated clot formation in all hypothermic studies as well all hemodilute plasma samples, except 25 % plasma (75% saline). PolyP-SNP's ability to accelerate clot formation is likely due to its ability to generate the thrombin burst quicker than FVIIa under the same conditions

The Morrissey lab has worked on improved coupling chemistries for fabricating polyP-bearing nanoparticles. This has included defining the optimal pH for phosphoramidate- versus phosphoester-based linkages, as well as a detailed investigation of the optimal times and temperatures for the coupling reactions. An important corollary to these studies is optimizing the stability of the resulting polyphosphate-linked organic molecules. The Morrissey lab has continued to define the effects of pH and divalent metal ions on the stabilities of polyphosphate-coupled compounds. Using amine- versus hydroxyl-containing PEG-biotin as the model compound, we have been able to enhance the efficiency of the coupling chemistry and continue to work toward further enhancement of the extent of derivatization of polyphosphate. We also extended these studies to coupling a variety of short, amine-containing synthetic peptides with a variety of functional groups attached to them, including biotin and free sulfhydryls. Additionally, we were able to couple peptides to the terminal phosphates of polyP that contained reactive groups compatible with click chemistry (alkynes or azides). We are currently preparing a manuscript for submission to *Biomacromolecules* based on these studies.

Task 4 — Design and utilize microfluidic devices that reproduce shear flow and surface chemistries relevant to internal hemorrhage.

Progress and completion of Milestone 4 by the Ismagilov lab and Kastrup lab was summarized in the December 2014 annual report. A manuscript describing this work has been submitted for publication to *Thrombosis and Haemostasis*, entitled “Localization of short-chain polyphosphate enhances its ability to clot flowing blood plasma,” by Ju Hun Yeon, Nima Mazinani, Travis S. Schlappi, Karen Y. T. Chan, James R. Baylis, Stephanie A. Smith, Alexander J. Donovan, Damien Kudela, Galen D. Stucky, Ying Liu, James H. Morrissey, Rustem F. Ismagilov, and Christian J. Kastrup.

4. KEY RESEARCH ACCOMPLISHMENTS

Numerical simulations

- Numerical simulations were completed that reflect the activity of polyP on clotting.
- Simulations successfully predicted that the localization of polyP increases its coagulability, including when blood is flowing.

Raw materials for conjugation to nanoparticles:

- Synthesized and characterized silica and iron oxide nanoparticles as a carrier for polyP.

Coupling chemistries for conjugation of polyP to nanoparticles:

- Applied both adsorbed and covalently bound polyP techniques to silica.
- For covalently bound polyP to silica, used APTMS or APTES to form the amide bond followed by EDAC cross-linker.
- An alternative to EDAC as a cross-linker for covalent binding of polyP to silica was through the use of NHS-OPSS.
- We increased the scope of EDAC-mediated coupling chemistry by coupling a variety of peptides (each with different functional groups) onto the terminal phosphates.
- Esterification was used to couple polyP to silica and iron oxide particles.
- Iron oxide-polyP conjugates were prepared using Lewis acid chemistry.

Microfluidics:

- Devices were used to measure clot times simultaneously at various shear rates.
- Found that polyP with chain-lengths similar to platelet polyP can initiate clotting when surface-localized far more efficiently than when present in bulk solution.

PolyP-based procoagulant nanoparticles:

- Reported that size-controlled nanoprecipitation of polyP in aqueous solutions containing biologically relevant concentrations of divalent metal cations (e.g. Ca^{2+} , Mg^{2+} , Zn^{2+} etc.)
- Reported Artificial Dense Granules as a drug delivery system (DDS) for treating incompressible hemorrhage
- Reported that particles of polyP initiate clotting faster than solubilized macromers of polyP.
- Found that polyP nanoparticles initiate clotting in a shear-dependent manner, where they clot plasma at the low shear rates typical of blood that is pooling in wounds.

5. CONCLUSION

This past year, we made completed a series of studies, described in detail in the December 2014 annual report, involving synthesizing, characterizing, and understanding the properties of iron oxide, silica, and iron oxide core-silica shell nanoparticles with respect to the blood clotting process. We also further expanded the coupling chemistries available for covalently linking various functional groups to the terminal phosphates of polyP, including ester-bonded compounds as well as phosphoramidate-linked peptides containing a variety of exploitable functional groups. These studies have now further expanded the repertoire of techniques for fabricating pro-hemostatic nanoparticles of varying compositions and properties.

We also were able to create "Artificial Dense Granules" via the size-controlled synthesis of monodisperse polyP NPs at physiological concentrations of calcium and magnesium, and reported this in a publication. We found that the solubility is related nonlinearly to the polymer length, with very long-chain polyP precipitating much more facilely than platelet-sized polyP.

Our studies of "Artificial Dense Granules", gold nanoparticles, and nanoparticles based on silica, iron oxide, and iron oxide core-silica functionalized with polyP have now matured to the point that we are ready to test their hemostatic function in a hemostasis model (mouse tail bleeding model), as soon as regulatory approval is obtained.

The goal is to test if our polyP-functionalized NPs can serve as a foundation for the future development of targeted procoagulant nanotechnologies to control internal hemorrhage.

6. PUBLICATIONS, ABSTRACTS, AND PRESENTATIONS (from project inception to date)

Published and In Press in peer-reviewed scientific journals:

- (1) Hebbard CF, Wang Y, Baker CJ, and Morrissey JH. Synthesis and evaluation of chromogenic and fluorogenic substrates for high-throughput detection of enzymes that hydrolyze inorganic polyphosphate. *Biomacromolecules*. **2014**, 15(8):3190-3196. DOI: 10.1021/bm500872g
- (2) Donovan AJ, Kalkowski J, Smith SA, Morrissey JH, and Liu Y. Size-controlled synthesis of granular polyphosphate nanoparticles at physiologic salt concentrations for blood clotting. *Biomacromolecules*. **2014**, 15(11): 3976-3984. DOI: 10.1021/bm501046t
- (3) Kudela D, Smith SA, May-Masnou A, Braun GB, Pallaoro A, Nguyen CK, Chuong TT, Nownes S, Allen R, Parker NR, Rashidi HH, Morrissey JH, and Stucky GD. Clotting activity of polyphosphate functionalized silica nanoparticles. *Angew Chem Int Ed Engl*. **2015**, 54(13): 4018-4022. DOI: 10.1002/anie.201409639
- (4) Szymusiak M, Donovan AJ, Smith SA, Ransom R, Shen H, Kalkowski J, Morrissey JH, Liu Y. colloidal confinement of polyphosphate on gold nanoparticles robustly activates the contact pathway of blood coagulation. *Bioconjug Chem*, In Press.

Conference Presentations:

- (1) A.J. Donovan, J. Kalkowski, S.A. Smith, J.H. Morrissey, and Y. Liu. "Size-controlled synthesis of granular polyphosphate nanoparticles at physiologic salt concentrations for blood clotting." 15th Annual Midwest Platelet Conference, 8-10th October 2014.
- (2) Damien Kudela, Stephanie A. Smith, Ju Hun Yeon, Anna May-Masnou, Gary B. Braun, Alessia Pallaoro, Tracy Chuong, James R. Baylis, Christian J. Kastrup, James H. Morrissey and Galen D. Stucky. "Treating non-compressible hemorrhage with functionalized nanoparticles," Military Health System Research Symposium (MHSRS), Orlando, Florida, 2014.
- (3) Damien Kudela, Stephanie A. Smith, Ju Hun Yeon, Anna May-Masnou, Gary B. Braun, Alessia Pallaoro, Tracy Chuong, James R. Baylis, Christian J. Kastrup, James H. Morrissey and Galen D. Stucky. "Treating non-compressible hemorrhage with functionalized nanoparticles," Nanotech, Washington, D.C., 2014.

7. INVENTIONS, PATENTS AND LICENSES

Issued United States Patents:

Damien Kudela, Galen D. Stucky, Anna May-Masnou, Gary B. Braun, James H. Morrissey, Stephanie A. Smith. "Polyphosphate-Functionalized Inorganic Nanoparticles as Hemostatic Compositions and Methods of Use." U. S. Patent number 9,186,417 (issued November 17, 2015).

Patent (PCT) Applications:

Y. Liu and A.J.Donovan. "Artificial Platelets for Treatment of Catastrophic Bleeding." PCT/US2015/051814, filed 24 September 2015.

8. REPORTABLE OUTCOMES

This research has led to the development of a company, Cayuga Biotech, which seeks to commercialize treatments for hemorrhage.

9. OTHER ACHIEVEMENTS

None (the above categories list our progress and outcomes appropriately).

10. REFERENCES

- [1] Smith SA, Mutch NJ, Baskar D, Rohloff P, Docampo R, Morrissey JH. Polyphosphate modulates blood coagulation and fibrinolysis. *Proc Natl Acad Sci U S A*. 2006;103:903-8.
- [2] Morrissey JH, Choi SH, Smith SA. Polyphosphate: an ancient molecule that links platelets, coagulation, and inflammation. *Blood*. 2012;119:5972-9.
- [3] Muller F, Mutch NJ, Schenk WA, Smith SA, Esterl L, Spronk HM, et al. Platelet Polyphosphates Are Proinflammatory and Procoagulant Mediators In Vivo. *Cell*. 2009;139:1143-56.
- [4] Shoffstall AJ, Atkins KT, Groynom RE, Varley ME, Everhart LM, Lashof-Sullivan MM, et al. Intravenous hemostatic nanoparticles increase survival following blunt trauma injury. *Biomacromolecules*. 2012;13:3850-7.

11. APPENDIX

PDF "reprints" of the following 4 papers resulting from this project are attached as an appendix:

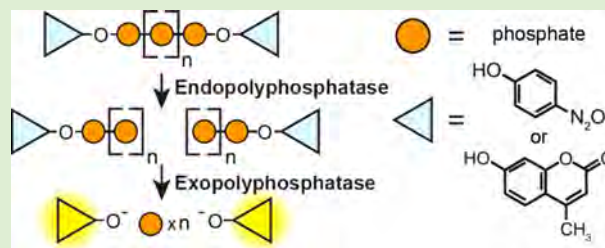
- (1) Hebbard CF, Wang Y, Baker CJ, and Morrissey JH. Synthesis and evaluation of chromogenic and fluorogenic substrates for high-throughput detection of enzymes that hydrolyze inorganic polyphosphate. *Biomacromolecules*. **2014**, 15(8):3190-3196. DOI: 10.1021/bm500872g
- (2) Donovan AJ, Kalkowski J, Smith SA, Morrissey JH, and Liu Y. Size-controlled synthesis of granular polyphosphate nanoparticles at physiologic salt concentrations for blood clotting. *Biomacromolecules*. **2014**, 15(11): 3976-3984. DOI: 10.1021/bm501046t
- (3) Kudela D, Smith SA, May-Masnou A, Braun GB, Pallaoro A, Nguyen CK, Chuong TT, Nownes S, Allen R, Parker NR, Rashidi HH, Morrissey JH, and Stucky GD. Clotting activity of polyphosphate functionalized silica nanoparticles. *Angew Chem Int Ed Engl*. **2015**, 54(13): 4018-4022. DOI: 10.1002/anie.201409639
- (4) Szymusiak M, Donovan AJ, Smith SA, Ransom R, Shen H, Kalkowski J, Morrissey JH, Liu Y. colloidal confinement of polyphosphate on gold nanoparticles robustly activates the contact pathway of blood coagulation. *Bioconjug Chem*, In Press.

Synthesis and Evaluation of Chromogenic and Fluorogenic Substrates for High-Throughput Detection of Enzymes That Hydrolyze Inorganic Polyphosphate

Carleigh F. F. Hebbard,^{†,§} Yan Wang,[†] Catherine J. Baker,[†] and James H. Morrissey^{*,†}

[†]Department of Biochemistry and [§]College of Medicine, University of Illinois at Urbana–Champaign, Urbana, Illinois 61801, United States

ABSTRACT: Inorganic polyphosphates, linear polymers of orthophosphate, occur naturally throughout biology and have many industrial applications. Their biodegradable nature makes them attractive for a multitude of uses, and it would be important to understand how polyphosphates are turned over enzymatically. Studies of inorganic polyphosphatases are, however, hampered by the lack of high-throughput methods for detecting and quantifying rates of polyphosphate degradation. We now report chromogenic and fluorogenic polyphosphate substrates that permit spectrophotometric monitoring of polyphosphate hydrolysis and allow for high-throughput analyses of both endopolyphosphatase and exopolyphosphatase activities, depending on assay configuration. These substrates contain 4-nitrophenol or 4-methylumbelliferone moieties that are covalently attached to the terminal phosphates of polyphosphate via phosphoester linkages formed during reactions mediated by EDAC (1-ethyl-3-(3-(dimethylamino)propyl)carbodiimide). This report identifies Nudt2 as an inorganic polyphosphatase and also adds to the known coupling chemistry for polyphosphates, permitting facile covalent linkage of alcohols with the terminal phosphates of inorganic polyphosphate.



INTRODUCTION

Inorganic polyphosphates (polyP) are linear polymers of orthophosphate joined by high-energy phosphoanhydride bonds and can range in length from tens to thousands of phosphates. PolyP is widespread throughout biology and implicated in a multitude of physiologic processes in organisms from bacteria to man,^{1–4} although many of its biological functions likely remain to be discovered and characterized. PolyP is also an industrial chemical with applications in areas such as water treatment, food processing, fertilizers, and flame retardants.³ The biodegradable and versatile nature of polyP makes it an attractive material with many uses, and it would be desirable to understand how polyP is turned over. Known polyP-digesting enzymes include exopolyphosphatases which sequentially remove terminal phosphates from polyP, and endopolyphosphatases which hydrolyze internal phosphoanhydride bonds.¹ Although some of the enzymes responsible for degrading polyP have been identified in unicellular organisms, they remain relatively poorly studied in higher eukaryotes, with a few notable exceptions.^{1,5} Two examples are mammalian alkaline phosphatase,⁶ a highly potent exopolyphosphatase, and the human protein, h-prune, a short-chain exopolyphosphatase implicated as a regulator of metastasis.⁷ Recent work has shown that polyP is secreted from activated human platelets⁸ and mast cells⁹ and that it is an important regulator of blood clotting⁴ and complement.¹⁰ PolyP is degraded in human plasma with a half-life of about 90 min,¹¹ which is no doubt important in

controlling polyP's biological action, yet the mechanism of its degradation *in vivo* is currently unknown.

An impediment to identifying and studying the properties of polyP-degrading enzymes is the dearth of high-throughput means for detecting inorganic polyphosphatases and quantifying their activities. Many of the existing methods for quantifying enzymatic polyP degradation are cumbersome, of low sensitivity, or require the use of specialized equipment. The methods also typically rely on multiple steps including chromatography, gel electrophoresis, laborious physical extraction protocols coupled with chemical detection of liberated inorganic orthophosphate, or the use of radiolabeled polyP.¹ On the other hand, recently reported, more facile methods for detecting exopolyphosphatase activity include the continuous recording of released inorganic monophosphate, which was successfully employed to determine the kinetic parameters of the exopolyphosphatase, h-prune.⁷ Detecting and quantifying the action of endopolyphosphatases remains substantially more time-consuming, however, as it typically involves resolving the digested polyP products using gel electrophoresis.¹² We therefore sought to develop chromogenic and fluorogenic polyP substrates that would allow polyP degradation to be followed spectrophotometrically and, in particular, a method that would allow high-throughput detection of endopolyphos-

Received: June 13, 2014

Revised: July 2, 2014

Published: July 7, 2014

phatase activity. Ideally, we would covalently attach chromogenic or fluorogenic dyes to the terminal phosphates of polyP. Chromogenic and fluorogenic substrates are available for a number of hydrolases and are readily adaptable to high-throughput assays in multiwell formats. We previously showed that primary amines can be covalently coupled via phosphoramidate linkages to the terminal phosphates of polyP in a reaction promoted by the zero-length cross-linking reagent, 1-ethyl-3-(3-(dimethylamino)propyl)carbodiimide (EDAC).¹³ In the present study, we now show that EDAC can also be used to promote the efficient formation of phosphoester linkages with the terminal phosphates of polyP, and we apply this chemistry to create chromogenic or fluorogenic polyphosphatase substrates in which polyP is end-labeled with either 4-nitrophenol (NOL) or 4-methylumbelliferone (MU). We also show that these polyP derivatives can be used to detect the action of endo- and exopolyphosphatases, depending on assay configuration.

■ EXPERIMENTAL SECTION

Materials. Specified reagents were purchased from Sigma-Aldrich (St. Louis, MO) unless otherwise noted. NOL was recrystallized using hot water and ethanol. All experiments in this report used a polyP preparation (Natriumpolyphosphat P70) that was a kind gift from BK Giulini GmbH (Ludwigshafen, Germany). The polymer lengths of this preparation ranged from about 20 to 100 phosphates, with a mean length of approximately 45 to 50. PolyP concentrations were quantified using malachite green after acid hydrolysis¹⁴ and are reported here in terms of phosphate monomer (monomer formula: NaPO_3). PolyP was end-labeled with spermidine via phosphoramidate linkages as described.¹³

Methods. EDAC-Mediated End-Labeling of PolyP by Esterification with Methanol. A mixture of 5.9 mM polyP, 150 mM freshly dissolved EDAC, and 6.4 M methanol in 100 mM MES buffer pH 6.5 was incubated for either 5 h at 37 °C or 1 h at 65 °C, after which the reaction mixtures were cooled on ice. Reaction volumes varied from 0.35 to 6.5 mL. PolyP-methanol was purified by acetone precipitation; briefly, NaCl was added to the reaction mixture (to 535 mM) followed by two reaction volumes of acetone, with mixing after each addition. The mixture was then centrifuged at $11,000 \times g$ for 7 min at room temperature, after which the supernatant was discarded. The polyP pellet was washed twice by adding acetone to the tube followed by centrifugation. Pellets were then dried and redissolved in water.

Prior to NMR analyses, polyP-methanol was further purified by adsorption to a suspension of silica particles ("glass milk"). Glass milk was produced by a modification of the method of Vogelstein and Gillespie,¹⁵ in which 250 mL silica (325 mesh) was stirred in 400 mL water for 1 h, then allowed to settle for 1 h to remove large particles. The supernatant was then centrifuged for $4000 \times g$ for 15 min after which the pellet was collected and resuspended in 200 mL 50% nitric acid. This was then stirred and heated to close to boiling, after which it was cooled to room temperature. The silica fines were then collected by centrifugation and washed five times with water by resuspension and centrifugation. The final pellet of washed silica fines was resuspended as a 50% slurry by volume (glass milk). PolyP was purified by binding to, and elution from, glass milk as described,¹⁴ except that the solutions were kept chilled throughout, and the polyP was eluted with 95 °C water instead of buffer.

EDAC-Mediated End-Labeling of PolyP by Esterification with NOL. A mixture of 5.9 mM polyP, 150 mM freshly dissolved EDAC, and 200 to 525 mM NOL was incubated for 1 h at 65 °C. Reaction volumes varied from 0.35 to 40 mL, and mixtures were agitated throughout, since the NOL concentrations exceeded solubility limits even in hot water. Completed reactions were cooled on ice and polyP was isolated by acetone precipitation. Because some free NOL coprecipitated with polyP in the first acetone precipitation, three full cycles of acetone precipitation were employed in which the collected polyP pellets were completely resuspended in water and reprecipitated

by addition of NaCl and acetone followed by centrifugation. PolyP-NOL was then further purified using Bio-Gel P-6 desalting columns (Bio-Rad; Hercules, CA). The polyP-containing column fractions were identified by toluidine blue staining,¹⁶ pooled, and lyophilized.

EDAC-Mediated End-Labeling of PolyP by Esterification with MU. A mixture of 5.5 mM polyP, 150 mM freshly dissolved EDAC, and 280 mM MU in a reaction volume of 1 mL was incubated for 1 h at 65 °C with agitation because the concentrations of MU used exceeded solubility limits. The reactions were then cooled on ice and polyP-MU was isolated using acetone precipitation as described above for the preparation of polyP-NOL.

NMR Analyses. Purified polyP and polyP derivatives were dissolved in water containing 10% (v/v) D_2O . All solution NMR spectra were collected on a Varian Unity INOVA 600 MHz proton frequency spectrometer with a 5 mm Varian AutoTuneX 1H/X PFG Z probe at 23 °C. 1D ^{31}P and ^{13}C spectra were acquired with a 2 s recycle delay. 1D ^1H spectra were acquired with a 1 s recycle delay, and solvent suppression was done by presaturation. 2D ^1H – ^{13}C Heteronuclear Single Quantum Coherence (HSQC) spectra were acquired with 2048 and 160 points in the ^1H and ^{13}C dimensions, respectively. ^1H and ^{13}C spectra were referenced with external tetramethylsilane at 0 ppm, and ^{31}P spectra were referenced with external phosphoric acid at 0 ppm. 1D spectra were processed with MNOVA (Mestrelab Research), and 2D spectra with NMRPipe.¹⁷ polyP: ^{31}P NMR (90% H_2O 10% D_2O , 243 MHz) δ : -7.01 (s), -21.14 , -21.65 . polyP-methanol: ^{31}P NMR (90% H_2O 10% D_2O , 243 MHz) δ : -9.36 (d, $J_{\text{P,P}} = 17.8$ Hz), -21.67 . ^1H NMR (90% H_2O 10% D_2O , 600 MHz) δ : 3.51 (d, $J_{\text{H,P}} = 11.42$ Hz). ^{13}C NMR (90% H_2O 10% D_2O , 151 MHz) δ : 53.7. polyP-NOL: ^{31}P NMR (90% H_2O 10% D_2O , 243 MHz) δ : -10.43 , -16.81 (d, $J_{\text{P,P}} = 17.7$ Hz), -21.43 , -21.61 .

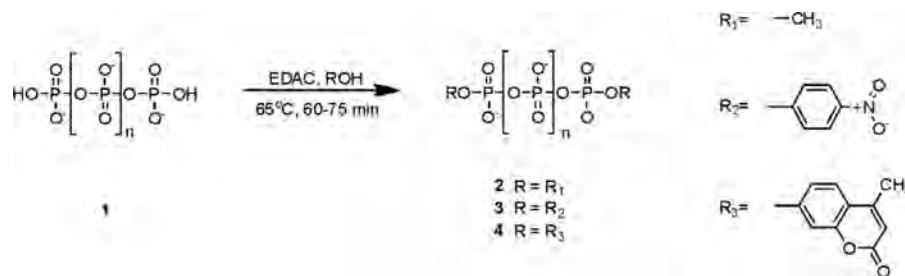
Gel Electrophoresis of PolyP. PolyP preparations were resolved on urea-containing 15% polyacrylamide gels and visualized using DAPI negative staining as described.¹⁸

Alkaline Phosphatase Digestion of PolyP. Protection against exopolyphosphatase-mediated degradation was employed to determine the extent to which polyP molecules were doubly end-labeled, as previously described.¹³ Such digestions used calf intestinal alkaline phosphatase (CIAP, Promega; Madison, WI), a highly active exopolyphosphatase.⁶ Typical reactions included 250 μM polyP and 20 units/mL CIAP; the liberated monophosphate was quantified using malachite green analysis.¹⁴

PolyP-NOL preparations often varied in the extent to which both ends of polyP were derivatized. To rid these preparations of singly labeled polyP, some were digested to completion with recombinant shrimp alkaline phosphatase (SAP, New England BioLabs; Ipswich, MA) by incubating 50 mM derivatized polyP with 50 U/mL SAP for 2 h at 37 °C in the manufacturer's buffer. SAP then was inactivated by heating at 65 °C (7 min), after which the remaining polyP was reupurified by acetone precipitation. These preparations were termed SAP-treated polyP-NOL.

Endopolyphosphatase Digestion of PolyP. Certain nudix hydrolases were examined for endopolyphosphatase activity, typically in a two-stage assay. In the first stage, polyP-MU or SAP-treated polyP-NOL was incubated with endoacting enzyme (Nudt2 or Nudt3, Fitzgerald Industries International; Acton, MA) in the appropriate buffer at 37 °C, after which the reactions were chilled on ice. Buffer conditions were the following: for Nudt2, 8 mM SAP-treated polyP-NOL or 2 mM polyP-MU, 50 mM HEPES pH 7.4, and 5 mM MgCl_2 ; for Nudt3: 5.5 mM SAP-treated polyP-NOL or 2 mM polyP-MU, 25 mM HEPES pH 7.4, 20 mM NaCl, 10 mM MgCl_2 , and 1 mM dithiothreitol.

For the second stage, a solution of CIAP in 100 mM Tris-HCl pH 8.8, 0.2 mM ZnCl_2 was prepared and warmed to 37 °C in 96-well polystyrene plates (Corning; Tewksbury, MA). The second stage was initiated by pipetting 100 μL of the chilled nudix-polyP reaction into prewarmed wells containing 100 μL CIAP solution, after which the rate of dye release was monitored spectrophotometrically at 37 °C. For polyP-NOL substrate, absorbance at 400 nm was measured using a SpectraMax M2 microplate reader (Molecular Devices; Sunnyvale, CA); for polyP-MU substrate, fluorescence was quantified in

Scheme 1. EDAC-Mediated Esterification of the Terminal Phosphates of PolyP^a

^aCompounds: 1, polyP; 2, polyP-methanol; 3, polyP-NOL; 4, polyP-MU.

fluorescence mode using excitation at 360 nm, emission at 450 nm, and a 435 nm cutoff filter.

RESULTS

EDAC-Mediated Esterification of the Terminal Phosphates of PolyP with Methanol. EDAC has been used to promote the formation of ester linkages between alcohols and carboxylates,¹⁹ as well as phosphoester linkages between alcohols and certain organic phosphates.²⁰ We therefore examined whether EDAC could promote the formation of ester linkages between alcohols and the terminal phosphate groups of inorganic polyP (Scheme 1).

As proof of principle, and to identify reaction conditions more readily, we examined EDAC-mediated esterification of polyP with methanol. The reaction resulted in a product that was protected from exopolyphosphatase (CIAP) digestion to an extent comparable to polyP that had been end-labeled with spermidine via phosphoramidate linkages (Table 1).

Table 1. Resistance of PolyP Derivatives to Hydrolysis by Alkaline Phosphatase (CIAP)

reactant	end label	% hydrolysis		
(none)	—	96.0	±	16.7
spermidine	NH ₂ (CH ₂) ₃ NH(CH ₂) ₄ NH—	20.8	±	2.1
methanol	H ₃ CO—	19.8	±	2.0
NOL	O ₂ NC ₆ H ₄ O—	27.0	±	2.0
MU	C ₁₀ H ₇ O ₃ —	3.9	±	1.6

We used solution-state NMR to further verify the product's identity. In the ³¹P spectra, unmodified polyP displayed a relatively broad alpha (terminal) phosphorus peak at about 7 ppm (Figure 1A); the broadness likely reflects exchange of protonation states of the phosphate group.

Methylated polyP displayed an alpha peak shifted to 9.4 ppm (Figure 1B), which was also much sharper than the alpha peak of underivatized polyP. The methylated polyP alpha peak sharpness likely is caused by attenuation of the exchange broadening. This shifted alpha peak displayed as a doublet (Figure 1C) owing to the ³¹P–³¹P J-coupling between the alpha- and beta-phosphorus atoms. We next utilized the ³J_{H–P} coupling between the methyl protons and alpha-phosphorus atom to confirm end modification and map connectivity. When proton decoupling was turned off, each peak of the alpha phosphorus doublet signal was split into a quartet pattern (Figure 1D), indicating the presence of three neighboring protons. To assign the chemical shift of the methyl protons, we acquired a 1D ¹H spectrum with heteronuclear decoupling irradiation at the alpha phosphorus frequency. The resulting spectrum, when compared to the spectrum without decoupling

(compare Figure 1E and F), shows that the peak at around 3.5 ppm is converted from a doublet to a singlet. This transformation is consistent with a proton signal being coupled to a single neighboring phosphorus atom. To identify the carbon signal of the methyl group, we used ¹³C-enriched (20%) methanol to synthesize methylated polyP. The resulting 1D ¹³C spectrum (Figure 1H) shows significant enhancement of the carbon peak at ~53.6 ppm, which was almost unobservable in natural abundance methyl-polyP preparation (Figure 1G). To confirm that coupling existed between the carbon peak and the previously identified methyl proton signal, we performed 2D ¹H–¹³C HSQC on the ¹³C-enriched sample, with clearly observable correlation between the two signals (Figure 1I).

PolyP End-Labeled with NOL or MU. NOL is used often in making chromogenic substrates, as its absorption spectrum shifts dramatically when ester-linked to carboxylates or a single phosphate. MU is also extensively employed in synthesizing fluorogenic substrates because its fluorescence is quenched when ester-linked to carboxylates. Reacting polyP with NOL and EDAC resulted in a polyP preparation that was nearly as resistant to CIAP digestion as was polyP end-labeled with spermidine or methanol (Table 1). Reacting polyP with MU and EDAC resulted in a product with even greater CIAP resistance (Table 1) than that of polyP derivatized with spermidine or methanol. Absorption spectra of polyP-NOL before and after hydrolysis reveal an absorption maximum of 285 nm before hydrolysis (indicating covalent coupling of the NOL dye to phosphate) and 398 nm after hydrolysis (characteristic of free NOL; Figure 2C).

Analyzing polyP-NOL by 1D ³¹P NMR produced an alpha peak shifted from ~7 ppm in underivatized polyP (Figure 1A) to a doublet at ~17 ppm in polyP-NOL (Figure 3A), consistent with covalent modification of the terminal phosphates. Resolving polyP and polyP-NOL by gel electrophoresis indicated little change in the distribution of polymer lengths after reacting the polyP with NOL and EDAC (Figure 3B).

Exopolyphosphatase (CIAP) Digestion of PolyP-NOL. End-labeling efficiency was calculated after complete acid hydrolysis of polyP-NOL and quantification and comparison of liberated NOL and monophosphate ratios (and assuming a mean polymer length of 50 phosphates). Using a polyP-NOL preparation in which approximately 40% of the polyP molecules were singly end-labeled, we added CIAP and monitored A₄₀₀ versus time at 37 °C (Figure 3C). These results show that singly labeled polyP-NOL can be used to follow the progress of exopolyphosphatase digestion. The curvilinear progress curves probably reflect the fact that the substrate is ~50 phosphates long but the chromophore is

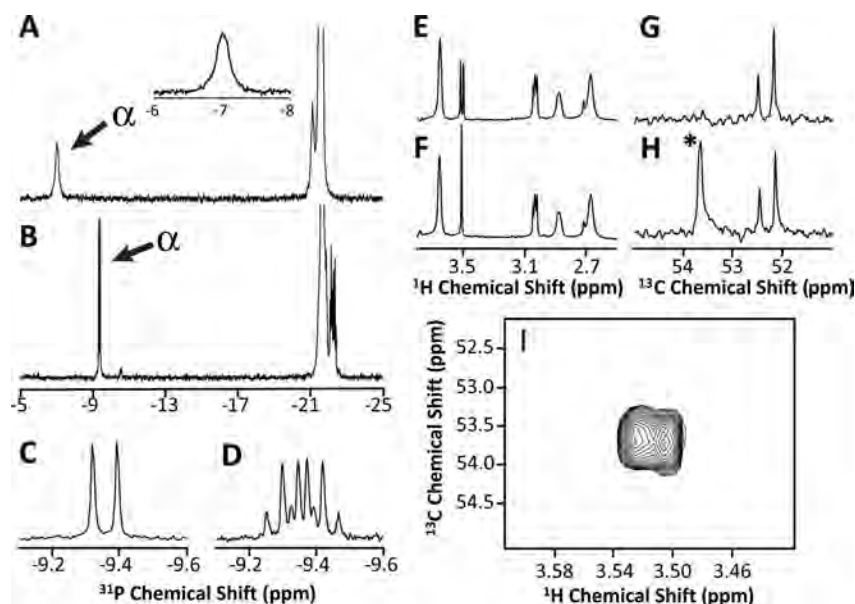


Figure 1. NMR analyses of end-methylated polyP. 1D ^{31}P spectra of (A) unmodified polyP and (B) polyP following reaction with methanol and EDAC. The terminal phosphate (alpha) peaks are indicated by arrows, and the inset in panel A is an expanded view of the alpha peak region of this spectrum. (C) The expanded view shows that the sharp alpha peak in panel B is resolved as a doublet. (D) Without ^1H decoupling, the alpha peak from methylated polyP expands into quartets as a result of J couplings from methyl protons. (E,F) 1D ^1H spectra of methylated polyP with (E) and without (F) applied decoupling irradiation at the alpha-phosphate frequency. The doublet peak at ~ 3.5 ppm (E) converts into a singlet (F) after irradiation because the proton peak is coupled to a phosphorus atom. (Other peaks in the ^1H spectra are from the MES buffer used in product purification and thus not affected by the decoupling.) 1D ^{13}C spectra of methylated polyP prepared with (G) natural abundance methanol or (H) 20% ^{13}C -enriched methanol. Use of ^{13}C -enriched methanol in the reaction greatly enhanced the signal at ~ 53.7 ppm (asterisk). (Other ^{13}C peaks are from the MES buffer.) (I) 2D HSQC analysis of the 53.7 ppm ^{13}C peak confirmed that the ^{13}C atoms are connected to the methyl protons.

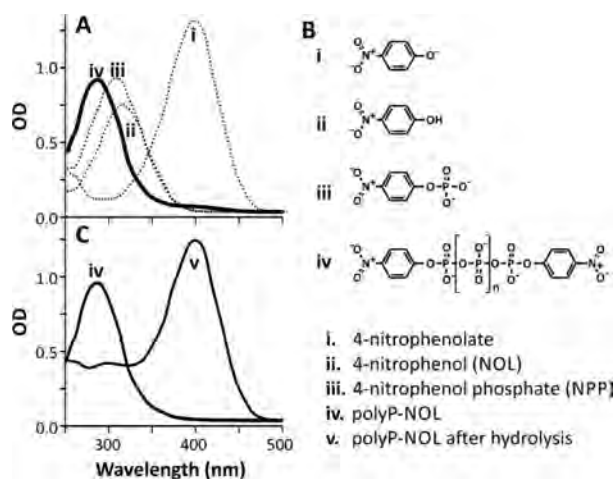


Figure 2. Product analysis and NOL substitution series using UV-vis spectroscopy. (A) Absorbance spectra of NOL substitution series with (B) the accompanying compounds' chemical structures. Each compound (except (ii)) was brought to a final concentration of 150 μM in alkaline conditions (1.5 M Tris-HCl buffer pH = 8.8, final) and scanned spectrally; NOL (ii) was scanned under acidic conditions. Absorbance maxima were the following: 398 nm (i), 317 nm (ii), 310 nm (iii), and 285 nm (iv). (C) Absorption spectra of polyP end-labeled with NOL, before (iv) and after (v) acid hydrolysis (1 M HCl for 1 h at 100 $^\circ\text{C}$) followed by alkalization to pH 8.8.

released only when the last phosphate is removed from the substrate.

Endopolyphosphatase Digestion of PolyP-NOL and PolyP-MU. Covalent modification of polyP on both ends protects polyP against exopolyphosphatase (CIAP) digestion (Table 1). We therefore reasoned that two-stage assays for

endopolyphosphatase activity could be devised using polyP that is completely labeled on both ends with chromophore or fluorophore. Digestion by exopolyphosphatase should be possible only after the action of endopolyphosphatase has exposed free polyP ends. In such an assay one could employ either sequential or simultaneous digestion with endo- and exopolyphosphatases. Accordingly, polyP-NOL was predigested to completion with SAP to eliminate singly labeled molecules, after which the polyP-NOL was repurified. We then used this SAP-treated polyP-NOL in a two-stage endopolyphosphatase assay in which we first digested the substrate with either Nudt3 (a hydrolase with known endopolyphosphatase activity¹²) or Nudt2 (another nudix hydrolase that cleaves dinucleotide polyphosphates, "Np_nNs", but whose endopolyphosphatase activity was not known) and then monitored product release during digestion with CIAP. Figure 4 shows that few dye molecules from SAP-treated polyP-NOL were released upon incubating the substrate with either endopolyphosphatase (Nudt2 or Nudt3) or exopolyphosphatase (CIAP) alone. However, polyP-NOL was readily hydrolyzed by CIAP following pretreatment with either Nud2 or Nudt3. Additionally, this experiment demonstrated that Nudt2 has endopolyphosphatase activity (Figure 4B).

The efficiency of polyP labeling with MU was usually greater than that with NOL (Table 1), so predigestion of polyP-MU (Figure 5A) with SAP was typically not required before using this substrate to detect endopolyphosphatase activity. Figure 5B shows the reaction curves for two-stage assays of polyP-MU digestion with Nudt2 followed by CIAP. Neither Nudt2 nor CIAP alone released significant MU, while polyP-MU was efficiently digested by CIAP after incubation with Nudt2.

This experiment also demonstrates the amount of CIAP required for maximal rates of product release. Figure 5C shows

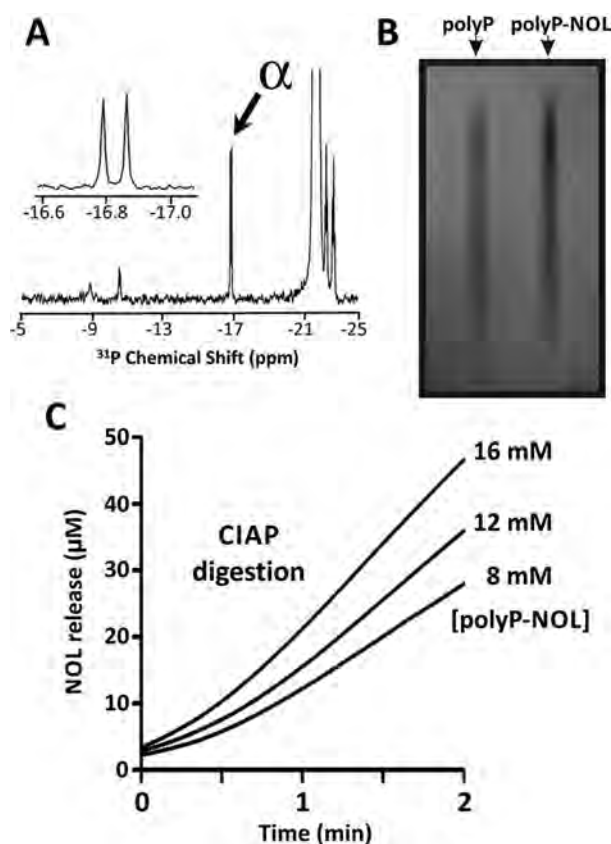


Figure 3. Analysis of polyP end-labeling with NOL. (A) 1D ^{31}P spectrum of polyP-NOL highly labeled at both ends. The alpha phosphate peak, indicated by an arrow, is resolved as a doublet (inset) upon axis expansion. (B) Comparison of polyP and polyP-NOL resolved by gel electrophoresis and detected by DAPI negative staining. (C) Enzymatic degradation of varying concentrations of incompletely end-labeled polyP-NOL (8 to 16 mM phosphate) by CIAP, with NOL release detected spectrophotometrically at 400 nm.

a much shorter time course of the second stage of this two-stage assay, using saturating levels of CIAP. We tested Nudt1 (a nudix hydrolase known to cleave Ap_3A but not long-chain Np_nN molecules) in a similar two-stage assay, but under the various conditions we used, the enzyme did not support MU release by CIAP (data not shown). We also examined a one-stage assay employing polyP-MU incubated simultaneously with CIAP plus varying concentrations of Nudt2. We found limited product release with CIAP alone but robust product release by the combination of CIAP and Nudt2 (Figure 5D).

DISCUSSION

This study had two goals: expand the covalent coupling chemistry for polyP, allowing for facile linkage of alcohols to the terminal phosphates of polyP via phosphoester bonds; and use this chemistry to develop high-throughput methods for detecting and quantifying the enzymatic digestion of polyP. We now report that the water-soluble cross-linker, EDAC, can be used to efficiently generate phosphoester linkages between alcohols and the terminal phosphates of polyP. We utilized this coupling chemistry to generate new chromogenic and fluorogenic substrates for detecting the enzymatic hydrolysis of polyP, based on phosphoester end-labeling of polyP with NOL or MU, respectively. Additionally, with our polyP

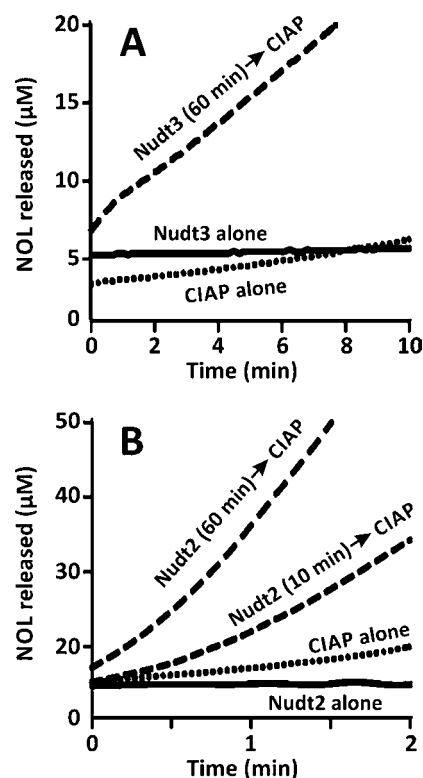


Figure 4. Sequential digestion of doubly end-labeled polyP-NOL with endopolyphosphatases and exopolyphosphatases. In both panels, doubly end-labeled polyP-NOL was first incubated with or without endopolyphosphatase (Nudt2 or Nudt3) for 10 or 60 min at 37 °C. Exopolyphosphatase (120 U/mL CIAP) was then added to the indicated samples and NOL release was quantified over time. (A) Treatment with 850 nM Nudt3. (B) Treatment with 250 nM Nudt2.

substrates, we were able to monitor and distinguish endo- and exopolyphosphatase activities in real time.

Previously, we reported that EDAC could be used efficiently to couple compounds with primary amines to the terminal phosphates of polyP via phosphoramidate linkages, and this chemistry has allowed us to link a variety of probes to polyP;¹³ for example, we used this method to biotinylate polyP, which we then employed to detect and quantify interactions between polyP and blood clotting proteins.^{21,22} Although phosphoramidate linkages are relatively stable under neutral and alkaline conditions, the linkages are highly acid-labile.²³ It would be advantageous, therefore, to be able to efficiently link the terminal phosphates of polyP to organic compounds via phosphoester linkages, which, unlike phosphoramidate linkages, resist acid hydrolysis at physiological temperatures.²³ A previous study used combinations of carbodiimides (other than EDAC) in conjunction with polyP and alcohols in anhydrous organic solvents to generate phosphoester linkages to polyP; however, the reactions also caused substantial polyP hydrolysis to much shorter polyP chains and the apparent formation of cyclic and branched polyP adducts (which are unstable in aqueous solution).²⁴ In this report we identified aqueous coupling conditions for EDAC-mediated formation of phosphoester linkages to polyP that resulted in labeling just the terminal phosphates and that did not appreciably shorten the polyP chains.

Full-length polyP capped on either end with chromogenic or fluorogenic dyes was used to detect phosphatase activity. PolyP-

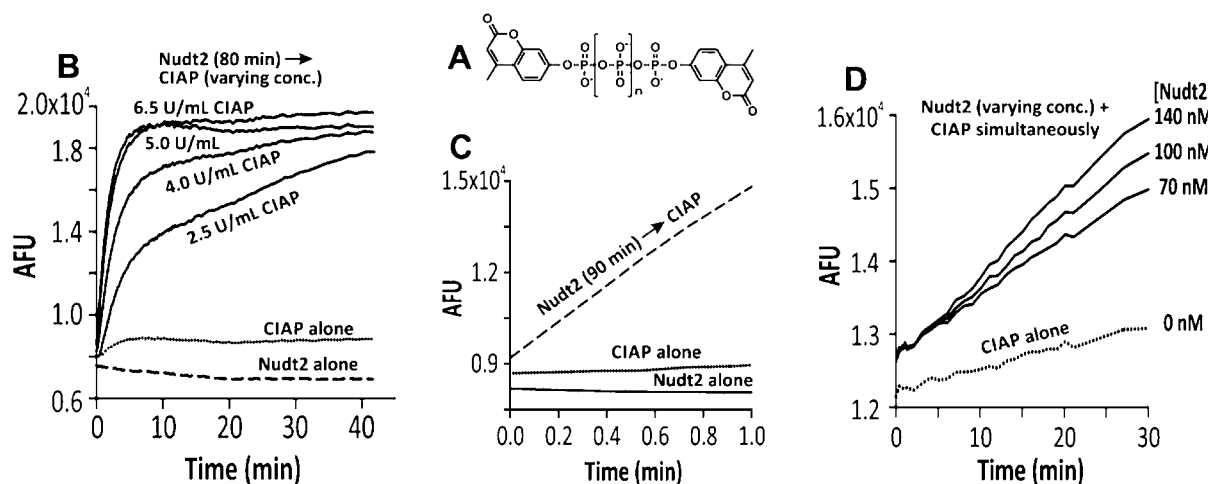


Figure 5. Digestion of polyP-MU by mixtures of endo- and exopolyphosphatases. (A) Structure of doubly end-labeled polyP-MU. (B) Sequential digestion of doubly end-labeled polyP-MU with endopolyphosphatase and exopolyphosphatase. PolyP-MU was first incubated with or without endopolyphosphatase (250 nM Nudt2) for 80 min at 37 °C, after which varying concentrations of exopolyphosphatase (CIAP) were added to the indicated samples and the increase in fluorescence (AFU) was quantified over time. (C) Sequential digestion of doubly end-labeled polyP-MU, first, with or without 250 nM Nudt2 for 90 min at 37 °C, after which 5 U/mL CIAP was added to the indicated samples and fluorescence was quantified over time. (D) Simultaneous digestion of polyP-MU with the indicated concentrations of Nudt2 and 55 U/mL CIAP, during which fluorescence was quantified over time.

NOL preparations that were incompletely labeled on both polyP ends were useful substrates for detecting exopolyphosphatase activity, which released free NOL upon the complete hydrolysis of the singly end-labeled polyP. On the other hand, polyP-NOL and polyP-MU preparations that were fully labeled on both polyP ends were highly resistant to exopolyphosphatase digestion, and this property was used as the basis of a two-stage assay in detecting endopolyphosphatase activity. In such assays, endopolyphosphatase digestion creates free polyP ends which are then substrates for exopolyphosphatase (CIAP) digestion, which in turn releases free dye from polyP-NOL or polyP-MU.

Not surprisingly, assays using the fluorogenic substrate, polyP-MU, could be conducted using lower substrate concentrations than those using the chromogenic substrate, polyP-NOL, owing to the greater sensitivity of fluorescence-based detection methods; however, assays using fluorogenic substrates require more specialized equipment and sample handling than do simple chromogenic assays, prompting us to develop both types of substrates in this study.

We constructed a two-stage assay to demonstrate the activity of a known endopolyphosphatase (Nudt3), and to demonstrate that another nudix hydrolase (Nudt2) also exhibits endopolyphosphatase activity. Nudt3, sometimes called DIPPI, or simply DIPPI, is a nudix-type enzyme with multiple known *in vitro* substrates: capped mRNA, oxo-8-dGTPase, inositol pyrophosphates, dinucleotide polyphosphates, and inorganic polyphosphate (reviewed by McLennan²⁵). Many nudix-type phosphatases are clinically important enzymes and their overexpression can be markers of disease. Nudt2 (Aph1), for example, is an Ap_4A hydrolase that, when overexpressed in breast cancer, correlates with poor prognosis.²⁶ In addition to processing Ap_4A , Nudt2 can hydrolyze long-chain Np_nNs such as Ap_6A . We hypothesized that this nudix enzyme, though previously not described as having endopolyphosphatase activity on inorganic polyP, might be able to cleave polyP and that we might detect this cleavage using our substrates in conjunction with CIAP. This was confirmed with our novel

substrates. Like Nudt2, the human short-chain exopolyphosphatase, h-prune, is also implicated in tumor survival,⁷ again providing a connection between alterations in polyP degradation and human health.

It should also be noted that the substrates only release a signal (free dye) when the last phosphate of the polyP chain is removed by an exopolyphosphatase. While this reaction was efficiently catalyzed by CIAP, other exopolyphosphatases might digest polyP to very short chains but not completely to monophosphate and therefore would not be expected to release the dye from these substrates. Such enzymes could be studied using these substrates in sequential assays employing CIAP.

We anticipate that the utilization of chromogenic and fluorogenic polyP substrates will aid further inquiry into how polyphosphates are turned over enzymatically. For example, an additional class of enzymes that could conceivably be studied using these substrates are kinases that utilize polyP as a substrate/phosphate donor. Also important is the development of a method for making stable ester linkages to the ends of polyP. Applications for such phosphoester linkages could include attaching polyP to surfaces, fabricating polyP-containing nanoparticles, and attaching fluorescent probes to polyP, in addition to creating the chromogenic and fluorogenic substrates for polyP-degrading enzymes reported here.

CONCLUSIONS

Using carbodiimide-mediated chemistry, we selectively esterified the terminal phosphates of inorganic polyP polymers with various alcohols. In a proof-of-principle experiment, we used methanol in esterification reactions and confirmed the product through 1D and 2D ^{31}P , ^1H , and ^{13}C NMR analyses. We also showed that polyP could be similarly end-labeled with chromogenic or fluorogenic alcohols to form adducts. These adducts were shown to be useful substrates for polyP-degrading enzymes, allowing us to monitor enzyme activity spectrophotometrically in real time; furthermore, we used these substrates to identify a new function for the clinically significant enzyme,

Nudt2. The chemistry and substrates developed in this work are likely to be useful for synthetic and clinical applications.

AUTHOR INFORMATION

Corresponding Author

*E-mail: jhmmorris@illinois.edu. Telephone: (217) 265-5424. Fax: (217) 265-5290.

Notes

The authors declare no competing financial interest.

ACKNOWLEDGMENTS

We thank Dr. M. Burke for helpful discussions about chemical synthesis and Dr. A. Jahromi for help with recrystallization. This work was supported in part by grant R01 HL047014 from the National Heart, Lung and Blood Institute of the NIH, and by Award WQ81XWH-11-2-0021 from the U.S. Army Medical Research and Materiel Command. The U.S. Army Medical Research Acquisition Activity, 820 Chandler Street, Fort Detrick, MD 21702-5014 is the awarding and administering acquisition office. The contents of this article do not necessarily reflect the position or the policy of the Government, and no official endorsement should be inferred.

REFERENCES

- (1) Rao, N. N.; Gomez-Garcia, M. R.; Kornberg, A. *Annu. Rev. Biochem.* **2009**, *78*, 605–647.
- (2) Moreno, S. N.; Docampo, R. *PLoS Pathol.* **2013**, *9* (5), e1003230.
- (3) Kulakovskaya, T. V.; Vagabov, V. M.; Kulaev, I. S. *Process Biochem.* **2012**, *47* (1), 1–10.
- (4) Morrissey, J. H.; Choi, S. H.; Smith, S. A. *Blood* **2012**, *119* (25), 5972–5979.
- (5) Azevedo, C.; Saiardi, A. *Biochem. Soc. Trans.* **2014**, *42* (1), 98–102.
- (6) Lorenz, B.; Schröder, H. C. *Biochim. Biophys. Acta* **2001**, *1547* (2), 254–261.
- (7) Tammenkoski, M.; Koivula, K.; Cusanelli, E.; Zollo, M.; Steegborn, C.; Baykov, A. A.; Lahti, R. *Biochemistry* **2008**, *47* (36), 9707–9713.
- (8) Ruiz, F. A.; Lea, C. R.; Oldfield, E.; Docampo, R. *J. Biol. Chem.* **2004**, *279* (43), 44250–44257.
- (9) Moreno-Sanchez, D.; Hernandez-Ruiz, L.; Ruiz, F. A.; Docampo, R. *J. Biol. Chem.* **2012**, *287* (34), 28435–28444.
- (10) Wat, J. M.; Foley, J. H.; Krisinger, M. J.; Ocariza, L. M.; Lei, V.; Wasney, G. A.; Lameignere, E.; Strynadka, N. C.; Smith, S. A.; Morrissey, J. H.; Conway, E. M. *Blood* **2014**, *123* (5), 768–776.
- (11) Smith, S. A.; Mutch, N. J.; Baskar, D.; Rohloff, P.; Docampo, R.; Morrissey, J. H. *Proc. Natl. Acad. Sci. U. S. A.* **2006**, *103* (4), 903–908.
- (12) Lonetti, A.; Szigyarto, Z.; Bosch, D.; Loss, O.; Azevedo, C.; Saiardi, A. *J. Biol. Chem.* **2011**, *286* (37), 31966–31974.
- (13) Choi, S. H.; Collins, J. N.; Smith, S. A.; Davis-Harrison, R. L.; Rienstra, C. M.; Morrissey, J. H. *Biochemistry* **2010**, *49* (45), 9935–9941.
- (14) Smith, S. A.; Choi, S. H.; Davis-Harrison, R.; Huyck, J.; Boettcher, J.; Rienstra, C. M.; Morrissey, J. H. *Blood* **2010**, *116* (20), 4353–4359.
- (15) Gailani, D.; Broze, G. J., Jr. FXI and the contact system. In *Metabolic and Molecular Basis of Inherited Disease*; Scriver, C., Beaudet, A., Sly, W., Valle, D., Childs, B., Kinzler, K., Vogelstein, B., Eds.; McGraw-Hill: New York, 2001; Vol. 8, pp 4433–4453.
- (16) Damle, S. P.; Krishnan, P. S. *Arch. Biochem. Biophys.* **1954**, *49* (1), 58–70.
- (17) Delaglio, F.; Grzesiek, S.; Vuister, G. W.; Zhu, G.; Pfeifer, J.; Bax, A. *J. Biomol. NMR* **1995**, *6* (3), 277–293.
- (18) Smith, S. A.; Morrissey, J. H. *Electrophoresis* **2007**, *28* (19), 3461–3465.

(19) Otera, J.; Nishikido, J. Reaction of alcohols with carboxylic acids and their derivatives. In *Esterification: Methods, Reactions and Applications*, 2nd ed.; Wiley-VCH Verlag GmbH & Co. KGaA, 2010; pp 3–157.

(20) Jordan, S. W.; Cronan, J. E., Jr. *J. Bacteriol.* **2003**, *185* (5), 1582–1589.

(21) Choi, S. H.; Smith, S. A.; Morrissey, J. H. *Blood* **2011**, *118* (26), 6963–6970.

(22) Smith, S. A.; Choi, S. H.; Collins, J. N.; Travers, R. J.; Cooley, B. C.; Morrissey, J. H. *Blood* **2012**, *120* (26), 5103–5110.

(23) Duclos, B.; Marcandier, S.; Cozzzone, A. J. *Methods Enzymol.* **1991**, *201*, 10–21.

(24) Glonek, T.; Kleps, R. A.; Van Wazer, J. R.; Myers, T. C. *Bioinorg. Chem.* **1976**, *5* (4), 283–310.

(25) McLennan, A. G. *Cell. Mol. Life Sci.* **2013**, *70* (3), 373–385.

(26) Oka, K.; Suzuki, T.; Onodera, Y.; Miki, Y.; Takagi, K.; Nagasaki, S.; Akahira, J.; Ishida, T.; Watanabe, M.; Hirakawa, H.; Ohuchi, N.; Sasano, H. *Int. J. Cancer* **2011**, *128* (8), 1770–1782.

Size-Controlled Synthesis of Granular Polyphosphate Nanoparticles at Physiologic Salt Concentrations for Blood Clotting

Alexander J. Donovan,[†] Joseph Kalkowski,[†] Stephanie A. Smith,[‡] James H. Morrissey,[‡] and Ying Liu^{*,†,§}

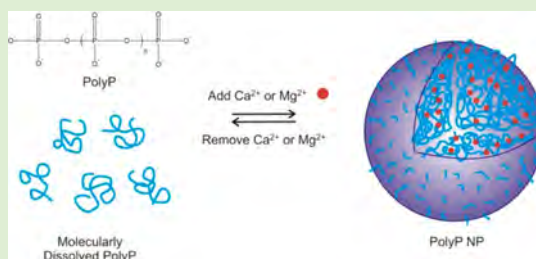
[†]Department of Chemical Engineering, University of Illinois at Chicago, Chicago, Illinois 60607, United States

[‡]Department of Biochemistry, University of Illinois at Urbana–Champaign, Urbana, Illinois 61801, United States

[§]Department of Biopharmaceutical Sciences, University of Illinois at Chicago, Chicago, Illinois 60607, United States

S Supporting Information

ABSTRACT: Size-controlled granular polyphosphate (PolyP) nanoparticles were synthesized by precipitation in aqueous solutions containing physiological concentrations of calcium and magnesium. We demonstrate using dynamic light scattering (DLS) that the solubility is correlated inversely with PolyP chain length, with very long chain PolyP (PolyP1000+, more than 1000 repeating units) normally found in prokaryotes precipitating much more robustly than shorter chains like those found in human platelet dense granules (PolyP80, range 76–84 repeating units). It is believed that the precipitation of PolyP is a reversible process involving calcium coordination to phosphate monomers in the polymer chain. The particles are stable in aqueous buffer and albumin suspensions on time scales roughly equivalent to catastrophic bleeding events. Transmission electron microscopy images demonstrate that the PolyP nanoparticles are spherical and uniformly electron dense, with a particle diameter of 200–250 nm, closely resembling the content of acidocalcisomes. X-ray elemental analysis further reveals that the P/Ca ratio is 67:32. The granular nanoparticles also manifest promising procoagulant effects, as measured by *in vitro* clotting tests assaying contact pathway activity.



INTRODUCTION

Inorganic polyphosphate (PolyP) is an anionic linear polymer composed of orthophosphate subunits found in a broad array of organisms, ranging from the simplest prokaryotes to the most complex mammals including humans.¹ Dating from evolution's primordial stages, PolyP exhibits a diversity of functions depending upon its environment and polymer length, including highly regulated cellular tasks such as biofilm formation,² pathogen virulence,³ cell motility,⁴ quorum sensing,⁵ transmembrane ion conductance,^{6,7} metal chelation,⁸ blood coagulation,^{9–14} and energy storage.¹⁵ PolyP's chemical simplicity despite its ubiquity, age, and biological versatility suggests that its precipitation into condensed granules may play a part in its myriad of biochemical tasks. Present across nearly all phylogenetic taxa are acidic subcellular storage compartments containing large quantities of PolyP.¹⁶ Acidocalcisomes are acidic intracellular compartments found in prokaryotes that contain extremely high levels of ionized alkali earth and transition metal cations. Electron microscopy has revealed that these structures are electron dense, and elemental analysis confirms the presence of phosphate-containing compounds.¹⁷ Ruiz et al. recently showed that this structure is conserved through the evolutionary tree to humans in the form of dense granules in human platelets.¹⁸

PolyP precipitates could wield different procoagulant effects than the molecularly dissolved polymer, possibly serving as an anionic contact "surface" for activation of FXII like kaolin and collagen.¹⁹ Alternatively, these bodies could have evolved in

evolution's early stages merely as condensed stores of large concentrations of PolyP for later downstream cellular functions requiring rapid nonlinear responses. PolyP has been known for approximately a century to reversibly bind to calcium, magnesium, iron, copper, zinc, barium, and other metals.²⁰ The calcium concentration within the platelet dense granules is as high as 2.2 M,²¹ and the dissociation constants for Ca²⁺ and Mg²⁺ have even been quantified.²²

Although successful synthesis of aluminum PolyP nanoparticles has been reported, the established synthetic routes require harsh organic solvents and intensive separation processes and lead to inadequate size control.²³ Momeni et al. investigated polyphosphate gels, or "coacervates," for potential utilization as hemostatic agents and examined the chelation of Ca²⁺, Ba²⁺, and Sr²⁺ to PolyP glasses of varied polymer lengths and its effects on solution pH and chain degradation of the PolyP solution.^{24,25} However, systematic measurements of PolyP precipitation into particles with controlled sizes have never been reported. Moreover, the potential downstream therapeutic potential of PolyP precipitation has not been adequately addressed in the literature.

Herein, we show that the precipitation of inorganic PolyP into granular nanostructures is based on polymer length, with very long polymer lengths condensing much more robustly

Received: July 17, 2014

Revised: September 26, 2014

Published: September 30, 2014

than shorter chains like those found in human platelet dense granules. Furthermore, these condensed PolyP granules are stable in aqueous buffer and albumin suspensions on the same time scale as catastrophic bleeding events and possess potent procoagulant function, when assaying for activation of the contact pathway. Precipitation of inorganic PolyP in aqueous calcium and/or magnesium could potentially serve as a facile therapy to mitigate the deleterious effects of serious trauma via the delivery of high concentrations of PolyP stores locally to bleeding sites to rapidly induce coagulation.

■ EXPERIMENTAL SECTION

Materials and Reagents. Tris(hydroxymethyl)aminomethane, $\text{CaCl}_2 \cdot 6\text{H}_2\text{O}$, $\text{MgCl}_2 \cdot 6\text{H}_2\text{O}$, NaCl, KCl, and bovine serum albumin (BSA) were purchased from Sigma-Aldrich (St. Louis, MO). Water was deionized to 18.2 M Ω -cm (Nanopure II, Barnstead, Dubuque, IA). Citrated, pooled normal plasma was purchased from George King Biomedical (Overland Park, KS). L- α -Phosphatidylcholine (PC), L- α -phosphatidylserine (PS), and Avanti Mini-Extruder with 200 nm pore diameter polycarbonate membrane were purchased from Avanti Polar Lipids (Alabaster, AL). All materials were purchased at standard grades and used as received. PolyP80 (76–84 repeating units), PolyP250, (100–390 repeating units), PolyP305 (242–383 repeating units), and PolyP1000+ (more than 1000 repeating units) was size fractionated via preparative electrophoresis as previously described¹⁴ or by differential isopropanol precipitation of heterogeneous long chain PolyP. Natriumpolyphosphat P70 (BKGP70, 20–125 repeating units, mode ~45) was purchased from BK Guilini GmbH (Ludwigshafen am Rhein, Germany). PolyP concentrations are given throughout in terms of the concentration of phosphate monomer (monoP).

PolyP Nanoprecipitation. Aqueous size-fractionated PolyP was micropipetted into 8 mM Tris-HCl, pH 7.4 solutions containing combinations of the following: 1.2 mM, 5.0 mM, or 7.5 mM CaCl_2 ; 0.4 mM MgCl_2 ; 4.35 mM KCl; and 150 mM NaCl. The nanoparticles were then vortexed for 5 s. Precipitation was characterized by dynamic light scattering (DLS) (Brookhaven NanoDLS, Brookhaven, NY).

Determination of PolyP Solubility. The measurements of PolyP solubility are similar to the procedure used to determine the critical micelle concentration (CMC) of surfactants, copolymers, and phospholipids using DLS. PolyP samples were prepared as described above and injected into the DLS, beginning at exceedingly low concentrations (typically 100 nM to 1 μM monoP), where the scattering count rate resembled that of molecularly dissolved PolyP. The PolyP concentration was slowly titrated up until the scattering count rate increased and the correlation function was a well-behaved exponential decay on the baseline, suggesting that the PolyP sample was supersaturated. The scattering count rate was then plotted against the logarithm of the monoP concentration, producing a plot with two clear regimes representing: (1) molecularly dissolved PolyP and (2) precipitated PolyP. A linear regression was then performed on each regime and the point of intersection was found, which was defined as the solubility concentration. For consistency, all measurements were done on low laser intensity.

PolyP Nanoparticle (NP) Stability. Stability in Aqueous Buffer. NPs were synthesized using PolyP250 (125 μM) in either 1.2 mM or 5 mM CaCl_2 buffered with 8 mM Tris-HCl, pH 7.4 as discussed previously. Immediately after vortexing, particle size was characterized by DLS using at least a 1 min scattering time every 5 min for 1 h at room temperature.

Stability in BSA Suspensions. A solution of BSA (70 mg/mL) containing 8 mM Tris-HCl, pH 7.4 was prepared both with and without 2.5 mM CaCl_2 the day before experiments were conducted. PolyP250 (125 μM) was nanoprecipitated in 5 mM CaCl_2 , 8 mM Tris-HCl, pH 7.4, and the particle diameter was determined immediately by DLS. The PolyP NPs were then mixed 1:1 (v:v) with the BSA suspensions. The resulting BSA and CaCl_2 concentrations were thus 35 mg/mL and 1.25 mM, respectively. Particle size was measured using DLS every 5 min for 1 h and subsequently every 30 min until 3 h

had elapsed. The dispersion viscosity was calculated to be 1.2 cP,²⁶ and the refractive index was kept the same as water (1.331).

Transmission Electron Microscopy. Sample Preparation. PolyP250 (125 μM) was nanoprecipitated in 5 mM CaCl_2 , 8 mM Tris-HCl, pH 7.4 as described above. The sample (10 μL) was micropipetted onto a 300-mesh carbon-coated Formvar grid (Structure Probe Inc., West Chester, PA) and allowed to dry in air for 10 min. The remaining liquid was wicked away with a Kim wipe and the process was repeated two more times to increase particle density and minimize aggregation. The sample was viewed in a JEOL JEM-1220 transmission electron microscope (JEOL, Japan).

X-ray Microanalysis. PolyP250 NPs (10 μL) were micropipetted onto a 300-mesh Holey Formvar carbon grid. The sample was dried for 15 min and examined in a JEOL JEM-3010 transmission electron microscope (JEOL, Japan).

Preparation of Large Unilamellar Vesicles (LUV). LUVs (200 nm) of PC to PS (80:20 molar ratio) were made by extrusion.²⁷ Briefly, 158 μL of 10 mg/mL L- α -PC and 42 μL of 10 mg/mL L- α -PS dissolved in chloroform were pipetted into a glass scintillation vial and dried under argon gas. The resulting lipid film was then placed under vacuum for an additional 1 h to remove any residual chloroform. The lipid cake was subsequently rehydrated with 1 mL Tris buffer, pH 7.4 and passed through an extruder with a polycarbonate membrane with 200 nm pore size 11 times to generate monodisperse LUV. Liposome diameter and polydispersity were verified by DLS.

Clotting Assays. Clotting was evaluated using a microplate-based assay as previously described⁹ with minor modifications. The citrated plasma was prewarmed to 37 °C for 20 min, and PolyP was nanoprecipitated at room temperature and evaluated by DLS before proceeding with the assay. Wells contained 50 μL of citrated pooled normal plasma, 50 μL of PolyP NPs in 5 mM CaCl_2 , 8 mM Tris-HCl, pH 7.4, and coagulation was initiated with 50 μL of 25 mM CaCl_2 , 75 μM LUV, 8 mM Tris-HCl, pH 7.4. Final excess free calcium was estimated to be 4.72 mM. LUVs containing a small amount of phosphatidylserine (~20 mol %) were added in contact activation assays, because the prothrombinase complex, consisting of Factor Va and Factor Xa, assembles on negatively charged phospholipid membranes in the presence of calcium. In the absence of negatively charged phospholipids, thrombin formation would be significantly hindered. Absorbance was read at 405 nm at room temperature on a Finstriments Microplate Reader (MTX Lab Systems Inc., Vienna, Virginia) every minute for 30 min. The sigmoidal absorbance traces were fitted to a standard Boltzmann growth function in Origin Pro 8.6 (OriginLab Corp., Northampton, MA). The x -coordinate of the inflection point (parameter x_0) was defined as the time at which clotting occurred.

■ RESULTS AND DISCUSSION

In this study, the solubilities of PolyP of differing polymer lengths were first investigated by employing DLS. Analogous to determining the critical micelle concentration of a surfactant, the light scattering count rate begins to markedly increase when PolyP begins to precipitate into NPs. The scattering intensity of very long chain PolyP (PolyP1000+, similar to the long chains in prokaryotes) in aqueous solutions containing various concentrations of mono- and divalent cations is shown in Figure 1A. PolyP precipitated in the presence of divalent metal cations at biologically relevant concentrations (5 and 1.2 mM CaCl_2 and 1.2 mM CaCl_2 + 0.4 mM MgCl_2); however, monovalent cations exerted far less precipitative effects than their divalent counterparts. At 5 mM CaCl_2 , concentrations typical of conventional clotting assays, PolyP nanoprecipitated much more easily than at physiological concentrations (1.2 mM CaCl_2). K^+ at normal physiological concentration does not statistically change the scattering intensity profile, while Na^+ at a relatively high ionic strength of 150 mM combined with 5 mM CaCl_2 causes the scattering intensity to increase at a

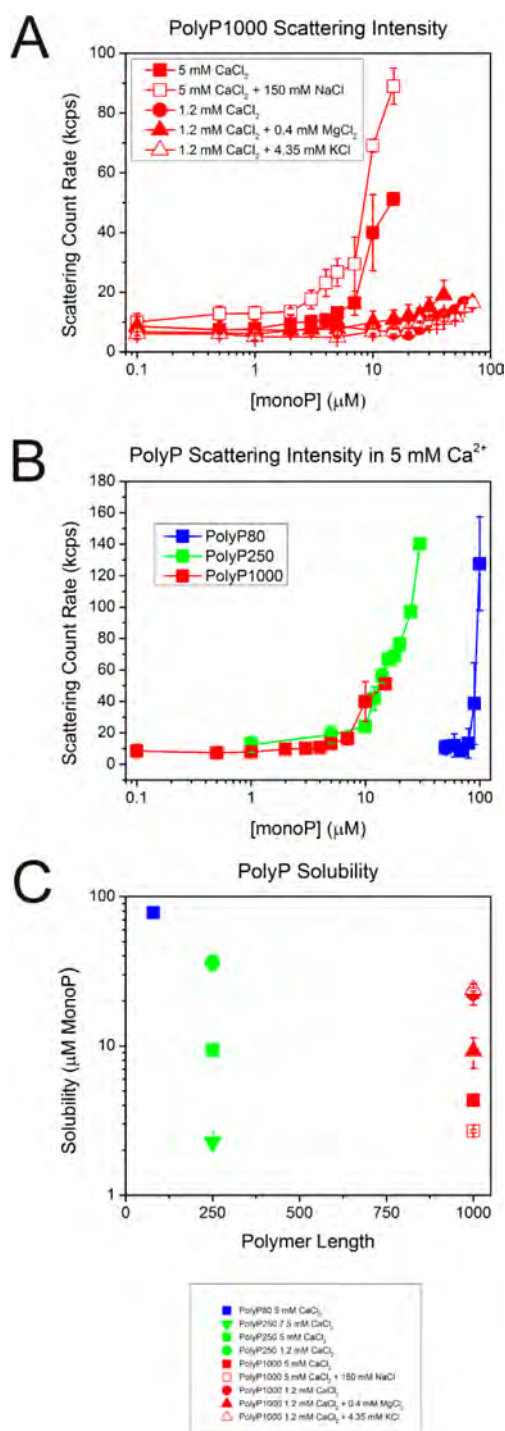


Figure 1. Solubility of PolyP as determined by DLS. (A) The precipitative effects of different metal cations on very long chain PolyP. Divalent metal cations such as Ca²⁺ and Mg²⁺ cause PolyP1000+ to robustly nanoprecipitate at physiological concentrations, as evidenced by the steep rise in the scattering intensity count rate, whereas monovalent cations such as Na⁺ and K⁺ at biologically relevant concentrations exert negligible effects on the polymer's solubility. (B) 5 mM CaCl₂ yields divergent precipitative effects on PolyP depending on the polymer length. PolyP1000+ precipitates most robustly with a steep rise in scattering intensity at 4.3 μM monoP concentration. PolyP250 is more soluble than PolyP1000+, with the count rate increasing near 9.4 μM. Platelet-size PolyP (PolyP80) is more soluble than both very long- and intermediate-chain length PolyP, with the scattering intensity markedly increasing at a monoP concentration almost a magnitude higher than PolyP250. (C) Solubility of PolyP of

Figure 1. continued

different polymer lengths. PolyP's solubility in various aqueous salt solutions buffered with 8 mM Tris-HCl, pH 7.4 plotted against polymer length in monoP units. There is a strongly nonlinear relationship, with very long chains (i.e., PolyP1000+) being much more readily precipitated than shorter polymers, e.g., polyP80. Divalent metal cations like Ca²⁺ and Mg²⁺, which are known to chelate strongly to phosphate-containing compounds, exert precipitative effects at biologically relevant concentrations, while monovalent ions such as Na⁺ and K⁺ induce little or no significant effects on PolyP's solubility.

modestly lower monoP concentration. Ca²⁺ and Mg²⁺ function synergistically to promote nanoprecipitation. The solubility in 1.2 mM CaCl₂ + 0.4 mM MgCl₂ is more than 60% lower than in 1.2 mM CaCl₂ alone.

Nanoprecipitation was also a function of polymer length, with very long chains precipitating much more robustly than intermediate-length PolyP (PolyP250) or platelet-size polyP (PolyP80) at 5 mM CaCl₂ (Figure 1B). The solubility for each precipitative condition was determined by finding the intersection of the two linear regressions representing molecularly dissolved PolyP and PolyP NP regimes as plotted in Figure 1C. The solubilities for PolyP1000+ and PolyP250 at 5 mM CaCl₂ were 4.3 and 9.4 μM, respectively, while platelet-sized PolyP's solubility at the same condition was about 78 μM. Although not measured, it is safe to assume that PolyP80s solubility concentration is at or above 78 μM in 1.2 mM CaCl₂. Upon platelet activation, the concentration of PolyP in whole blood can reach up to 2–7 μM,¹⁴ which suggests that platelet PolyP likely exerts its procoagulant effects while remaining largely molecularly dissolved. However, the next experiments demonstrate that PolyP nanoparticles exhibit dilution hysteresis, keeping open the possibility that condensed PolyP precipitates remain in NP format after secretion from activated platelets, despite being below the thermodynamic solubility limit. In addition, the local concentration of secreted PolyP could be orders of magnitude higher than 2–7 μM inside platelet-rich thrombi.

The solubility of platelet-sized PolyP in 5 mM CaCl₂ as a function of pH was also investigated. PolyP is stored intracellularly under mildly acidic conditions (~pH 5.4) together with extremely concentrated levels of calcium cations, serotonin, and pyrophosphate under the tight regulation of a H⁺-ATPase pump in human platelet dense granules.¹⁸ Given that this is the case in prokaryotic organisms as well, one could speculate that PolyP may be more easily precipitated under acidic conditions. However, at least for platelet-sized PolyP, the solubility is nearly identical at both mildly acidic and basic conditions (see Supporting Figure S5 and Supporting Table S3 in the Supporting Information).

PolyP250 was chosen as a paradigmatic polymer to study nanoparticle stability. First, nanoparticle growth kinetics were examined in an aqueous buffer containing biologically relevant concentrations of ionic calcium for 1 h, a time scale approximating a traumatic bleeding event and the half-life of PolyP in plasma or serum.⁹ PolyP250 was nanoprecipitated in 8 mM Tris-HCl, pH 7.4 with 1.2 mM and 5 mM CaCl₂ (Figure 2A). Particle aggregation behavior follows power law kinetics, typical of metastable colloidal dispersions. Initial particle diameters were 169 and 58 nm for 5 mM and 1.2 mM CaCl₂, respectively. This suggests that the phosphate/calcium

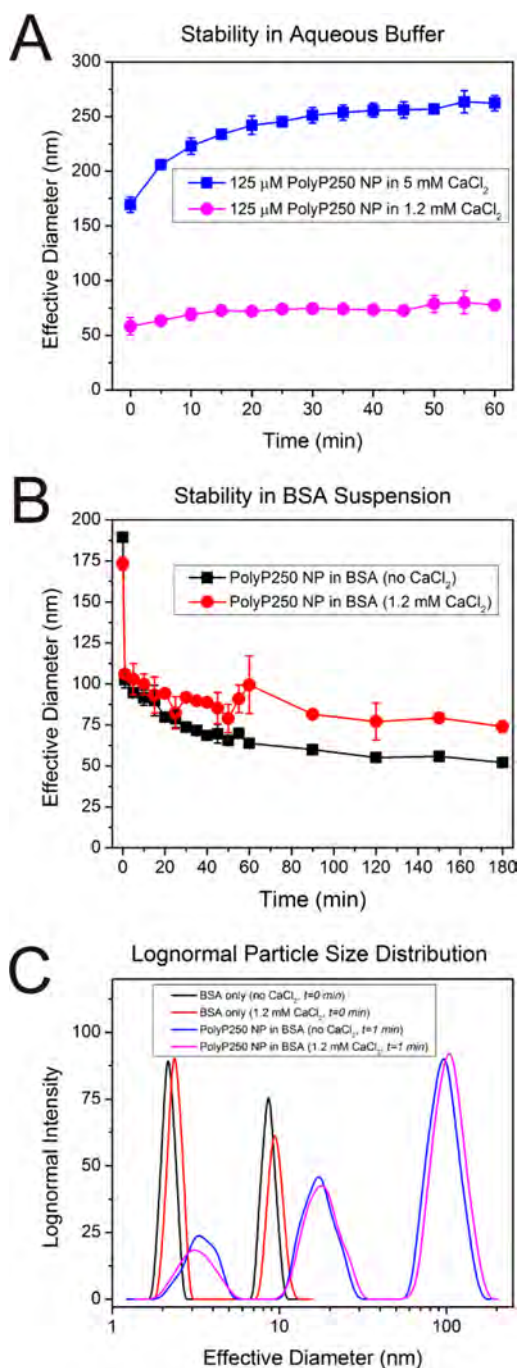


Figure 2. PolyP nanoparticle stability. (A) PolyP250 nanoparticle stability in aqueous buffer. 125 μ M PolyP250 was nanoprecipitated in 8 mM Tris-HCl, pH 7.4 containing 1.2 mM or 5 mM CaCl_2 . Average effective diameter was assessed every 5 min for 1 h, a typical time scale for a bleeding event. At 5 mM CaCl_2 , the initial particle diameter was 169 nm and slowly grew to be approximately 260 nm after 1 h. At 1.2 mM CaCl_2 , the particles were initially 58 nm and steadily increased to \sim 80 nm. The growth behavior of both suspensions appears to follow power-law kinetics typical of many metastable colloidal dispersions. (B) PolyP250 nanoparticle stability in suspensions containing BSA. 125 μ M PolyP250 was precipitated in aqueous buffer containing 5 mM CaCl_2 as described previously and then mixed 1:1 (v:v) with 70 mg/mL BSA suspension buffered to pH 7.4 with or without 1.2 mM CaCl_2 . Final BSA and CaCl_2 concentrations were 35 mg/mL and 1.2 mM, respectively. In both cases, the PolyP250 NPs shrank from approximately 170–180 nm before mixing with the BSA solution to 100 nm immediately after mixing with the BSA solution. This was not

Figure 2. continued

due to changes in dispersion viscosity or multiple scattering effects (confirmed by more measurements presented in the Supporting Information, Table S1). After 3 h, the PolyP NPs in BSA without CaCl_2 equilibration shrank to approximately 50 nm in diameter, while the NPs in the BSA equilibrated with 1.2 mM CaCl_2 were roughly the same size (\sim 80 nm). It is hypothesized that BSA may be initially forming a complex with PolyP (the rapid shrinkage upon addition to the suspension) and then competitively binding Ca^{2+} , unless it has been pre-equilibrated. (C) Lognormal size distributions for (1) BSA suspension without Ca^{2+} pretreatment; (2) BSA suspension with 1.2 mM CaCl_2 ; (3) immediate addition of PolyP 250 NPs in 35 mg/mL BSA without CaCl_2 pre-equilibration; and (4) immediate addition of PolyP 250 NPs in 35 mg/mL BSA with 1.2 mM CaCl_2 .

ratio may be the major driving force in the thermodynamic equilibrium of PolyP nanoprecipitation. Stoichiometry and PolyP supersaturation ratio as it relates to nanoparticle formation will be discussed systematically below. The stability of PolyP1000+ NPs precipitated at mildly acid conditions was also examined (see Supporting Figure S3 in the Supporting Information), resembling the environment in acidocalcisomes. The growth behavior manifests power law kinetics identical to physiologic pH. However, the scattering count rate remains more stable.

Aqueous buffer is only a poor approximation of the environment in circulation as it lacks many of the proteins and peptides that contribute to hemostasis and that regulate pH and plasma ionic strength. In addition to examining the nanoparticle growth behavior in aqueous buffer, stability was also investigated in Tris-buffered suspensions containing 35 mg/mL BSA to better approximate the conditions found in human serum. Serum albumin is the most abundant protein in circulation. It binds to a myriad of pharmaceuticals and foreign substances,²⁸ tightly regulates serum pH,²⁹ and robustly and competitively binds to metal cations,^{30–35} most notably Ca^{2+} , Zn^{2+} , and Cu^{2+} . Because of BSA's functionality, two conditions were considered for PolyP250 NP stability: (1) BSA not pre-equilibrated with CaCl_2 and (2) BSA pre-equilibrated with 1.2 mM CaCl_2 . Briefly, 125 μ M PolyP250 NPs were nanoprecipitated in 5 mM CaCl_2 as described previously and mixed 1:1 (v:v) with the BSA suspensions. The particle size evolution was then monitored for 3 h (Figure 2B). At both salt conditions, the particles immediately shrank from 170 to 180 nm to approximately 100 nm when they were added to the BSA suspensions. The shrinkage is too rapid to suggest that this is due to enzymatic degradation. Moreover it is not an artifact of multiple scattering or changes in dispersion viscosity (see the Supporting Information, Table S1). PolyP250 NPs in BSA not pretreated with CaCl_2 continued to shrink to \sim 50 nm after 3 h, whereas the PolyP250 NPs in BSA pre-equilibrated with 1.2 mM CaCl_2 maintained approximately the same particle diameter, with the final size after 3 h being \sim 80 nm. It is conjectured that serum albumin may extract Ca^{2+} from the PolyP- Ca^{2+} complex. However, much further study is needed to prove this claim conclusively.

Figure 2C shows the log-normal particle population for the following conditions: (1) BSA without Ca^{2+} pre-equilibration; (2) BSA with 1.2 mM CaCl_2 pre-equilibration; (3) immediate addition of 125 μ M PolyP250 NPs to BSA not pre-equilibrated with Ca^{2+} ; and (4) immediate addition of PolyP250 NPs to BSA pre-equilibrated with 1.2 mM CaCl_2 . BSA without PolyP in the presence or absence of calcium displayed two peaks. The

first peak centered around 3 nm represents the hydrodynamic diameter of the BSA monomer. The second peak at approximately 15 nm constitutes multimeric BSA. The hydrodynamic radius has been previously reported in the literature to be 3.42 nm.³⁶ Quasielastic light scattering data demonstrates that the BSA monomer is a prolate ellipsoid. BSA dimerizes side-to-side, with significant overlap, leading to the dimer being less than twice the size of the monomer.³⁷

Addition of CaCl_2 has minimal effects on the size distribution of the BSA protein. The particle populations representing conditions 3 and 4 show that there is an additional peak with a mean diameter of approximately 100 nm. This peak must be the effective diameter of the PolyP250 NPs. Moreover, the middle peak representing the BSA dimer has shifted to the right, further evidence that PolyP may be interacting directly with BSA and forming an adduct mediated by calcium. The striking discrepancy in the hydrodynamic diameter of the PolyP NPs in aqueous buffer and in BSA suspension deserves special scrutiny. Further study is needed to measure PolyP- Ca^{2+} binding constants at these conditions to corroborate the hypothesis that the evolution in PolyP particle diameter, characterized first by a steep drop and then a gradual shrinkage over a time scale of hours, is due to a competitive equilibrium process governed by the differential Ca^{2+} binding affinities of BSA and PolyP.

The initial effective diameter of the PolyP granular NPs was systemically investigated against the polymer's supersaturation ratio at three different calcium concentrations: 1.2 mM (free calcium concentration in human plasma), 5 mM (calcium concentration in *in vitro* coagulation assays), and 7.5 mM. Figure 3A shows the particle size plotted against monoP concentrations up to 1 mM for intermediate-length PolyP (PolyP250). PolyP precipitated in 5 mM CaCl_2 at monoP concentrations of 250 μM or greater had to be diluted with more Tris-buffered 5 mM CaCl_2 solution before being characterized by DLS (PolyP NP diameter is hysteretic after dilution; see the Supporting Information, Table S2). No trends between particle diameter and monoP concentration are manifest at first glance until the monoP concentration is divided by the solubility of PolyP250 at the given calcium concentration and plotted nondimensionally as the supersaturation ratio, as in Figure 3B. At low to moderate supersaturation ratios (~ 1 –50) the particle size is only a function of the calcium concentration.

After it was established that the solubility of PolyP250 was 9.4 μM in 5 mM CaCl_2 , 8 mM Tris-HCl, pH 7.4, a sample well above the solubility concentration (in this case 30 μM) was diluted progressively with more 5 mM CaCl_2 to decrease the PolyP concentration and keep the calcium concentration constant, and the scattering intensity was measured after each dilution. As can be seen in Figure 3C, the system exhibits hysteresis: the count rate remains much higher even below the solubility concentration despite a thermodynamic driving force for some of the particles to resolubilize. Evidence that PolyP NP formation manifests dilution-dependent hysteresis has potentially profound ramifications: for example, a bolus of condensed PolyP could be delivered to a trauma site at locally high concentrations and be dispersed further downstream in the circulation without losing its NP format due to its hysteretic behavior, maintaining its associated biological functionality as a procoagulant and proinflammatory agent. However, in human plasma other mechanisms may come into play, such as binding of PolyP to membrane-associated proteins on vessel walls

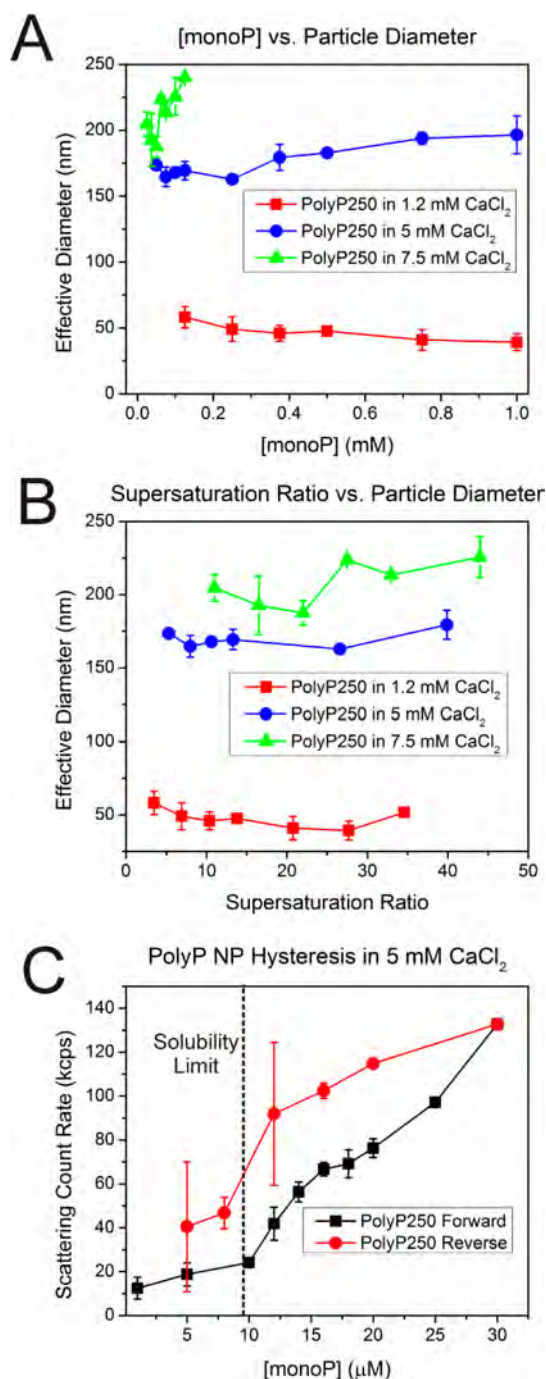


Figure 3. PolyP NP effective diameter as a function of supersaturation ratio. (A) PolyP250 NP initial effective diameter versus monoP and Ca^{2+} concentrations. Initial PolyP250 NP sizes were measured with up to 1 mM monoP concentration at three different calcium concentrations: 1.2, 5, and 7.5 mM Ca^{2+} . No trends are manifest except for a dependence on calcium concentration. (B) PolyP250 NP initial effective diameter as a function of supersaturation ratios and Ca^{2+} concentrations. When the monoP concentrations are divided by the solubility of PolyP250 at the respective calcium concentrations, it appears that at moderate supersaturation ratios (~ 1 –50), the PolyP particle diameter is only a function of the calcium concentration. (C) PolyP NP solubility hysteresis. The 30 μM PolyP250 was nanoprecipitated in 5 mM CaCl_2 , generating a supersaturated colloidal dispersion of PolyP250 NPs. The suspension was then serially diluted with 5 mM CaCl_2 , 8 mM Tris-HCl, pH 7.4 in order to decrease monoP concentration, while maintaining constant $[\text{Ca}^{2+}]$. As is evident from the reverse solubility curve (shown in red above), the

Figure 3. continued

scattering intensity remains elevated, even approaching PolyP250s solubility ($9.4 \mu\text{M}$) in 5 mM CaCl_2 despite a thermodynamic driving force for resolubilization. This suggests that PolyP colloidal dispersions manifest hysteresis, a characteristic that may have profound ramifications for potential downstream therapeutic usage of PolyP NPs as clotting agents.

adjacent to thrombi, which may prevent PolyP NPs from being convected away from the wound site, thereby curtailing a potentially disastrous or even fatal scenario.

We have found that PolyP exerts its most robust procoagulant effects at roughly the $10\text{--}500 \mu\text{M}$ when assayed

at 5 mM CaCl_2 .¹⁴ Indeed, this concentration range almost exactly corresponds to a supersaturation ratio of $1\text{--}50$ for PolyP250 at 5 mM Ca^{2+} . However, at physiological calcium concentration, the particle diameter for this polymer length is roughly constant between $36 \mu\text{M}$ and 1.8 mM . One could speculate that organisms have specifically developed techniques to store and condense PolyP in subcellular compartments such as acidocalcinsomes and platelet dense granules in a controlled manner by exploiting PolyP's roughly constant particle diameter at low to moderate supersaturation ratios. Upon secretion, these PolyP precipitates could potentially serve as concentrated stores of the polymer for biochemical processes requiring rapid, nonlinear, or threshold-switchable behavior such as coagulation or quorum sensing.

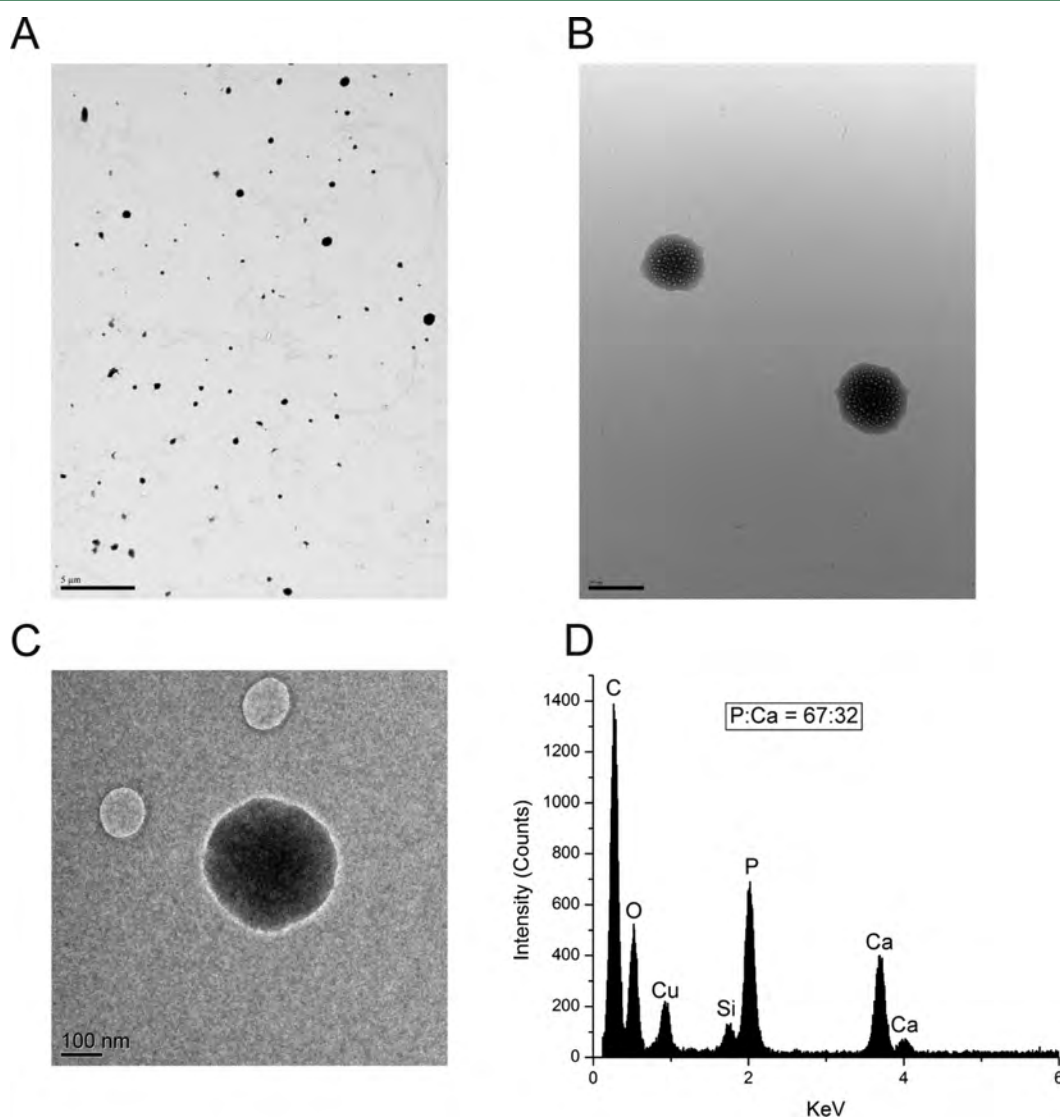


Figure 4. PolyP NP morphology, structure and elemental composition. (A) PolyP forms monodisperse particles in solution. The $125 \mu\text{M}$ PolyP250 was precipitated in 5 mM CaCl_2 , $8 \text{ mM Tris}\cdot\text{HCl}$, pH 7.4. PolyP250 forms monodisperse particle populations in the presence of 5 mM CaCl_2 . Scale bar: $5 \mu\text{m}$. (B) PolyP NPs appear spongy after prolonged electron beam exposure just like acidocalcinsomes and platelet dense granules. Even though PolyP250 NPs are uniformly electron dense, after sustained exposure to the electron beam, white spots begin to appear so that the particles appear like round sponges or porous balls. This same phenomenon was also observed in Ruiz et al.'s investigation¹⁸ of PolyP-containing dense granules in platelets. (C) A granular PolyP250 nanoparticle. A single PolyP 250 NP is shown at higher magnification revealing that the granule is roughly spherical and approximately $200\text{--}250 \text{ nm}$ in diameter, in good agreement with DLS data. Scale bar: 100 nm . (D) Elemental composition of the synthetic PolyP250 NPs. Copper, carbon, and silicon are from the grid. The ratio of the phosphorus to the calcium peak is $67:32$. Ruiz et al. performed the equivalent analysis with human platelet dense granules, and their resulting X-ray microspectrogram is quasi-identical, except for the presence of a small K peak.¹⁸ However, potassium was not used here for PolyP nanoprecipitation.

Transmission electron microscopy was used to examine the PolyP particle structure, elemental composition, and morphology. Figure 4A is an electron micrograph taken at low magnification with a large population of PolyP250 NPs, showing that the granules are spherical in shape and relatively monodisperse, despite the presence of some larger aggregates. The particle diameter is a function of the calcium concentration; inevitably, some aggregation is bound to occur during the drying process and grid preparation. When the particles undergo substantial exposure from the electron beam, the PolyP250 NPs develop white spherical spots, resulting in the granules resembling round sponges or soccer balls, despite their uniform electron density as seen in Figure 4B. Indeed, Ruiz et al. has shown using TEM that PolyP bodies in acidocalcisomes and human platelet dense granules also appear spongy after bleaching with the electron beam, resembling the PolyP NPs synthesized here.¹⁸

Figure 4C shows a single PolyP250 nanoparticle at high magnification. The PolyP granule is spherical and approximately 200–250 nm in diameter, corroborating DLS data. Figure 4D is an X-ray microspectrum of the particle in part C showing its elemental composition. Copper, carbon, and silicon are from the grid. It is very typical for X-ray microspectra to have small peaks (~1–2%) of Si and alkali earth metals arising from the detector itself or, more rarely, from silicon-containing oils deposited on the Formvar grids during the manufacturing process. In fact, a small Si peak was also observed in the X-ray microanalysis of human platelet dense granules in the past.¹⁸ The P/Ca ratio is 67:32. Ruiz et al., in their investigation of human platelet dense granules, also determined the elemental composition of the PolyP bodies, yielding very similar results.¹⁸ The P/Ca was 1.76 with trace amounts of K⁺. However, dense granules are mildly acidic subcellular compartments, which may lead to a different P/Ca stoichiometry, and platelets contain substantial cellular stores of potassium.³⁸ Potassium was not used here to precipitate PolyP into synthetic PolyP granules.

Smith et al. demonstrated that PolyP is a potent activator of the contact pathway of coagulation, and its activity is related nonlinearly with its polymer length,¹⁴ with long polymers being more robust activators than shorter chains, which exert their effects at different points in the cascade such as via acceleration of FV activation and alteration of fibrin clot architecture and morphology. Figure 5B shows a schematic representation of the intrinsic pathway of coagulation and the points in which PolyP exerts its effects. It is well accepted in the literature that anionic “surfaces” such as collagen, glass, or kaolin are required to form the primary complex consisting of FXII (Hageman Factor) and its activation partners, plasma prekallikrein and high molecular weight kininogen (HMWK).¹⁹ However, countless other soluble substances serve as scaffolds for the (auto)activation of FXII. Examples include ellagic acid, lipopolysaccharides, dextran sulfate, and phospholipids.³⁹ It has been reported previously that there exists a threshold molecular weight for activation of the intrinsic pathway for polystyrene polymers and dextran derivatives, with contact activity for both polymer types rising sharply ~25 000 Da.⁴⁰ Others have communicated that the threshold molecular weight for dextran sulfate is as low as 10 000 Da.⁴¹ Nonetheless, the mechanism by which PolyP acts on FXII has yet to be clearly elucidated.

Previous studies assaying the procoagulant effects of PolyP were performed under conditions where the polymer would presumably exist in its molecularly dissolved state. Typically, PolyP was incubated together with pooled normal plasma

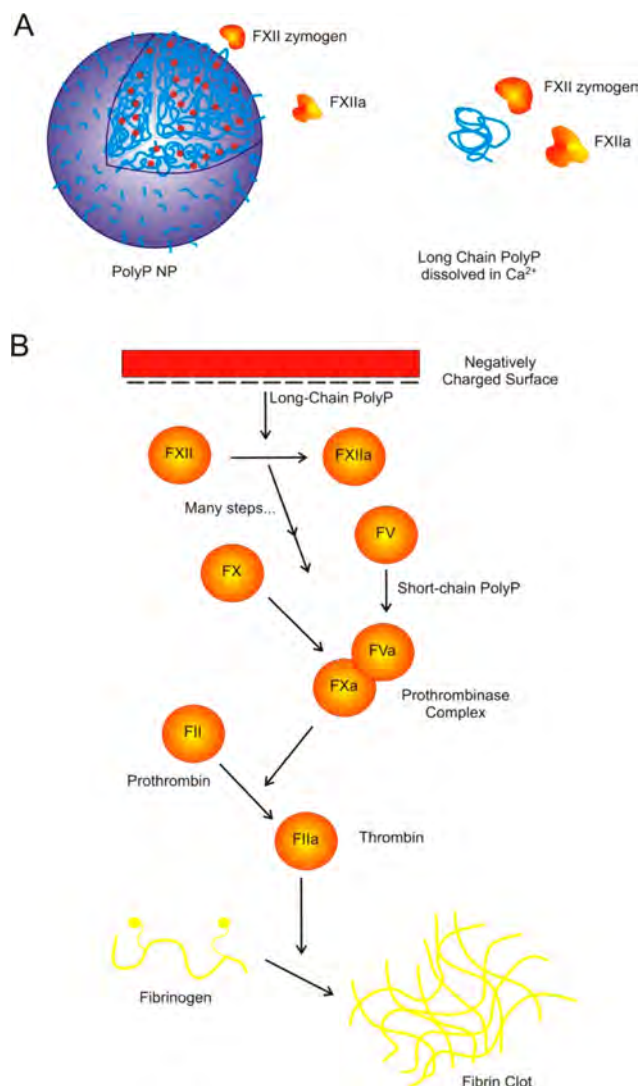


Figure 5. PolyP NPs as contact activators. (A) Possible mechanisms by which PolyP exerts its contact pathway activity. PolyP could serve as a surface for FXII activation as a colloidal particle like kaolin (left) or as a soluble anionic polymer like dextran sulfate (right) with a threshold molecular weight needed to elicit a conformational change in the FXII zymogen. (B) Schematic of the intrinsic pathway of blood coagulation. A negatively charged surface serves as the site for assembly of the primary complex consisting of FXII, kallikrein, and high molecular weight kininogen. Long-chain PolyP is able to support activation of the contact pathway, while shorter polymer lengths (like those in human platelets) are weak contact activators. PolyP also exhibits procoagulant effects further downstream in the final common pathway of blood clotting.

(PNP) for 3–5 min prior to recalcification. Since the plasma is citrated, there would be very little ionic calcium available to chelate PolyP, and thus no calcium-dependent precipitation would take place. The activation of contact enzymes and the generation of FXIIa are calcium-independent; therefore, prior studies investigating PolyP's contact activity are confined to an examination of the polymer in the absence of calcium-dependent precipitation. Moreover, plasma contains countless proteins and peptides such as serum albumin which may prevent or hinder its precipitation after recalcification. Because of PolyP's role in the early stages of natural selection, predating the arrival of polypeptides and quite possibly serving as the

precursor to deoxyribonucleic and ribonucleic acid, it is only natural that PolyP would serve as the paradigmatic anionic scaffold for plasma and cytosolic proteins, emerging as a favored binding partner for peptides with cationic amino acid residues.

Figure 6 shows the clotting time of PolyP molecules or nanoparticles when assaying for contact activity using citrated

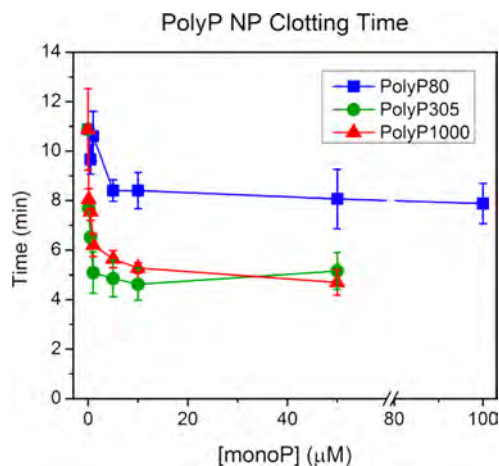


Figure 6. Initiation of the contact pathway by PolyP based on polymer length and concentration. Clotting time of PolyP is plotted as a function of monoP concentration from 0 to 100 μM . PolyP was added to 5 mM CaCl_2 , 8 mM Tris-HCl, pH 7.4 at concentrations above and below its solubility. The presence of precipitated PolyP was monitored by DLS before addition to plasma. Intermediate- and very long-chain length PolyP (PolyP305 and PolyP1000+) are clearly more robust contact activators than platelet-sized PolyP (PolyP80). The concentration dependence on clotting time for PolyP305 and PolyP1000+ are identical, suggesting that a “saturating condition” has been established.

PNP. The polyphosphates (PolyP80, PolyP305, and PolyP1000+) were first added to 5 mM CaCl_2 , 8 mM Tris-HCl, pH 7.4 at three times the final assay concentration and characterized by DLS (data not shown). Once the PolyP was incubated with the calcium solution, it was added to the PNP and immediately recalcified to initiate coagulation. Platelet-size PolyP (PolyP80) weakly shortened time to clot formation, saturating near 10–50 μM monoP. PolyP305 and PolyP1000+, on the other hand, were robust contact activators, drastically reducing clotting times even at submicromolar concentrations. Interestingly, the clotting activities of the two longer polymer sizes are quasi-identical (the error bars overlap for every concentration except one).

These data suggest that platelet PolyP only weakly promotes the activation of FXII, with the reduction in clotting time deriving mostly from effects on the final common pathway of clotting. On the other hand, the longer polymer sizes are large enough to serve as scaffolds for primary complex formation after treatment with calcium. One possibility is that there is a threshold polymer length (molecular weight) (as was previously reported for polystyrene and dextran sulfate) needed to exert the conformation change on the FXII zymogen (or to recruit a sufficiently high local surface density of FXII and its activators) as shown in Figure 5A. Interestingly, PolyP305’s molecular weight is approximately 24 kDa, corroborating past results on threshold contact activation measured using polystyrene and dextran sulfate polymers. The fact that the concentration dependence is identical for PolyP305 and

PolyP1000+ also suggests that the nanoparticle solubility is not the threshold condition for contact pathway activation for polymers over the threshold size, as PolyP1000+’s solubility is approximately 2-fold lower in 5 mM CaCl_2 . If the solubility were the limiting condition, then PolyP1000+’s clotting time would drop at $\sim 4 \mu\text{M}$, whereas PolyP305’s would drop at $\sim 9 \mu\text{M}$. However, there are several important caveats that limit the completeness of this analysis: (1) PolyP NPs have been shown to exhibit dilution-dependent hysteresis; (2) the solubility of PolyP in plasma or serum with its diversity of proteins and peptides and additional polyvalent cations such as Mg^{2+} , Cu^{2+} , Zn^{2+} , Mn^{2+} , and $\text{Fe}^{2+}/\text{Fe}^{3+}$ (see Supporting Figures S2 and S4 in the Supporting Information) could be vastly different than in aqueous buffer containing only calcium; and (3) the effect of citrate and other calcium chelators such as EDTA on PolyP nanoparticle stability has yet to be investigated.

The zeta potential of the PolyP NPs was determined to be between -15 and -20 mV independent of particle diameter and polymer length (see Supporting Tables S4 and S5 in the Supporting Information). The negative surface charge of PolyP precipitates could therefore conceivably support autoactivation of Factor XII or recruitment of its activators, plasma prekallikrein, and high molecular weight kininogen independent of polymer molecular weight, discounting other factors that would influence PolyP NP stability in human plasma mentioned above.

Regardless of the physical interpretation, the fact remains that PolyP precipitation under aqueous conditions at physiologic salt concentrations is a facile means to synthesize large amounts of condensed PolyP granules similar in structure to human platelet dense granules for potential downstream uses such as a biocompatible procoagulant agent.

CONCLUSION

Herein, we demonstrate the size-controlled synthesis of monodisperse PolyP NPs at physiological concentrations of calcium and magnesium. The solubility is related nonlinearly to the polymer length, with very long-chain PolyP precipitating much more readily than platelet PolyP. Further, the NP size is only a function of the calcium concentration across a wide supersaturation range. The granules are stable for at least an hour in aqueous buffer solutions, displaying typical power-law growth kinetics and are stable in BSA suspensions for 3 h.

The PolyP NPs possess promising procoagulant activity. Given that the PolyP particles are stable on the same time scale as a catastrophic bleeding event raises the question that PolyP’s powerful procoagulant effects on the intrinsic pathway may be related to its precipitation into micron or submicron granular particles serving as negatively charged surfaces for FXII activation. The facile, size-controlled synthesis of these particles in the laboratory serves as a foundation for the future development of targeted procoagulant nanotechnologies exploiting PolyP precipitation to mitigate the effects of a diversity of bleeding phenomena such as internal hemorrhage and hemophilia in a minimally invasive manner.

ASSOCIATED CONTENT

Supporting Information

Scattering intensity of PolyP250 in 7.5 mM CaCl_2 , 8 mM Tris-HCl, pH 7.4. Determination of any multiple scattering effects in BSA suspensions containing PolyP250 NPs. PolyP250 NP diameter hysteresis after dilution with more 5 mM CaCl_2 . PolyP1000+ precipitation and log-normal particle size dis-

tribution in 5 mM MgCl₂, 8 mM Tris-HCl, pH 7.4. Stability of PolyP1000+ NPs in acidic and basic conditions. Particle size distribution of PolyP1000+ NPs in Fe²⁺/Fe³⁺. Scattering intensity of platelet-sized PolyP as a function of monoP concentration at acidic and basic conditions. Solubility of PolyP as a function of molecular weight and pH. Zeta potential and particle effective diameter as a function of polymer length in 5 mM CaCl₂, pH 7.4. Zeta potential and particle effective diameter of PolyP at various precipitating conditions. This material is available free of charge via the Internet at <http://pubs.acs.org>.

AUTHOR INFORMATION

Corresponding Author

*Phone: +1(312) 996-8249. Fax: +1(312) 996-0808. E-mail: liuying@uic.edu.

Author Contributions

Experiments were conducted by A.J.D. and J.K. and were designed and interpreted by Y.L., A.J.D., J.K., S.A.S., and J.H.M. Polyphosphates were prepared by S.A.S. The manuscript was composed by A.J.D. and Y.L. with editorial contributions from S.A.S. and J.H.M. All authors have given approval to the final version of the manuscript.

Notes

The authors declare no competing financial interest.

ACKNOWLEDGMENTS

The authors would like to extend their gratitude to Dr. Alan Nicholls and Linda Juarez of the UIC Research Resource Center for their excellent technical assistance with transmission electron microscopy characterization. The study was sponsored by the U.S. Army Medical Research and Materiel Command (Grant WQ81XWH-11-2-0021). The U.S. Army Medical Research Acquisition Activity, 820 Chandler Street, Fort Detrick MD 21702-5014 is the awarding and administering acquisition office. The contents of this article do not necessarily reflect the position or the policy of the government, and no official endorsement should be inferred.

REFERENCES

- Morrissey, J. H.; Choi, S. H.; Smith, S. A. *Blood* **2012**, *119* (25), 5972–5979.
- Shi, X. B.; Rao, N. N.; Kornberg, A. *Proc. Natl. Acad. Sci. U.S.A.* **2004**, *101* (49), 17061–17065.
- Kim, K. S.; Rao, N. N.; Fraley, C. D.; Kornberg, A. *Proc. Natl. Acad. Sci. U.S.A.* **2002**, *99* (11), 7675–7680.
- Rashid, M. H.; Rao, N. N.; Kornberg, A. *J. Bacteriol.* **2000**, *182* (1), 225–227.
- Brown, M. R. W.; Kornberg, A. *Proc. Natl. Acad. Sci. U.S.A.* **2004**, *101* (46), 16085–16087.
- Reusch, R. N.; Huang, R. P.; Bramble, L. L. *Biophys. J.* **1995**, *69* (3), 754–766.
- Fleischer, B.; Xie, J. P.; Mayrleitner, M.; Shears, S. B.; Palmer, D. J.; Fleischer, S. *J. Biol. Chem.* **1994**, *269* (27), 17826–17832.
- Kornberg, A.; Rao, N. N.; Ault-Riche, D. *Annu. Rev. Biochem.* **1999**, *68*, 89–125.
- Smith, S. A.; Mutch, N. J.; Baskar, D.; Rohloff, P.; Docampo, R.; Morrissey, J. H. *Proc. Natl. Acad. Sci. U.S.A.* **2006**, *103* (4), 903–908.
- Smith, S. A.; Morrissey, J. H. *Blood* **2008**, *112* (7), 2810–2816.
- Muller, F.; Mutch, N. J.; Schenk, W. A.; Smith, S. A.; Esterl, L.; Spronk, H. M.; Schmidbauer, S.; Gahl, W. A.; Morrissey, J. H.; Renne, T. *Cell* **2009**, *139* (6), 1143–1156.
- Choi, S. H.; Smith, S. A.; Morrissey, J. H. *Blood* **2011**, *118* (26), 6963–6970.
- Smith, S. A.; Morrissey, J. H. *J. Thromb. Haemost.* **2008**, *6* (10), 1750–1756.
- Smith, S. A.; Choi, S. H.; Davis-Harrison, R.; Huyck, J.; Boettcher, J.; Rienstra, C. M.; Morrissey, J. H. *Blood* **2010**, *116* (20), 4353–4359.
- Kornberg, A. *J. Bacteriol.* **1995**, *177* (3), 491–496.
- Docampo, R.; de Souza, W.; Miranda, K.; Rohloff, P.; Moreno, S. N. *J. Nat. Rev. Microbiol.* **2005**, *3* (3), 251–261.
- Docampo, R.; Moreno, S. N. *J. Parasitol. Today* **1999**, *15* (11), 443–448.
- Ruiz, F. A.; Lea, C. R.; Oldfield, E.; Docampo, R. *J. Biol. Chem.* **2004**, *279* (43), 44250–44257.
- Renne, T.; Schmaier, A. H.; Nickel, K. F.; Blomback, M.; Maas, C. *Blood* **2012**, *120* (22), 4296–4303.
- Jensen, T. E.; Baxter, M.; Rachlin, J. W.; Jani, V. *Environ. Pollut. A* **1982**, *27* (2), 119–127.
- Holmsen, H.; Weiss, H. *J. Annu. Rev. Med.* **1979**, *30*, 119–134.
- Bonting, C. F. C.; Kortstee, G. J. J.; Boekestein, A.; Zehnder, A. J. B. *Arch. Microbiol.* **1993**, *159* (5), 428–434.
- Monteiro, V. A. D.; de Souza, E. F.; de Azevedo, M. M. M.; Galembeck, F. *J. Colloid Interface Sci.* **1999**, *217* (2), 237–248.
- Momeni, A.; Filiaggi, M. J. *J. Non-Cryst. Solids* **2013**, *382*, 11–17.
- Momeni, A.; Filiaggi, M. J. *Langmuir* **2014**, *30* (18), 5256–5266.
- Einstein, A. *Ann. Phys.* **1906**, *19* (2), 289–306.
- Mui, B.; Chow, L.; Hope, M. J. *Methods Enzymol.* **2002**, *367*, 3–14.
- Sjoholm, I.; Ekman, B.; Kober, A.; Ljungstedtpahlman, I.; Seiving, B.; Sjodin, T. *Mol. Pharmacol.* **1979**, *16* (3), 767–777.
- Van Slyke, D. D.; Hastings, A. B.; Hiller, A.; Sendroy, J. *J. Biol. Chem.* **1928**, *79* (2), 769–780.
- Pedersen, K. O. *Scand. J. Clin. Lab. Inv.* **1972**, *30* (1), 89–94.
- Pedersen, K. O. *Scand. J. Clin. Lab. Inv.* **1972**, *29* (4), 427–432.
- Pedersen, K. O. *Scand. J. Clin. Lab. Inv.* **1971**, *28* (4), 459–469.
- Foghandersen, N. *Clin. Chem.* **1977**, *23* (11), 2122–2126.
- Pedersen, K. O. *Scand. J. Clin. Lab. Inv.* **1972**, *29* (1), 75–83.
- Masuoka, J.; Saltman, P. *J. Biol. Chem.* **1994**, *269* (41), 25557–25561.
- Axelsson, I. *J. Chromatogr.* **1978**, *152* (1), 21–32.
- Squire, P. G.; Moser, P.; O'Konski, C. T. *Biochemistry* **1968**, *7* (12), 4261–4272.
- Zieve, P. D.; Gamble, J. L., Jr.; Jackson, D. P. *J. Clin. Invest.* **1964**, *43*, 2063–2069.
- Samuel, M.; Pixley, R. A.; Villanueva, M. A.; Colman, R. W.; Villanueva, G. B. *J. Biol. Chem.* **1992**, *267* (27), 19691–19697.
- Corrette, E.; Nigretto, J. M. *Thromb. Res.* **1990**, *59* (3), 463–473.
- Silverberg, M.; Diehl, S. V. *Biochem. J.* **1987**, *248* (3), 715–720.

Clotting Activity of Polyphosphate-Functionalized Silica Nanoparticles**

Damien Kudela,* Stephanie A. Smith, Anna May-Masnou, Gary B. Braun, Alessia Pallaoro, Chi K. Nguyen, Tracy T. Chuong, Sara Nownes, Riley Allen, Nicholas R. Parker, Hooman H. Rashidi, James H. Morrissey,* and Galen D. Stucky*

Abstract: We present a silica nanoparticle (SNP) functionalized with polyphosphate (polyP) that accelerates the natural clotting process of the body. SNPs initiate the contact pathway of the blood-clotting system; short-chain polyP accelerates the common pathway by the rapid formation of thrombin, which enhances the overall blood-clotting system, both by accelerating fibrin generation and by facilitating the regulatory anti-coagulation mechanisms essential for hemostasis. Analysis of the clotting properties of bare SNPs, bare polyP, and polyP-functionalized SNPs in plasma demonstrated that the attachment of polyP to SNPs to form polyP-SNPs creates a substantially enhanced synergistic effect that lowers clotting time and increases thrombin production at low concentrations. PolyP-SNP even retains its clotting function at ambient temperature. The polyP-SNP system has the potential to significantly improve trauma-treatment protocols and outcomes in hospital and prehospital settings.

Controlling hemorrhage is a major focus in the treatment and stabilization of many trauma patients. Uncontrolled blood loss is the leading cause of battlefield deaths, even though less than 5% of soldiers who subsequently reach a hospital die of their wounds.^[1] In civilian hospitals, hemorrhage results in 15–25% of trauma deaths.^[2] These data suggest that treatment should focus on stopping bleeding

prior to hospital arrival. Bleeding management is currently aimed at volume resuscitation and surgical intervention to limit blood loss.^[3] However, these measures often do not address the source or mechanism of the bleeding and ultimately can limit the possible options to control it, especially in the prehospital setting.

Currently, there are three major approaches for controlling prehospital hemorrhage. The oldest method employs mechanical devices that compress the wound to minimize the area through which blood can escape the damaged vessel.^[4] Agents such as kaolin or chitosan (Figure 1) are useful as field therapeutics for the management of external hemorrhage and are widely utilized by military forces as a first-response treatment.^[5,6] However, these compounds cannot be administered systemically and therefore lack utility for internal injuries with an intrinsic noncompressible hemorrhage.

Recombinant human factor VIIa (rFVIIa) is currently licensed for the management of bleeding episodes in patients with hemophilia and certain cases of warfarin overanticoagulation. Off-label use of rFVIIa is also commonly seen in certain other hemorrhagic conditions.^[7] Although anecdotal reports of clinical response abound, a significant number of concerns regarding safety remain owing to reported thrombotic complications.^[7] Drug-storage requirements and the

[*] D. Kudela, A. May-Masnou, A. Pallaoro, C. K. Nguyen, T. T. Chuong, S. Nownes, R. Allen, Prof. G. D. Stucky
Department of Chemistry and Biochemistry
University of California, Santa Barbara
Santa Barbara, CA 93106 (USA)
E-mail: dkudela@chem.ucsb.edu
stucky@chem.ucsb.edu

S. A. Smith, Prof. J. H. Morrissey
Department of Biochemistry, College of Medicine
University of Illinois at Urbana-Champaign
Urbana, IL 61801 (USA)
E-mail: jhmmorris@illinois.edu

A. May-Masnou
Departament d'Enginyeria Química, Universitat de Barcelona
c/Martí i Franquès, 1–11, 08028 Barcelona, Catalunya (Spain)

G. B. Braun
Sandford-Burnham Medical Research Institute
10901 North Torrey Pines Road, La Jolla, CA 92037 (USA)

N. R. Parker
Department of Mechanical Engineering
University of California, Santa Barbara

Prof. H. H. Rashidi
Department of Pathology and Laboratory Medicine
University of California, Davis, Sacramento, CA 95817 (USA)

Prof. G. D. Stucky
Materials Department, University of California, Santa Barbara

[**] This research was funded by the US Army Medical Research and Materiel Command under Contract Number WQ81XWH-11-2-0021, by the US Army Medical Research and Materiel Command and the Telemedicine and Advanced Technology Research Center under Contract Number W911NF-10-2-0114, and by NIH grant R01 HL047014. Partial support was provided by the Institute for Collaborative Biotechnologies grant W911NF-09-0001 from the U.S. Army Research Office. The content of the information does not necessarily reflect the position or the policy of the Government, and no official endorsement should be inferred. The MRL Shared Experimental Facilities are supported by the MRSEC Program of the NSF under Award No. DMR 1121053; a member of the NSF-funded Materials Research Facilities Network. A.M.-M. thanks the Spanish MINECO for financial support within the framework of project number CTQ2011-29336-C03-02.

Supporting information for this article, including experimental details of the synthesis and characterization of all new compounds as well as clotting assays, is available on the WWW under <http://dx.doi.org/10.1002/anie.201409639>.

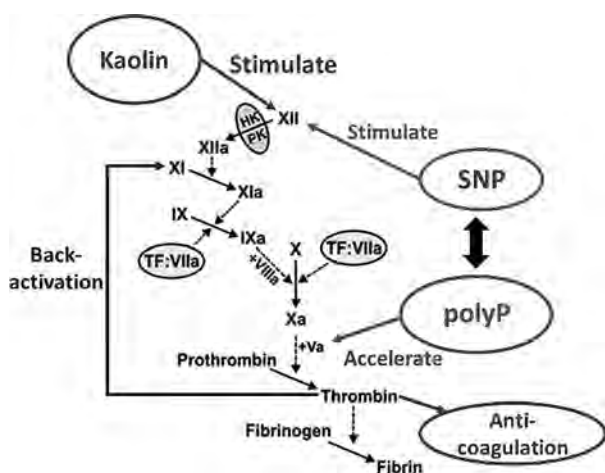


Figure 1. Simplified coagulation cascade. The SNP surface induces the activation of FXII, whereas short-chain polyP enhances the rates of activation of FV and FXI, thus leading to an earlier thrombin burst. Rapid thrombin generation leads to back-activation of FXIa to accelerate the coagulation cascade and facilitate increased activity in the anticoagulation pathway, which is designed to limit the spread of coagulation to uninjured vessels. Kaolin acts only to activate FXII through the intrinsic pathway.

extreme cost of recombinant-protein medication further limit field use.^[8]

The ideal agent to control noncompressible hemorrhage in the prehospital setting would have the following properties: 1) long shelf life and stability in weather extremes, 2) reasonable cost, 3) promotion of key functions of the blood-clotting system at the injury site through the common pathway, including coagulation, regulatory anticoagulation, and fibrin formation, and 4) lack of off-target adverse effects. Such an agent could initiate treatment during the transport phase when the patient is at the greatest risk for exsanguination. We propose that targeted short-chain-polyphosphate-laden silica nanoparticles (polyP-SNPs) have the potential to fulfill these requirements.

Because it accelerates through the common pathway the key functions of the blood-clotting system rather than initiating endogenous-coagulation-enzyme production, short-chain polyP is a reasonable candidate for the management of hemorrhage.^[9] The delivery of a polyP payload on a nanoparticle carrier could potentially be optimized to target the site of injury while minimizing the impact on the systemic circulation. Effective targeting and control would in theory minimize the risk of thrombotic complications that limit procoagulant therapy. Besides the potential for better biosystem safety, the production cost for polyP is low as compared to that of recombinant proteins. Upon attachment to inorganic oxides, polyP also has the potential for long-term stability under a variety of storage conditions.

In response to an injury, human platelets secrete short-chain polyP of approximately 60–100 monomers. Platelet-secreted polyP has a variety of wound-healing therapeutic effects, including enhanced activation of factors XI and V, which ultimately leads to enhanced factor X activity, and limitation of the activity of tissue factor pathway inhibitor,

thus resulting in accelerated thrombin generation.^[10] The incorporation of polyP also impacts clot structure and leads to resistance to fibrinolysis.^[11] As a result of the approximately 90 min half-life of polyP in plasma, the procoagulant effects are temporally limited.^[10–12] This endogenous metabolism of polyP offers much better biocompatibility than currently available agents, such as kaolin, which are not metabolized.

Whereas long-chain polyP is a potent activator of the contact pathway, short-chain polyP released from platelets has a relatively poor capacity to activate factor XII.^[9] We employed polyP with a relatively short chain length for these studies to maximize the enhancement of downstream coagulation enzymatic steps (common pathway), while minimizing contact-pathway activation.

As noted above, platelets serve as a polyP-delivery agent, secrete procoagulants and clotting factors that promote blood coagulation, and initiate the formation of a clot-dissolving enzyme that degrades blood clots during the healing process. In our studies following up on the extensive research originally carried out by the Morrissey group,^[9–12] we used free polyP as a benchmark. In the research we report herein, delivery-agent bifunctionality is introduced by using SNPs as a procoagulant carrier for the polyP.

Silica is generally considered to be a nontoxic material, and it is often used in drug-delivery studies.^[13] However, owing to its negative surface charge, silica is also a contact activator.^[5a,14] Consequently, the ideal construction of a polyP-bearing silica nanoparticle would shield the silica from exposure to the systemic circulation, with targeting and exposure of the silica carrier surface and polyP at the site of internal hemorrhage. Current materials used for treating external hemorrhage generally contain particles in the micrometer range, which are too large to readily traverse capillaries and unsuitable for use as intravenous therapeutics.^[15] We consequently developed an approach for the synthesis of particles with a diameter of 50–100 nm (Figure 2a, Table 1).^[5a,15]

Table 1: ζ potential and surface charge of the particles when dispersed in water or phosphate-buffered saline solution (pH 7.4).

Compound, medium ^{a)}	ζ potential [μ V]	Size [nm]
SNPs, H ₂ O	-24.4 ± 0.3	55.97 ± 2.19
SNPs, PBS	-52.5 ± 2.1	74.00 ± 6.24
PolyP-SNPs, H ₂ O	-44.3 ± 0.3	53.79 ± 1.75
PolyP-SNPs, PBS	-52.0 ± 3.2	78.18 ± 2.86

To attach the highly anionic polyP to an oxide, we followed the model of Lorenz et al., who used zirconia, which like silica has a negative surface potential, as the scaffold for applications in protein separation and purification.^[16] This attachment strategy exploits the Lewis acid properties of an oxide surface to bind polyP, thus overcoming the electrostatic repulsion.^[17]

³¹P NMR spectroscopy and the change in surface charge qualitatively demonstrated polyP attachment. PolyP-SNPs were digested in acid to break down polyP into phosphate monomers. ³¹P NMR spectroscopic tests on the digested

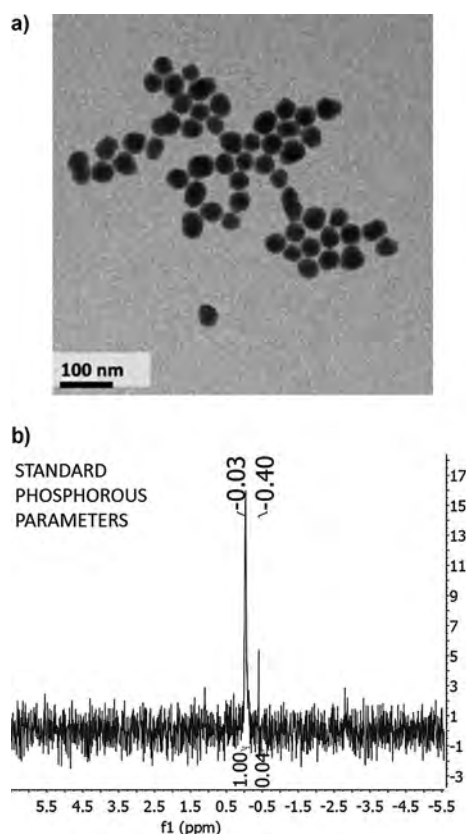


Figure 2. a) TEM images of polyP-SNPs. b) ^{31}P NMR spectrum of digested polyP-SNPs showing evidence of phosphorous.

sample detected the presence of phosphorous. The change in surface charge also suggested the presence of polyP in undigested polyP-SNPs (Table 1; see Figure 2 in the Supporting Information). Under physiological pH conditions in phosphate-buffered saline solution (PBS), both SNPs and polyP displayed a negative surface charge. In deionized water, the SNP surface charge ranged from -15 to -25 mV (Table 1; see Figure 2 in the Supporting Information). In simulated body fluid (SBF) under physiological pH conditions, SNPs had a surface charge between -50 and -60 mV. PolyP is negatively charged at this pH value as a result of a $\text{p}K_{\text{a}1}$ value between pH 1 and 2 (for all internal phosphates) and a $\text{p}K_{\text{a}2}$ value between pH 7.2 and 8.2 (for the two terminal phosphates).^[18] Upon functionalization of the SNP surface with polyP, the ζ potential of the nanoparticles decreased from -20 to -30 mV to roughly -40 to -50 mV in water, thus confirming the attachment of the polyP. In SBF, both types of particles exhibited a strongly negative charge below -45 mV.

To quantify the polyP loaded on the SNP surface, we examined the digested phosphate solutions with a malachite green assay and by inductively coupled plasma atomic emission spectroscopy (ICP-AES). Malachite green identified PO_3 concentrations of 56, 26, and 23 nmol per milligram of SNPs. ICP-AES indicated that the 26 nmol PO_3 sample had a PO_3 concentration of 29.6 nmol per milligram of SNPs. Assuming each polyP chain has 70 PO_3 monomers, these data suggest 100–200 polyP molecules are attached to each SNP.

By not using tissue factor to initiate clotting, we focused our clotting assays on the intrinsic (common) and the contact activation pathways. Negatively charged particles, such as the aluminosilicate kaolin (QuikClot Combat Gauze) used for external injuries, activate the contact pathway.^[4,5a] Because polyP is a poor clot initiator, polyP attachment shields SNPs in the systemic circulation, which is beneficial for intravenous control of haemorrhage. We measured the impact of both bare SNPs and polyP-SNPs on clot time by thromboelastography (TEG) on pooled normal plasma (PNP; Figure 3 a; see

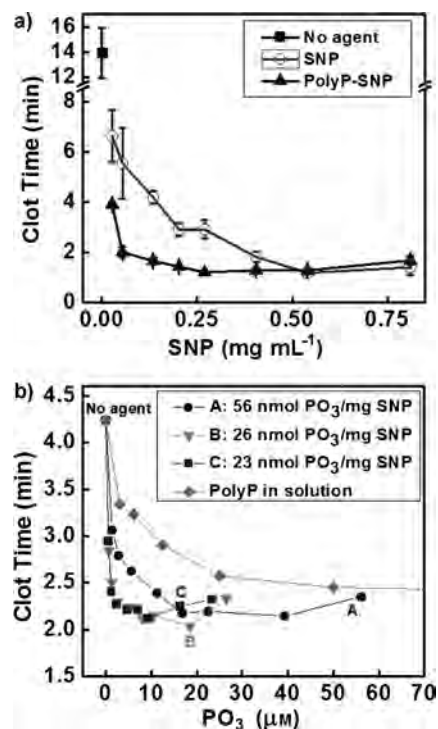


Figure 3. a) Graph showing that polyP-SNPs cut clot time (R value by TEG) roughly by half relative to that observed with bare SNPs below 0.3 mg mL^{-1} . b) Graph showing that polyP loaded onto silica lowers clot time relative to that observed with bare polyP, as measured by fibrometry.

Figures 4 and 5 in the Supporting Information). Both particles decreased the time to initial clot formation (R) in a concentration-dependent manner; however, polyP-SNP was more potent at concentrations below 0.5 mg mL^{-1} . The clot time reported in Figures 3 and 5 refers to the time to initial clot formation, which is key in illustrating how polyP-SNP successfully accelerates clotting. The agent used did not affect the overall size of the clot formed, only the time required to reach peak clot size. However, polyP has previously been shown to improve overall clot formation, in part by limiting the effect of fibrinolysis in plasma containing tissue plasminogen activator.^[11,12]

Next we evaluated the procoagulant activity of polyP-SNPs formed with differing loads of polyP. The ability to promote coagulation was measured by adding polyP-SNP or polyP in solution to PNP. Coagulation was evaluated by measuring the time to clot formation on a fibrometer (Fig-

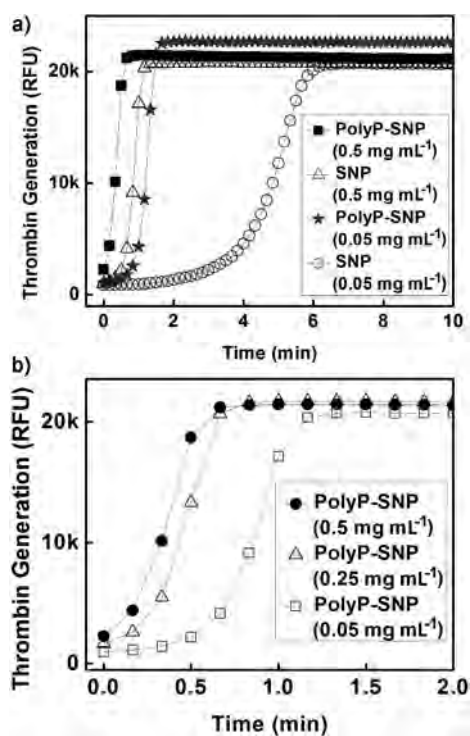


Figure 4. a) Graph showing that thrombin generation is more rapid with polyP-SNPs than with bare SNPs. b) Graph showing that polyP-SNPs are able to generate a rapid thrombin burst even at low concentrations. Thrombin generation was measured by the use of a thrombin-sensitive fluorescent dye.

ure 3b). In comparing the polyP payload, polyP-SNPs were more potent at activating the contact pathway than polyP in solution.

To further explore the relative activities of our materials, we evaluated the ability of the materials to generate thrombin, the terminal enzyme of the coagulation cascade and the primary determinant of the rate of fibrin formation.^[19] PolyP-SNP again substantially outperformed its bare counterpart (Figure 4a).

We next evaluated whether polyP-SNPs were able to enhance the generation of downstream coagulation enzymes (common pathway). We eliminated any potential impact on contact activation by utilizing factor XII deficient plasma and initiating coagulation with a small amount of relipidated tissue factor (LTF, 63 pM). As expected, bare SNPs did not affect TEG clot time in this system (Figure 5a). In contrast, polyP-SNP did shorten the time to physical clot formation. This result indicates that the polyP is accessible for binding to the relevant downstream coagulation proteins. Additionally, this response could also be evaluated in the clinical setting by comparing tests such as prothrombin time (PT) and partial thromboplastin time (PTT).

One of the problems facing emergency medical personnel is that current intravenous treatments have a significantly short half-life at ambient temperature. Even pure polyP nanoparticles remain stable for hours.^[9b] In comparison, the attachment of polyP to silica greatly enhanced the stability

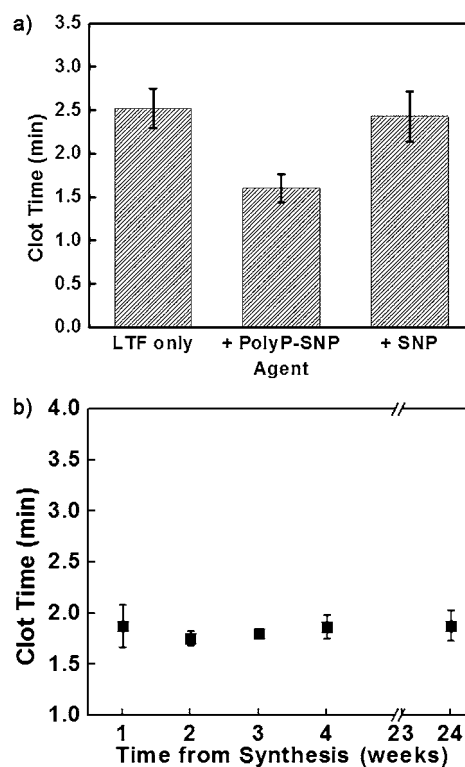


Figure 5. a) Graph showing that the addition of polyP-SNPs to LTF shortens clot time in FXII-deficient plasma relative to that observed with LTF only or LTF + SNP. LTF is required to initiate clotting. b) Graph showing that polyP-SNPs suspended in aqueous solution retained their procoagulant function after weeks of storage under ambient conditions.

and procoagulant function of polyP from hours to weeks. After bench-top storage at room temperature as both a powder and an aqueous suspension, polyP-SNP clotting times remained constant for weeks (Figure 5b). The strong negative surface charge of polyP-SNPs also minimized aggregation in aqueous suspensions over the same time period. Injectable drugs with a long shelf life can be used by emergency medical personnel prior to hospital arrival without concern that the particles will degrade without refrigeration. Thus, the polyP-SNP system could become the first prehospital intravenous injection designed to treat internal injuries by accelerating the clotting system at bleeding sites.

In this study, we successfully attached polyP to the surface of small-diameter SNPs and demonstrated that these polyP-SNPs are more potent than bare SNPs at promoting coagulation, probably owing to the ability of polyP to accelerate the common pathway for active clotting processes. PolyP-SNPs, like polyP in solution, are able to enhance downstream coagulation reactions, thus resulting in a shorter time to clot formation. Even after long-term storage at regular room temperature, the polyP-SNP system retained its procoagulant ability. The polyP-SNP construct is consequently promising as a prohemostatic agent. Further exploration of methods to limit contact activation in vivo will be necessary for its use as a systemic agent.

Keywords: hemorrhage · nanoparticles · polyphosphates · silicates · trauma

How to cite: *Angew. Chem. Int. Ed.* **2015**, *54*, 4018–4022
Angew. Chem. **2015**, *127*, 4090–4094

- [1] a) J. B. Holcomb, N. R. McMullin, L. Pearse, J. Caruso, C. E. Wade, L. Oetjen-Gerdes, H. R. Champion, M. Lawnick, W. Farr, S. Rodriguez, F. K. Butler, *Ann. Surg.* **2007**, *245*, 986–991; b) R. F. Bellamy, *Mil. Med.* **1984**, *149*, 55–62; c) H. R. Champion, R. F. Bellamy, C. P. Roberts, A. J. Leppaniemi, *Trauma* **2003**, *54*, S13–S19.
- [2] R. Pfeifer, I. S. Tarkin, B. Rocos, H.-C. Pape, *Injury* **2009**, *40*, 907–911.
- [3] P. I. Johansson, J. Stensballe, *Transfusion* **2010**, *50*, 701–710.
- [4] B. S. Kheirabadi, I. B. Terrazas, M. A. Hanson, J. F. Kragh, Jr., M. A. Dubick, L. H. Blackburne, *J. Trauma. Acute. Care. Surg.* **2013**, *74*, 1260–1265.
- [5] a) S. E. Baker, A. M. Sawvel, N. Zheng, G. D. Stucky, *Chem. Mater.* **2007**, *19*, 4390–4392; b) D. Johnson, B. Gegel, J. Burgert, J. Gasko, C. Cromwell, M. Jaskowska, R. Steward, A. Taylor, *ISRN Emerg. Med.* **2012**, *2012*, 927678.
- [6] a) B. G. Kozen, S. J. Kircher, J. Henao, F. S. Godinez, A. S. Johnson, *Acad. Emerg. Med.* **2008**, *15*, 74–81; b) Y. Li, A. M. Sawvel, Y.-S. Jun, S. Nownes, M. Ni, D. Kudela, G. D. Stucky, D. Zink, *Toxicol. Res.* **2013**, *2*, 136–144; c) P. D. Bowman, X. Wang, M. A. Meledeo, M. A. Dubick, B. S. Kheirabadi, *J. Trauma* **2011**, *71*, 727–732.
- [7] J. F. Barletta, C. L. Ahrens, J. G. Tyburski, R. F. Wilson, *J. Trauma* **2005**, *58*, 646–651.
- [8] P. M. Mannucci, M. E. Mancuso, E. Santagostino, *Blood* **2012**, *119*, 4108–4114.
- [9] a) S. A. Smith, S. H. Choi, R. Davis-Harrison, J. Huyck, J. Boettcher, C. M. Rienstra, J. H. Morrissey, *Blood* **2010**, *116*, 4353–4359; b) A. J. Donovan, J. Kalkowski, S. A. Smith, J. H. Morrissey, Y. Liu, *Biomacromolecules* **2014**, *15*, 3976–3984.
- [10] S. A. Smith, J. H. Morrissey, *J. Thromb. Haemostasis* **2008**, *6*, 1750–1756.
- [11] S. A. Smith, J. H. Morrissey, *Blood* **2008**, *112*, 2810–2816.
- [12] S. A. Smith, N. J. Mutch, D. Baskar, P. Rohloff, R. Docampo, J. H. Morrissey, *Proc. Natl. Acad. Sci. USA* **2006**, *103*, 903–908.
- [13] a) V. Cauda, H. Engelke, A. Sauer, D. Arcizet, C. Brauchle, J. Radler, T. Bein, *Nano Lett.* **2010**, *10*, 2484–2492; b) D. Tarn, C. E. Ashley, M. Xue, E. C. Carnes, J. I. Zink, C. J. Brinker, *Acc. Chem. Res.* **2013**, *46*, 792–801.
- [14] J. Margolis, *J. Exp. Biol.* **1961**, *39*, 249–258.
- [15] N. Singh, A. Karambelkar, L. Gu, K. Lin, J. S. Miller, C. S. Chen, M. J. Sailor, S. N. Bhatia, *J. Am. Chem. Soc.* **2011**, *133*, 19582–19585.
- [16] B. Lorenz, S. Marmé, W. E. G. Müller, K. Unger, H. C. Schröder, *Anal. Biochem.* **1994**, *216*, 118–126.
- [17] W.-C. J. Wei, S.-C. Wang, F.-Y. Ho, *J. Am. Ceram. Soc.* **1999**, *82*, 3385–3392.
- [18] A. Lee, G. M. Whitesides, *Anal. Chem.* **2010**, *82*, 6838–6846.
- [19] a) T. Myles, T. H. Yun, S. W. Hall, L. L. K. Leung, *J. Biol. Chem.* **2001**, *276*, 25143–25149; b) Y. Xiao, A. A. Lubin, A. J. Heeger, K. W. Plaxco, *Angew. Chem. Int. Ed.* **2005**, *44*, 5456–5459; *Angew. Chem.* **2005**, *117*, 5592–5595.

Received: September 30, 2014

Revised: December 19, 2014

Published online: January 29, 2015

Colloidal Confinement of Polyphosphate on Gold Nanoparticles Robustly Activates the Contact Pathway of Blood Coagulation

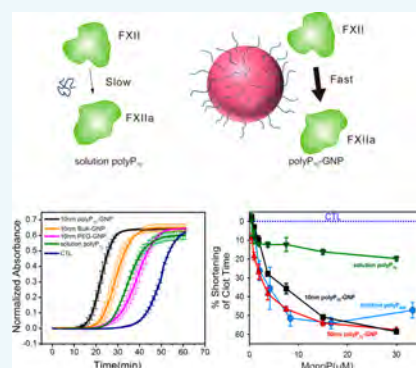
Magdalena Szymusiak,^{#,†} Alexander J. Donovan,^{#,†} Stephanie A. Smith,[‡] Ross Ransom,[†] Hao Shen,[†] Joseph Kalkowski,[†] James H. Morrissey,[‡] and Ying Liu^{*,†,§}

[†]Department of Chemical Engineering and [§]Department of Biopharmaceutical Sciences, University of Illinois at Chicago, Chicago, Illinois 60607, United States

[‡]Department of Biochemistry, University of Illinois at Urbana–Champaign, Urbana, Illinois 61801, United States

S Supporting Information

ABSTRACT: Platelet-sized polyphosphate (polyP) was functionalized on the surface of gold nanoparticles (GNPs) via a facile conjugation scheme entailing EDAC (*N*-(3-(dimethylamino)propyl)-*N*'-ethylcarbodiimide hydrochloride)-catalyzed phosphoramidation of the terminal phosphate of polyP to cystamine. Subsequent reduction of the disulfide moiety allowed for anchoring to the colloidal surface. The ability of the synthesized polyP-GNPs to initiate the contact pathway of clotting in human pooled normal plasma (PNP) was then assayed by quantifying changes in viscous, mechanical, and optical properties upon coagulation. It is revealed that the polyP-GNPs are markedly superior contact activators compared to molecularly dissolved, platelet-sized polyP (of equivalent polymer chain length). Moreover, the particles' capacity to mobilize Factor XII (FXII) and its coactivating proteins appear to be identical to very-long-chain polyP typically found in bacteria. These data imply that nanolocalization of anionic procoagulants on colloidal surfaces, achieved through covalent anchoring, may yield a robust contact surface with the ability to sufficiently cluster active clotting factors together above their threshold concentrations to cease bleeding. The polyP-GNPs therefore serve as a promising foundation in the development of a nanoparticle hemostat to treat a range of hemorrhagic scenarios.



INTRODUCTION

Polyphosphate (polyP) is an inorganic linear macromolecule consisting of orthophosphates connected by phosphoanhydride bonds.¹ The prevailing thought in the biochemistry community for decades contended that polyP was an early evolutionary casualty in Nature's endeavor to design information-dense, multifunctional biomacromolecules.² Arthur Kornberg and others³ in the last two decades have reasserted polyP's significant role in a multitude of organismal processes blurring across taxonomic boundaries: the polymer possesses potent hemostatic, inflammatory, and thrombotic properties,^{4–7} hinders tumor growth and angiogenesis,⁸ modulates bacterial pathogenicity,⁹ chelates toxic metals,¹⁰ aids in DNA transport,¹¹ and directs histological differentiation,^{12,13} among innumerable other functions. PolyP arguably performs its variegated cellular duties, even with its simple polyphosphoanhydride chemistry, by adopting different macrostructures depending on polymer length, local environment, and incoming stimuli similar (but perhaps on a much more rudimentary level) to the plethora of possible tertiary structures encountered with polypeptides. Some prokaryotes surface-pattern long-chain polyPs at varying surface densities on their exterior, with the polymer projecting outward from the cell membrane into their surroundings. For example, the human infectious agents *N. meningitidis* and *N. gonorrhoeae*, responsible for bacterial meningitis and gonorrhea, respectively, derive their resilience and virulence in large part

from storing a significant fraction of their inorganic phosphate as high-molecular-weight polyP on their capsules.¹⁴ The intensely anionic charge density on the exterior is hypothesized to confer protection from a myriad of environmental insults. DoCampo and co-workers discovered condensed polyP on the nanometer-scale in several protozoan species known to infect insects, notably *T. cruzi* and *T. brucei*, in spherical, mildly acidic organelles called acidocalcisomes,¹⁵ colocalized with concentrations of metal ions at levels orders of magnitude higher than in the cytosol. More recently, short-chain polyP has been found in nearly identical subcellular compartments called dense granules in human platelets.¹⁶ We recently established that polyP spontaneously self-assembles into granular nanoparticles in aqueous media containing concentrations of divalent metal cations such as Ca^{2+} and Mg^{2+} , at levels normally found in human blood plasma.¹⁷ The nanoprecipitation is a thermodynamic process governed by the polyP polymer size and the metal ion concentration, with the salt concentration controlling the nanoparticle diameter regardless of polymer supersaturation ratio.¹⁷

Considerable effort in recent years has centered on implementing novel conjugation chemistries for modifying

Received: September 26, 2015

Revised: November 20, 2015

polyP with various moieties, e.g., fluorescent dyes, biotin, chromogenic substrates, or primary amines, and attaching the polymer to solid substrates for facilitating *in vitro* and *in vivo* detection, quantitating interactions with various binding partners like thrombin, Factor XIIIa (FXIIIa), Factor XIa (FXIa), and kallikrein, and preventing or slowing enzymatic degradation.^{18,19} Phosphoramidation of the terminal phosphates does not abrogate polyP's physiological functionality, and polyP attached to solid supports retains robust procoagulant ability.¹⁸

The fact that polyP can exist in a variety of physical manifestations, be it molecularly dissolved, surface-immobilized, granular, or even supported on a colloidal particle scaffold, suggests that these forms might manifest differential procoagulant properties. The varied ability of inorganic polyP to initiate the contact pathway of blood coagulation could be interpreted to substantiate this hypothesis. It has been previously demonstrated that polyP exerts differential clotting effects as a function of polymer length,⁶ with high-molecular-weight polymers serving as powerful activators of the contact pathway, while intermediate and platelet-sized polyP are less potent contact activators. These shorter polymers are procoagulant through mechanisms impacting enzymes and inhibitors of other portions of the coagulation cascade.^{4,7} It has been shown that negatively charged surfaces are necessary to initiate the contact pathway of blood coagulation.²⁰ Foreign colloidal particles like ellagic acid²¹ and silicate minerals²² and highly anionic polymers of sufficient molecular weight like sulfated polysaccharides²³ present the FXII zymogen and its enzymatic binding partners (i.e., high-molecular-weight kininogen (HMWK) and prekallikrein) a sufficiently large nanosurface to trigger clotting. Sulfated polysaccharides such as heparin are generally considered powerful anticoagulants because of binding to antithrombin; however, in the absence of this enzyme inhibitor, we have previously demonstrated that heparin in actuality is a robust procoagulant molecule in many respects similar to polyP.²⁴ FXII has a molecular weight of 80 000 Da,²⁵ so its radius of gyration would be ~ 2 –5 nm. As such, long-chain polyP should possess significant ability to activate the contact pathway due to its high molecular weight and large surface area, with both the molecularly dissolved and nanoprecipitated forms arguably being large enough to activate FXII. On the other hand, the ability of molecularly dissolved, short-chain polyP to initiate the contact pathway is a matter of some dispute.^{26–28} Recent work by Mutch and colleagues provides evidence that platelet-sized polyP autoactivates FXII *in vitro*, with activity catalyzed by the presence of zinc cations.²⁹

In the present investigation we demonstrate that polyP of approximately the size released from platelets conjugated to colloidal gold nanoparticles (GNPs) via phosphoramidate linkages is able to robustly activate the contact pathway of coagulation, with potency equivalent to that of molecularly dissolved, long-chain polyP like that predominately found in bacteria. With further functionalization, polyP–GNP conjugates may be potentially used for targeted delivery as procoagulant agents to the bleeding site, especially benefiting the first-aid treatment of internal hemorrhage. As polyP is already secreted upon platelet activation and naturally exists in the human body, it is anticipated that the introduction of a colloidal anchored polyP drug delivery vehicle would have minimal side effects compared to other foreign procoagulants. In order to achieve hemostasis, polyP concentrations typically approach the micromolar range in near-vascular injury sites and

could potentially be much higher within a platelet-dense thrombus.⁶ PolyP–GNPs could potentially be of use in the management of bleeding episodes and provide further corroboration that polyP is able to wield its divergent effects by manifesting in a myriad of macrostructural forms.

RESULTS AND DISCUSSION

Binding of polyP₇₀ to GNPs was achieved by two-stage reaction: (1) PolyP₇₀ was first allowed to react with cystamine. (2) The polyP₇₀–cystamine conjugate was then reacted with GNPs by replacing the citrate groups (Figure 1).

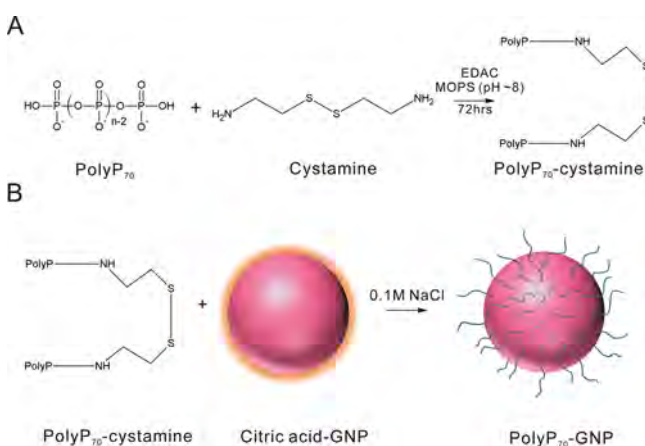


Figure 1. Process of synthesizing GNPs conjugated with polyP₇₀. (A) PolyP₇₀ is conjugated to cystamine. (B) PolyP₇₀–cystamine is attached to the surface of GNPs.

The primary amine-containing compounds like polyethylenimine, amine-PEG₂-biotin, and spermidine were used previously to study the covalent attachment of primary amine groups with the terminal phosphates of polyP via EDAC-mediated reaction.¹⁸ We modified this method for the coupling of polyP₇₀ with cystamine—a disulfide molecule, containing two primary amine groups. Reduction of the disulfide moiety in cystamine then allowed for the attachment to the GNP surface. Reaction conditions (including temperature, reaction time, pH, and buffering environment) were optimized to control the coupling of polyP₇₀ with cystamine. For the optimal conditions, polyP₇₀ was allowed to react with cystamine at room temperature and pH around 8 for 48 to 72 h. Higher temperature (37 °C) did not improve the yield. A fluorescamine assay was used to test the amount of the unreacted primary amines on cystamine, which indicated the conjugation efficiency. The highest yield of the reaction was approximately 90% as seen in Table 1.

An investigation of P–N bond hydrolysis was carried out to test the stability of the polyP₇₀–cystamine ligand. After 72 h of reaction, a fluorescamine assay was performed to detect the concentration of the unreacted cystamine. The samples were monitored for 2 weeks and hydrolysis of the P–N bonds was quantified. The P–N bond hydrolyzed in acidic conditions at pH 6.02. It was stable at pH above 7 as presented in Table 2 below. These results were in good agreement with other literature data on P–N bond hydrolysis.^{30–34}

The polyP₇₀–cystamine conjugate was allowed to react with GNPs of two different sizes (10 and 50 nm) by displacing the citrate group. After 24 h of reaction, salt addition was initiated to increase free GNP surface area available for polyP₇₀

Table 1. Conjugation Efficiency of polyP₇₀ and Cystamine at Various pH Conditions

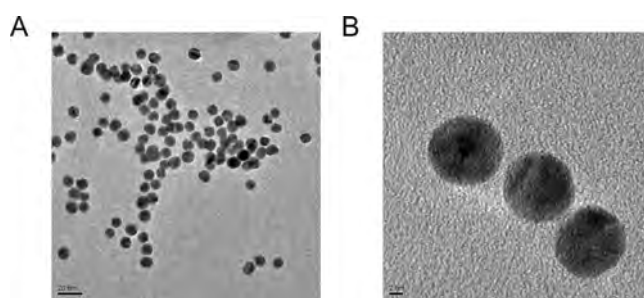
buffer	pH of reaction	efficiency (24 h)	efficiency (48 h)	efficiency (72 h)
MOPS (100 mM)	7.1	61.5%	65.0%	71.1%
MOPS (100 mM)	7.6	72.7%	74.3%	78.7%
MOPS (100 mM)	8.1	79.6%	87.3%	88.1%
MOPS (100 mM)	8.5	83.5%	87.3%	88.6%
MES (100 mM)	7.8	81.4%	89.5%	-

attachment.³⁵ The slow increase in salt concentration in the reaction over a period of 4 days (0.1 M NaCl final concentration) allowed the already attached polyP₇₀ to extend, creating more space for the unreacted ligands to access the gold surface, thus resulting in an increase in the number of polyP₇₀ chains per particle. The reaction conditions were modified from the conditions used to conjugate DNA on the surface of gold nanoparticles³⁵ and their detailed description is presented in the [Experimental Procedures](#). The full coverage is estimated from the theoretical calculations based on the ideal maximum ligand density of 0.22 per square nanometer^{36,37} and found to be 69 and 1727 for 10 and 50 nm GNPs, respectively. The maximized conjugation efficiencies were found to be 24.7% and 46.0% for 10 and 50 nm GNPs, respectively, comparing the number of conjugated ligands with the theoretical maxima.

Removal of excess, unreacted polyP₇₀ left in the solution was achieved via centrifugation. The detailed description of the centrifugation conditions and the centrifugation optimization experiments is provided in the [Experimental Procedures](#) and [Supporting Information](#). After each centrifugation, the supernatant was removed and the pellets were resuspended with a buffer at pH 7.2 to ensure the stability of the polyP₇₀-cystamine ligand and prevent polyP₇₀ hydrolysis.

Morphology and stability of the polyP₇₀-GNPs were confirmed by TEM ([Figure 2](#)), revealing that the polyP₇₀-GNP dispersion is largely free of aggregation, and the morphology of the GNPs is indistinguishable from commercially available citrated gold suspensions, that being spherical and uniformly electron dense. High magnification micrographs of 10 nm polyP₇₀-GNPs reveal the recognizable atomic lattices of the particles, clearly suggesting that the GNPs are nanocrystals.

After purification using centrifugation, concentrations of polyP₇₀ were measured using the malachite green assay and concentrations of GNPs were obtained by UV-vis spectroscopy. The number of polyP₇₀ on the surface of GNPs was calculated on the basis of the above measurements. The following polyP₇₀-GNPs were synthesized and characterized ([Table 3](#)) to investigate their ability to initiate the contact

**Figure 2.** Typical transmission electron micrographs of 10 nm polyP₇₀-GNPs. (A) polyP₇₀-GNPs are spherical and largely free of aggregation several days after synthesis. Scale bar: 20 nm. (B) Trio of polyP₇₀-GNPs with the crystal lattices very apparent. Scale bar: 2 nm.

pathway of blood coagulation in a concentration-dependent manner.

Table 3. Synthesized polyP₇₀-GNPs

sample	MonoP conc. (μM)	GNP conc. (nM)	number of polyP ₇₀ chains per particle	UV-vis peak for bulk GNP	UV-vis peak after centrifuging
10 nm polyP ₇₀ -GNP	90	75.399	17.052	519	521
50 nm polyP ₇₀ -GNP	90	1.619	794.195	531	532

PolyP₇₀-GNPs markedly reduce the time of coagulation in human plasma when assayed for contact activity using a mechanical coagulometer, a standard technique to measure clotting of both whole blood and plasma ([Figure 3](#)). Molecularly dissolved polyP₇₀ and polyP₈₀₀ were added as a positive control to citrated pooled normal plasma (PNP) at monoP concentrations ranging from 0 to 30 μM. Clotting was initiated by adding excess CaCl₂. Concentration for polyP₇₀-GNPs is given in terms of moles of GNPs (not elemental gold). Reduction in clotting time for polyP₇₀-GNPs follows typical kinetics of a surface-modulated reaction mechanism,³⁸ suggesting that the polyP₇₀-GNPs provide a templating surface for FXII activation. PolyP₇₀-cystamine ligands conjugated to GNPs of 10- and 50-nm diameter robustly activate the contact pathway of coagulation much more efficiently as compared to polyP₇₀ in solution.

The clotting activity of both 10 and 50 nm polyP₇₀-GNPs is comparable to that of much longer polyP (polyP₈₀₀) and even greater at monoP concentrations exceeding 20 μM. These results raise the question that colloidal confinement of polyP may yield divergent outcomes in complex, nonlinear biological processes such as blood coagulation, where threshold concentrations of activators must be attained before a response is generated. In this instance, chemical conjugation of platelet-

Table 2. Free Cystamine Concentration (μM) before and after pH Adjustment

pH	primary amine concentration (μM)				
	before pH adjustment	after 1 day	after 5 days	after 8 days	after 13 days
6.02	16.4 ± 0.49	30.0 ± 0.68	26.4 ± 0.82	27.6 ± 0.17	37.18 ± 1.41
7.07	16.4 ± 0.49	18.6 ± 1.29	14.5 ± 0.31	12.9 ± 0.12	13.72 ± 0.78
9.05	16.4 ± 0.49	17.1 ± 0.85	14.8 ± 0.44	14.2 ± 0.26	15.31 ± 1.36
10.01	16.4 ± 0.49	17.2 ± 0.90	14.8 ± 0.28	12.7 ± 1.2	14.73 ± 0.10

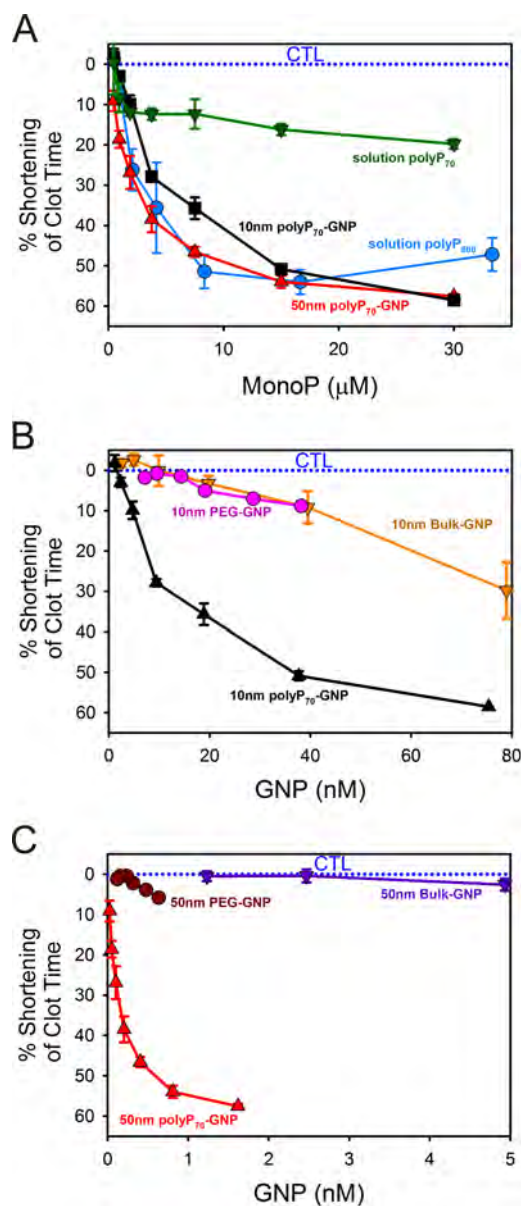


Figure 3. Shortening of clotting time of polyP₇₀-GNPs in human plasma when assayed for contact activation as a function of monoP and GNP concentration. (A) Reduction in clotting time of 10 nm polyP₇₀-GNPs and 50 nm polyP₇₀-GNPs compared to equivalent concentration of molecularly dissolved polyP₇₀ and heterogeneous long-chain polyP₈₀₀. (B) Reduction of clotting time of 10 nm polyP₇₀-GNPs compared to the equivalent concentration of 10 nm bulk-GNPs and 10 nm PEG-GNPs. (C) Shortening of clotting time of 50 nm polyP₇₀-GNPs compared against the same concentration of 50 nm bulk-GNPs and 50 nm PEG-GNPs.

sized polyP, itself a mediocre activator of the contact pathway, to an essentially inert colloidal surface, transforms the small polymer into an excellent contact activator comparable to polyP approximately ten times larger. Initiation of the contact pathway almost always necessitates a nanosurface of sufficient negative charge density and cross-sectional area to recruit the FXII zymogen. Subsequently, its fellow contact pathway components high-molecular-weight kininogen (HWMK) and prekallikrein must come in close proximity to FXII to accelerate and propagate the procoagulant stimulus. Anchoring highly anionic polyP₇₀ onto 10 and 50 nm GNPs likely generates such

an activating surface for the triad of proteins, whereas short-chain polymers that are molecularly dissolved like platelet-sized polyP₇₀ do not have adequate radii of gyration to localize FXII, HWMK, and prekallikrein together into the primary complex and propagate the signal. As prekallikrein and HWMK have been found to have a complexed molecular weight of 285 kDa in plasma, a surface larger than 5 nm would most likely be required to properly anchor these proteins together with FXII.³⁹ Bacterial polyPs, typically several hundred to thousands of orthophosphate residues, have molecular weights and radii of gyration comparable to large globular proteins, suggesting that these polymers are already above this threshold size for anchoring the primary complex, given that they robustly initiate the contact pathway of clotting in a fashion similar to foreign colloidal procoagulant agents.⁶ Long-chain polyP with robust contact-pathway activity can accordingly be used as a ruler for the measurement of hemostatic activity of polyP₇₀-GNPs and molecularly dissolved polyP₇₀ (Figure 3A).

The reduction in clotting time elicited by the polyP₇₀-GNPs was further analyzed as a function of the GNP concentration (Figure 3B,C). 50 nm polyP₇₀-GNPs are more procoagulant, as contrasted with the 10 nm polyP₇₀-GNPs, at equivalent GNP concentration: the 50 nm GNPs reduce the time to clot by 60% at less than 2 nM GNP concentration, whereas it takes approximately 80 nM for the equivalent drop with the 10 nm GNPs. This effect can be attributed to the 25-fold increase in the surface area of the 50 nm GNPs when compared with 10 nm GNPs, indicating larger localization of polyP₇₀ that could lead to a better recruitment of active clotting factors above their threshold concentration. The curvature of the particles may also affect the structural change of FXII. It is reported by Kushida et al. that nanoparticles of larger size with low curvature effect facilitated higher degree of FXII denaturation, whereas smaller size nanoparticles (high curvature) led to little or no denaturation/unfolding of FXII resulting in much weaker effects on the intrinsic coagulation.⁴⁰ Citrated (bulk) and PEGylated GNPs are used as controls to demonstrate that the GNPs themselves are not responsible for the marked reduction in clotting time. PEGylation of 10 nm citrated GNPs after 3–4 days of reaction reveals that the zeta potential drops from −20 to −5 mV, implying that the negatively charged citrate is being replaced by the neutral PEG-thiol (see Table 4). The zeta

Table 4. ζ Potential Measurements of the Synthesized Samples

sample	ζ potential (mV)
10 nm bulk	−19.5
10 nm polyP ₇₀ -GNPs	−27.5
10 nm PEG-GNP	−3.49
50 nm bulk	−22.3
50 nm polyP ₇₀ -GNP	−26.53
50 nm PEG-GNP	−2.30

potential of the synthesized polyP-GNPs is found to be −25 mV to −30 mV, which is comparable to silica particles with the zeta potential range from −25 mV to −40 mV and kaolin suspensions with the zeta potentials ranging from −20 mV to −30 mV.^{41,42} The silica particles and kaolin have been previously reported to be potent surfaces for contact pathway activation.^{43,44}

The contact activity of the polyP₇₀-GNPs was further corroborated by A₄₀₅ turbidity assays in pooled normal plasma

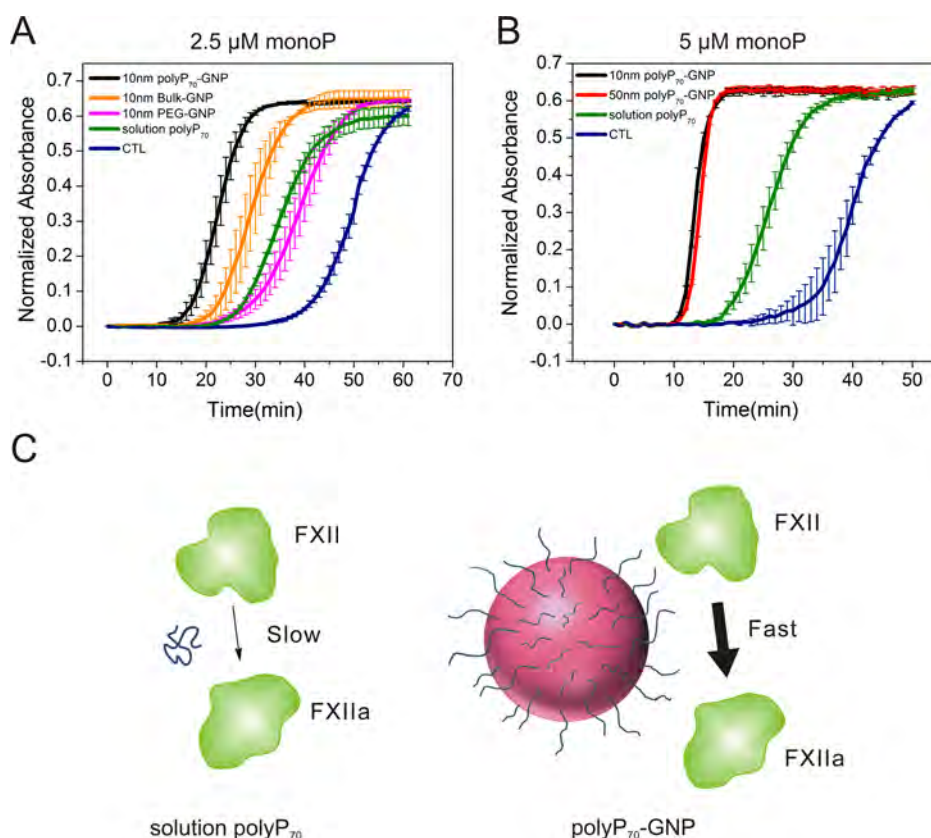


Figure 4. Procoagulant activity of polyP₇₀-GNPs assayed by A_{405} turbidity in PNP. (A) Normalized absorbance traces of 10 nm polyP₇₀-GNPs at 2.5 μ M monoP ($n = 3$, \pm S.E.) compared to PEGylated GNP and citrate GNP with the same GNP concentration, and molecularly dissolved polyP₇₀. (B) Normalized absorbance traces of 10 and 50 nm polyP₇₀-GNPs at 5 μ M monoP ($n = 3$, \pm S.E.) compared to molecularly dissolved polyP₇₀. (C) Differential clotting activation of colloidally anchored and solution-phase polyP₇₀. Colloidal clustering of polyP promotes rapid initiation of the contact pathway of clotting by serving as a surface for the assembly of the primary complex, whereas polyP₇₀ in solution is only marginally capable of FXII zymogen activation.

(PNP). 10 and 50 nm GNPs have intrinsic absorbance at 405 nm; hence, changes in absorbance values must be interpreted cautiously. As the coagulometric assay measures the mechanical and viscous properties of the clotting plasma, the turbidity tests provide complementary information on the optical density of the polymerizing fibrin mesh. Although fibrin clot density is being directly observed, and is a consequence of thrombin kinetics, it is linked to activation of FXII from interaction with a contact surface. Therefore, these two techniques can be used synergistically to evaluate the efficacy of the polyP₇₀-GNPs at initiating the contact pathway of clotting.

Before proceeding with the turbidity tests a series of control experiments were performed to ensure that the absorbance of citrated and polyP₇₀ conjugated GNPs does not change after incubation in PNP, and that the absorbance detector does not reach a saturating value during or after coagulation. SI Figure S2B,C,D demonstrates that the GNPs are colloidally stable in human plasma for at least 1 h, and that A_{405} remains constant. These observations also provide evidence that the GNPs did not aggregate during the clotting assays and that the quantified procoagulant outcomes emerge from the physical parameters we measured in the laboratory. SI Figure S2A,E,F shows that GNPs at considerably higher concentrations than used in the clotting tests still display a linear relationship with A_{405} turbidity, implying that absorbance values after coagulation will be well below the saturation limit of the detector. Therefore, the absorbance traces can be normalized by

subtracting their initial values and directly compared between samples to quantify their procoagulant efficacy. SI Figure S2A gives a representative raw absorbance trace of the polyP₇₀-GNPs at 5 μ M monoP before normalization. The time to initial fibrin formation is typically determined by fitting a line to the point at which the absorbance begins to increase and subsequently finding the intersection with the baseline absorbance value. Figure 4A shows the clotting outcomes (measured by increase in turbidity) of the 10 nm polyP₇₀-GNPs. PolyP₇₀-GNPs manifest a marked increase in turbidity long before polyP₇₀ in solution or control with no activator present. Completely PEGylated GNPs likewise do not robustly initiate the contact pathway, with a clotting time between molecularly dissolved polyP₇₀ in solution and the control (with no activator present). The citrated 10 nm GNPs (bulk), at the same GNP concentration as the 10 nm polyP₇₀-GNP sample, possess some ability to initiate the contact pathway of clotting, but they are significantly less efficacious than the 10 nm polyP₇₀-GNPs. Figure 4B depicts the clotting behavior of 10 and 50 nm polyP₇₀-GNPs at 5 μ M monoP. All GNPs conjugated with polyP₇₀ clot in approximately 10 min, while polyP₇₀ in solution coagulates at approximately 25 min, while the control (with no activator present) trails at 35–40 min. The turbidity measurements were all performed at room temperature, and the time to coagulation will in practice be much longer than those obtained by coagulometry at 37 $^{\circ}$ C. Regardless, the equivalent trends in procoagulant efficacy

between samples are apparent after short inspection. These data further corroborate coagulometric measurements presented above that nanoscale confinement of polyP₇₀ onto a colloidal surface transforms the weak contact activator polyP₇₀ into a robust agent, mimicking polyP chains more than ten times larger.

In the present investigation we lay the groundwork for the implementation of a novel, potentially injectable hemostat for treating a constellation of internal and external hemorrhagic phenomena through the conjugation of platelet-sized polyP to colloidal GNPs, facilitated by phosphoramidation to the disulfide cystamine. Although many negatively charged moieties have been shown to initiate the contact pathway of blood clotting,⁴⁵ using polyP has unique advantages, in that it is naturally secreted by human platelets and, in addition to FXII, polyP also interacts with FXI, FV, and thrombin to accelerate clotting. Moreover, our data indicated that the procoagulant effect of polyP conjugated on gold nanoparticles is orders of magnitude greater than any other (as yet) identified anionic polymer.^{4,6,7} Procoagulant outcomes, measured by conventional contact activity assays in human blood plasma, indicate that they exert significant reductions in the time to clot. Covalent conjugation to the colloidal surface transforms platelet-sized polyP₇₀ into a very robust contact surface, similar to that of the potent activator long-chain polyP. These data offer strong support to the claim that clustering of shorter polymers at high local concentrations is equivalent to having much longer polymers dispersed in solution phase for modulation of blood coagulation and other threshold-switchable networks.

The procoagulant activity characteristic of the polyP₇₀-GNPs is a meaningful step forward in the development of an on-demand, minimally invasive, targeted hemostat, and surprisingly reminiscent of the threshold-switchable properties of the coagulation cascade itself. Localization of procoagulant activators above crucial threshold concentrations accomplished in physiological contexts allows for swift propagation of the hemostatic signal to achieve wound healing. Organisms have adapted these nonlinear processes capable of exponential amplification, counterbalanced by negative feedback mechanisms, to harbor a rapid response to potentially catastrophic injury, always maintaining this delicate equilibrium of hemostasis essential for survival. The synthesis of polyP₇₀-GNPs therefore may fulfill a need for the treatment of a variety of bleeding phenomena, its methodology inspired by nature's nonlinear, threshold-switchable processes.

EXPERIMENTAL PROCEDURES

Materials and Reagents. Cystamine, EDAC (*N*-(3-(dimethylamino)propyl)-*N'*-ethylcarbodiimide hydrochloride), MES (2-(*N*-morpholino)ethanesulfonic acid), 4-morpholineethanesulfonic acid, NaCl, MOPS (3-(*N*-morpholino)propanesulfonic acid, 4-morpholinepropanesulfonic acid), imidazole, phosphorus standard solution, ammonium molybdate IV tetrahydrate, malachite green carbinol base, and poly(ethylene) glycol methyl ether thiol (Mn: 1000) were purchased from Sigma-Aldrich (St. Louis, Mo, U.S.A.). Colloidal gold citrate nanoparticles (10 and 50 nm diameter) were purchased from Ted Pella (Redding, CA). PolyP₇₀ ("Natrium polyphosphat", range 20–125 orthophosphates) was a kind gift from BK Giulini GmbH (Ludwigshafen am Rhein, Germany). PolyP₈₀₀ (range 200–1600) was prepared as previously described.⁶

Synthesis of PolyP₇₀-Cystamine Ligand. PolyP₇₀-cystamine ligand was conjugated via EDAC mediated reaction.¹⁸ PolyP₇₀ (70 mM monophosphate) was added to cystamine (0.1 mM) in the presence of EDAC (300 mM) and MES or MOPS (300 mM) buffers at various pH values (ranging from 6 to 10) and allowed to mix for 72 h at room temperature (20 °C). Control reactions containing all reagents except EDAC were also performed. The efficiency and stability of the reaction at different pH values (ranging from 6 to 10) were tested by the fluorescamine assay. Briefly, 10 μ L of the reaction sample was added to 95 μ L of 250 mM borate pH 10, and 45 μ L of fluorescamine reagent in acetone (1 mg/mL) in a 96-well black plate. The fluorescamine reagent is known to rapidly bind to the unreacted primary amine group in cystamine, which was measured by using a fluorescence plate reader with excitation wavelength of 365 nm and emission wavelength of 470 nm. A calibration curve was prepared with known concentrations of free cystamine to quantify the amounts of unreacted cystamine in the reaction.

Conjugation of PolyP₇₀-Cystamine to GNPs. PolyP₇₀-cystamine ligand was allowed to react with GNPs in eight 4 mL reaction vials for 10 nm GNPs and eight 2 mL reaction vials for 50 nm GNPs. Depending on the nanoparticle size (supplied in different starting particle concentrations or preconcentrated), the following reagent volumes and concentrations were chosen as indicated in Table 5 below.

Table 5. Experimental Conditions for Conjugation of polyP₇₀-Cystamine to GNPs

GNP size (nm)	GNP starting concentration (nM)	GNP suspension volume (μ L)	ligand solution (0.1 mM) volume (μ L)	MOPS buffer (pH 8) (μ L)
10	9.43	3850	30	120
50	0.374	1970	15	15

Control reactions of PEG-thiol (0.2 mM) with GNPs were also set up. The same reaction volumes were chosen for consistency. The ligands (polyP₇₀-cystamine or PEG-thiol) were used in a 2:1 excess ratio to GNP available binding sites. The reaction vials were first kept for 24 h at room temperature with constant slow mixing on a rotator. To increase binding efficiency, the salt addition was initiated to increase the ionic strength of the solution. 10 μ L of 5 M NaCl was added to the reaction vials while mixing. The procedure of salt addition was repeated eight times (two times a day with at least a 6 h break in between). The final concentration of salt was 0.1 M NaCl.

Removal of Unreacted PolyP₇₀. Unreacted polyP₇₀ and ligands were removed by using centrifugation in a Labnet Spectrafuge 16 M Microcentrifuge (Labnet International, Woodbridge, NJ). The samples from the polyP₇₀-cystamine ligand reactions with GNPs were distributed into 1.6 mL microcentrifuge tubes and centrifuged using optimized conditions (Table 6). After each centrifugation, the supernatant was collected and the GNP pellet was resuspended with the buffer (imidazole, pH 7.2) by vortexing for 30 s. After final

Table 6. Size-Dependent Centrifugation Conditions

GNP size (nm)	RPM	G-force	pelleting time (min)	centrifuge repeat
10	10000	8176	60	3×
50	8000	5223	10	3×

centrifugation for all GNP types, the pellets were resuspended with a smaller amount of buffer in order to achieve desired concentrations of polyP₇₀ and GNP.

Determination of Number of PolyP₇₀ Chains per Particle. The number of polyP₇₀ chains per particle was calculated by quantifying the concentrations of polyP₇₀ and GNPs in the concentrated samples after completion of the purification step. To quantify the amount of polyP₇₀ present in the sample, 101 μ L of sample was mixed with 9.1 μ L of 12.1 M HCl and heated at 100 °C for 30 min to first hydrolyze the polyP₇₀ chains into monophosphate (monoP). Then, 50 μ L of hydrolyzed sample was mixed with 100 μ L of malachite green reagent (mixing 0.1% malachite green and 42 mg/mL ammonium molybdate acid solution (5 M HCl) at 3:1 volume ratio) in a 96-well clear plate and allowed to react for 5 min. The amount of monoP present was quantified by measuring the absorbance at 620 nm using a plate reader and comparing the readings with the standardized curve. The amount of GNPs was determined by measuring the absorbance at 405 nm (for 10 nm GNPs) and 492 nm wavelengths (for 50 nm GNPs) and comparing it with the standard calibration. The final number of polyP₇₀ chains per particle was determined by the following formula:

$$\text{number of polyP}_{70}\text{chains per particle} = \frac{\text{monoP concentration/repeating unit}}{\text{gold nanoparticle concentration}}$$

Transmission Electron Microscopy (TEM). PolyP₇₀-GNPs or unmodified Au citrate suspension (10 μ L) was micropipetted onto a 300-mesh Formvar grid (Structure Probe Inc., West Chester, PA). After 10 min the liquid which had not evaporated was wicked away with the tip of a Kim Wipe. The samples were examined in a JEM-3010 transmission electron microscope (JEOL Inc., Tokyo, Japan).

Zeta (ζ) Potential Measurements. Zeta potentials of the synthesized polyP₇₀-GNPs and PEG-GNPs were measured by using a Zetasizer Nano ZS instrument (Malvern Instruments, Worcestershire, U.K.) in DI water at 20 °C.

Clotting Assays. Contact pathway activity of polyP₇₀-GNPs was determined by coagulometric assay.⁶ Clotting times of citrated human pooled normal plasma (PNP) (George King Biomedical, Overland Park, KS) were quantified at 37 °C using a Start 4 coagulometer (Diagnostica Stago, France). Prewarmed polyP or polyP₇₀-GNPs in imidazole buffer was incubated in coagulometer cuvettes with prewarmed plasma for 3 min, after which clotting was initiated by addition of phospholipid and CaCl₂. Tests of the contact pathway of blood clotting were conducted using final concentrations of GNPs as indicated, 33% plasma, 25 μ M phospholipid, 1.67 mM imidazole pH 7.0, and 8.33 mM CaCl₂.

A₄₀₅ Turbidity Measurements. Turbidity measurements of the same GNPs used above in the coagulometric assays were performed in clear, medium-binding 96-well microplates. A₄₀₅ was typically measured every min for 40–60 min at room temperature (20 °C). Each well contained 50 μ L of citrated human pooled normal plasma (George King Biomedical, Overland Park, KS) prewarmed to 37 °C containing 75 μ M phospholipid; 50 μ L of GNPs or polyP₇₀ (BKGP70) in solution in 5 mM imidazole, pH 7.2; and 50 μ L of 25 mM CaCl₂. GNPs and polyP₇₀ were preincubated in the citrated plasma on the microplate at 37 °C for 3 min before recalcification to ensure FXII activation.

■ ASSOCIATED CONTENT

● Supporting Information

The Supporting Information is available free of charge on the ACS Publications website at DOI: 10.1021/acs.bioconjchem.5b00524.

Centrifugation Optimization. Supporting Figures: Control centrifugation experiments for 10 nm GNPs, Control absorbance experiments, Clotting of 50 nm polyP₇₀-GNPs as a function of surface coverage. (PDF)

■ AUTHOR INFORMATION

Corresponding Author

*E-mail: liuying@uic.edu. Tel: (312) 996-8249. Fax: (312) 996-0808.

Author Contributions

M.S., A.J.D., S.A.S., R.R., H.S., and J.K. conceived and conducted experiments. M.S., A.J.D., S.A.S., R.R., H.S., J.K., J.H.M., and Y.L. interpreted the results. M.S., A.J.D., Y.L., and S.A.S. composed the manuscript, with editorial contributions from J.H.M. All authors have given consent to the final version of the manuscript.

Notes

The authors declare the following competing financial interest(s): J.H.M. and S.A.S. are co-inventors on patents and pending patent applications related to therapeutic usage of polyP. Y.L. and A.J.D. are co-inventors on a pending patent application associated with the pharmacologic application of polyP nanoparticles. The remaining authors declare no competing financial interests..

#Equivalent first authors.

■ ACKNOWLEDGMENTS

The study was sponsored by the U.S. Army Medical Research and Materiel Command (WQ81XWH-11-2-0021). The U.S. Army Medical Research Acquisition Activity, 820 Chandler Street, Fort Detrick MD 21702-5014 is the awarding and administering acquisition office. The contents of this article do not necessarily reflect the position or the policy of the government, and no official endorsement should be inferred. We would like to thank Dr. Seungpyo Hong at UIC for allowing us to access Malvern Zetasizer in his laboratory and Dr. Tad Daniel at UIC for assisting with TEM imaging.

■ REFERENCES

- (1) Brown, M. R. W., and Kornberg, A. (2004) Inorganic polyphosphate in the origin and survival of species. *Proc. Natl. Acad. Sci. U. S. A.* 101, 16085–16087.
- (2) Morrissey, J. H., Choi, S. H., and Smith, S. A. (2012) Polyphosphate: an ancient molecule that links platelets, coagulation, and inflammation. *Blood* 119, 5972–5979.
- (3) Kornberg, A. (1995) Inorganic Polyphosphate - toward Making a Forgotten Polymer Unforgettable. *J. Bacteriol.* 177, 491–496.
- (4) Smith, S. A., Mutch, N. J., Baskar, D., Rohloff, P., Docampo, R., and Morrissey, J. H. (2006) Polyphosphate modulates blood coagulation and fibrinolysis. *Proc. Natl. Acad. Sci. U. S. A.* 103, 903–908.
- (5) Smith, S. A., and Morrissey, J. H. (2008) Polyphosphate enhances fibrin clot structure. *Blood* 112, 2810–2816.
- (6) Smith, S. A., Choi, S. H., Davis-Harrison, R., Huyck, J., Boettcher, J., Reinstra, C. M., and Morrissey, J. H. (2010) Polyphosphate exerts differential effects on blood clotting, depending on polymer size. *Blood* 116, 4353–4359.

- (7) Choi, S. H., Smith, S. A., and Morrissey, J. H. (2011) Polyphosphate is a cofactor for the activation of factor XI by thrombin. *Blood* 118, 6963–6970.
- (8) Han, K. Y., Hong, B. S., Yoon, Y. J., Yoon, C. M., Kim, Y. K., Kwon, Y. G., and Gho, Y. S. (2007) Polyphosphate blocks tumour metastasis via anti-angiogenic activity. *Biochem. J.* 406, 49–55.
- (9) Rashid, M. H., Rumbaugh, K., Passador, L., Davies, D. G., Hamood, A. N., Iglewski, B. H., and Kornberg, A. (2000) Polyphosphate kinase is essential for biofilm development, quorum sensing, and virulence of *Pseudomonas aeruginosa*. *Proc. Natl. Acad. Sci. U. S. A.* 97, 9636–9641.
- (10) Keasling, J. D. (1997) Regulation of intracellular toxic metals and other cations by hydrolysis of polyphosphate. *Ann. N. Y. Acad. Sci.* 829, 242–249.
- (11) Reusch, R. N., and Sadoff, H. L. (1988) Putative Structure and Functions of a Poly-Beta-Hydroxybutyrate Calcium Polyphosphate Channel in Bacterial Plasma-Membranes. *Proc. Natl. Acad. Sci. U. S. A.* 85, 4176–4180.
- (12) Gezelius, K. (1974) Inorganic polyphosphates and enzymes of polyphosphate metabolism in the cellular slime mold *Dictyostelium discoideum*. *Arch. Microbiol.* 98, 311–329.
- (13) Zhang, H., Gomez-Garcia, M. R., Brown, M. R., and Kornberg, A. (2005) Inorganic polyphosphate in *Dictyostelium discoideum*: influence on development, sporulation, and predation. *Proc. Natl. Acad. Sci. U. S. A.* 102, 2731–2735.
- (14) Noegel, A., and Gotschlich, E. C. (1983) Isolation of a High Molecular-Weight Polyphosphate from *Neisseria-Gonorrhoeae*. *J. Exp. Med.* 157, 2049–2060.
- (15) Docampo, R., and Moreno, S. N. J. (1999) Acidocalcisome: A novel Ca²⁺ storage compartment in trypanosomatids and apicomplexan parasites. *Parasitol. Today* 15, 443–448.
- (16) Ruiz, F. A., Lea, C. R., Oldfield, E., and Docampo, R. (2004) Human platelet dense granules contain polyphosphate and are similar to acidocalcisomes of bacteria and unicellular eukaryotes. *J. Biol. Chem.* 279, 44250–44257.
- (17) Donovan, A. J., Kalkowski, J., Smith, S. A., Morrissey, J. H., and Liu, Y. (2014) Size-Controlled Synthesis of Granular Polyphosphate Nanoparticles at Physiologic Salt Concentrations for Blood Clotting. *Biomacromolecules* 15, 3976–3984.
- (18) Choi, S. H., Collins, J. N. R., Smith, S. A., Davis-Harrison, R. L., Rienstra, C. M., and Morrissey, J. H. (2010) Phosphoramidate End Labeling of Inorganic Polyphosphates: Facile Manipulation of Polyphosphate for Investigating and Modulating Its Biological Activities. *Biochemistry* 49, 9935–9941.
- (19) Hebbard, C. F. F., Wang, Y., Baker, C. J., and Morrissey, J. H. (2014) Synthesis and Evaluation of Chromogenic and Fluorogenic Substrates for High-Throughput Detection of Enzymes That Hydrolyze Inorganic Polyphosphate. *Biomacromolecules* 15, 3190–3196.
- (20) Renne, T., et al. (2012) In Vivo Roles for Factor XII. *Blood* 120, 4296–4303.
- (21) Bock, P. E., Srinivasan, K. R., and Shore, J. D. (1981) Activation of Intrinsic Blood-Coagulation by Ellagic Acid - Insoluble Ellagic Acid-Metal Ion Complexes Are the Activating Species. *Biochemistry* 20, 7258–7266.
- (22) Heimark, R. L., Kurachi, K., Fujikawa, K., and Davie, E. W. (1980) Surface Activation of Blood-Coagulation, Fibrinolysis and Kinin Formation. *Nature* 286, 456–460.
- (23) Tans, G., Rosing, J., and Griffin, J. H. (1983) Sulfatide-dependent autoactivation of human-blood coagulation factor-XII (Hageman-Factor). *J. Biol. Chem.* 258, 8215–8222.
- (24) Smith, S. A., and Morrissey, J. H. (2008) Heparin is procoagulant in the absence of antithrombin. *Thromb. Haemostasis* 100, 160–162.
- (25) Griffin, J. H. (1978) Role of Surface in Surface-Dependent Activation of Hageman-Factor (Blood-Coagulation Factor-Xii). *Proc. Natl. Acad. Sci. U. S. A.* 75, 1998–2002.
- (26) Faxälv, L., Boknäs, N., Strom, J. O., Tengvall, P., Theodorsson, E., Ramström, S., and Lindahl, T. L. (2013) Putting polyphosphates to the test: evidence against platelet-induced activation of factor XII. *Blood* 122, 3818–3824.
- (27) Nickel, K. F., Spronk, H. M., Mutch, N. J., and Renne, T. (2013) Time-dependent degradation and tissue factor addition mask the ability of platelet polyphosphates in activating factor XII-mediated coagulation. *Blood* 122, 3847–3849.
- (28) Müller, F., Mutch, N. J., Schenk, W. A., Smith, S. A., Esterl, L., Spronk, H. M., Schmidbauer, S., Gahl, W. A., Morrissey, J. H., and Renne, T. (2009) Platelet polyphosphates are proinflammatory and procoagulant mediators in vivo. *Cell* 139, 1143–1156.
- (29) Engel, R., Brain, C. M., Paget, J., Lionikiene, A. S., and Mutch, N. J. (2014) Single-chain factor XII exhibits activity when complexed to polyphosphate. *J. Thromb. Haemostasis* 12, 1513–1522.
- (30) Haake, P., and Koizumi, T. (1970) Hydrolysis of phosphinamides and the nature of the P-N bond. *Tetrahedron Lett.* 11, 4845–4848.
- (31) Garrison, A. W., and Boozer, C. E. (1968) The acid-catalyzed hydrolysis of a series of phosphoramidates. *J. Am. Chem. Soc.* 90, 3486–3494.
- (32) Mucha, A., Grembecka, J., Cierpicki, T., and Kafarski, P. (2003) Hydrolysis of the phosphoramidate bond in phosphono dipeptide analogues - The influence of the nature of the N-terminal functional group. *Eur. J. Org. Chem.* 2003, 4797–4803.
- (33) Mucha, A., Kunert, A., Grembecka, J., Pawelczak, M., and Kafarski, P. (2006) A phosphoramidate containing aromatic N-terminal amino group as inhibitor of leucine aminopeptidase - design, synthesis and stability. *Eur. J. Med. Chem.* 41, 768–772.
- (34) Jacobsen, N. E., and Bartlett, P. A. (1981) A Phosphoramidate Dipeptide Analog as an Inhibitor of Carboxypeptidase-A. *J. Am. Chem. Soc.* 103, 654–657.
- (35) Demers, L. M., Mirkin, C. A., Mucic, R. C., Reynolds, R. A., 3rd, Letsinger, R. L., Elghanian, R., and Viswanadham, G. (2000) A fluorescence-based method for determining the surface coverage and hybridization efficiency of thiol-capped oligonucleotides bound to gold thin films and nanoparticles. *Anal. Chem.* 72, 5535–5541.
- (36) Corbierre, M. K., Cameron, N. S., and Lennox, R. B. (2004) Polymer-stabilized gold nanoparticles with high grafting densities. *Langmuir* 20, 2867–2873.
- (37) Liu, Y. L., Shipton, M. K., Ryan, J., Kaufman, E. D., Franzen, S., and Feldheim, D. L. (2007) Synthesis, stability, and cellular internalization of gold nanoparticles containing mixed peptide-poly(ethylene glycol) monolayers. *Anal. Chem.* 79, 2221–2229.
- (38) Jackson, C. M., and Nemerson, Y. (1980) Blood-Coagulation. *Annu. Rev. Biochem.* 49, 765–811.
- (39) Mandle, R. J., Colman, R. W., and Kaplan, A. P. (1976) Identification of Prekallikrein and High-Molecular-Weight Kininogen as a Complex in Human-Plasma. *Proc. Natl. Acad. Sci. U. S. A.* 73, 4179–4183.
- (40) Kushida, T., Saha, K., Subramani, C., Nandwana, V., and Rotello, V. M. (2014) Effect of nano-scale curvature on the intrinsic blood coagulation system. *Nanoscale* 6, 14484–14487.
- (41) Kim, K. M., Kim, H. M., Lee, W. J., Lee, C. W., Kim, T. I., Lee, J. K., Jeong, J., Paek, S. M., and Oh, J. M. (2014) Surface treatment of silica nanoparticles for stable and charge-controlled colloidal silica. *Int. J. Nanomed.* 9, 29–40.
- (42) Greenwood, R., Lapcikova, B., Surynek, M., Waters, K., and Lapcik, L. (2007) The zeta potential of kaolin suspensions measured by electrophoresis and electroacoustics. *Chem. Pap. - Chem. Zvesti* 61, 83–92.
- (43) Margolis, J. (1961) The effect of colloidal silica on blood coagulation. *Immunol. Cell Biol.* 39, 249–258.
- (44) Zhu, S., and Diamond, S. L. (2014) Contact activation of blood coagulation on a defined kaolin/collagen surface in a microfluidic assay. *Thromb. Res.* 134, 1335–1343.
- (45) Oslakovic, C., Cedervall, T., Linse, S., and Dahlback, B. (2012) Polystyrene nanoparticles affecting blood coagulation. *Nanomedicine* 8, 981–986.